A FORMULATION AND VALIDATION OF RAIL-BOUND NAVIGATION

KWOK SHEUNG HUNG

Ph.D

The Hong Kong Polytechnic University

2017

The Hong Kong Polytechnic University

Department of Land Surveying and Geo-Informatics

A Formulation and Validation of Rail-bound Navigation

Kwok Sheung HUNG

A THESIS SUBMITTED IN PARTIAL FULFILMENT OF THE REQUIREMENTS FOR THE DEGREE OF DOCTOR OF PHILOSOPHY

September 2016

CERTIFICATE OF ORIGINALITY

I hereby declare that this thesis is my own work and that, to the best of my knowledge and belief, it reproduces no material previously published or written, nor material that has been accepted for the award of any other degree or diploma, except where due acknowledgement has been made in the text.

_____ (Signed)

Kwok Sheung HUNG (Name of student)

ABSTRACT

The advancement of Mobile Mapping Systems (MMS) has accelerated both commercial activities and academic research by efficient and flexible data acquisition. The Position and Orientation System (POS), which is a core component supporting direct georeferencing of mapping data, usually provides superior navigation performance by integrating the Inertial Navigation System (INS) and the Global Navigation Satellite System (GNSS). Its navigation accuracy, however, is primarily dependent on sensor quality and GNSS conditions, which leads to the necessity for additional data inspection and post-processing. Accordingly, the MMS are currently restricted to finite applications where GNSS is reliably available.

In railway environments, mobile mapping technology has considerable potential for supporting railway safety and management in real-time, but the conventional POS encounters a challenge of accuracy loss in GNSS-denied areas, especially in underground railways. To minimise the impact of this problem, an alternative configuration is presented to replace the GNSS component of a POS, with that of the railway track alignment to ensure navigation and geo-referencing accuracy is constantly maintained.

The concept of Rail-bound Navigation (RBN) is introduced in this thesis that directly substitutes the GNSS with the track constraints. Since a train is always bounded by the physical track under normal conditions, its relatively position and orientation are fundamentally constrained by the track alignment. With a valid rail-bound condition, the nominal position and orientation of train can be continuously determined, which provide alternative error control for a typical POS.

In this thesis, a generalised Track Alignment Positioning (TAP) method is established to realise the concept of track constraints, while the RBN solution is formulated with the integration of INS and TAP and the discussion for corresponding practical issues. To validate the RBN concept, a prototype RBN system has been built with consumer grade Inertial Measurement Units (IMU) for conducting a number of model-based and real world experiments. Despite the absolute position errors caused by poor sensor quality, results have demonstrated a significant improvement in attitude and velocity in that the error accumulation has been greatly constrained without additional measurements and external control data. Through the analysis of repeated measurements, the potential performance of RBN have been illustrated.

ACKNOWLEDGEMENTS

I would like to express my sincere gratitude to my former chief supervisor, Dr. Bruce King, for his continuous support and advices to my four-year research study, including the formulation of thesis direction, connections to relevant personnel, necessary resources, opportunity of exchange study at the University of Calgary, Canada, and academic and language assistance, which are irreplaceable for the completion of this thesis. Additionally, Dr. King, as a supervisor, is also my good friend who shares my happiness and worries throughout my study. I am proud to have been his last student before his retirement.

I also kindly thank Prof. Chen Wu, who was my final chief supervisor, for providing me with academic assistance and important advices. I extend my gratefulness to him for his academic and professional support during the guided study which established my basis of knowledge regarding the research study.

This research would have not completed without the support of the MTR Corporation. I am grateful to Mr. Andrew Lee, the former survey manager of the MTR Corporation, for his kind support and the resources during my preliminary study.

In addition, I would like to acknowledge the financial and academic support of the Hong Kong Polytechnic University and the Department of Land Surveying and Geo-Informatics. I would like to thank all the teaching staff and supporting staff of the department for their support during my four-year undergraduate study and four-year postgraduate study.

Last but not least, I want to thank my family and friends for giving supports in different aspects throughout my life.

TABLE OF CONTENTS

LIST OF FIGURES

LIST OF TABLES

LIST OF ABBREVIATIONS

ALS	Airborne Laser Scanning
ADMS	Automatic Deformation Monitoring Systems
AR	Auto-Regressive
ATO	Automatic Train Operation
CUPT	Coordinate Updates
DG	Direct Georeferencing
DCM	Direction Cosine Matrix
DMI	Distance Measuring Indicator
ECEF	Earth-centred Earth-fixed
ECI	Earth-centred Inertial
EKF	Extended Kalman Filter
FOG	Fibre-Optic Gyroscope
GNSS	Global Navigation Satellite System
GLONASS	Global Navigation Satellite System
GPS	Global Positioning System
GOA	Grade of Automation
GUI	Graphical User Interface
HKPD	Hong Kong Principal Datum
IMU	Inertial Measurement Unit
INS	Inertial Navigation System
IAE	Innovation-based Adaptive Estimation
UITP	International Association of Public Transport
LMU	Landmark Update
LiDAR	Light Detection And Ranging
LKF	Linearised Kalman Filter
MTR	Mass Transit Railway
MTRC	Mass Transit Railway Corporation
MATLAB	Matrix Laboratory
MEMS	Micro-Electro-Mechanical System
MLS	Mobile Laser Scanning
MMS	Mobile Mapping System
NASA	National Aeronautics and Space Administration
POS	Position and Orientation System
RBN	Rail-bond Navigation
RLG	Ring Laser Gyroscopes
RMS	Root Mean Squared
SLAM	Simultaneous Localisation and Mapping
SMO	Survey and Mapping Office
TAP	Track Alignment Positioning
URLS	Underground Railway Laser Scanning
VUPT	Velocity Updates
WGS	World Geodetic System
ZUPT	Zero Velocity Updates

Chapter 1: Introduction

Rail transport, especially underground rapid transit, has an irreplaceable role in modern society with complex railway networks forming the public transportation backbone of cities such as Hong Kong, London, Moscow, New York, Shanghai and Tokyo. The railway systems generally aim at meeting the great demand of passenger transport, service safety and reliability. In Hong Kong, the Mass Transit Railway (MTR), operated by the Mass Transit Railway Corporation (MTRC), is a heavily patronized railway network carrying on average 4.71 million passengers per day ("Hong Kong: The Facts", 2015), thus any service disruption will cause unpredictable social and financial impacts, especially during rush hours. Despite the use of highly automated train control systems, mishaps such as train malfunctions, signal failure, derailment and even train collision ("Island Line Closed …", 2012; Ngo, 2013; Lau, 2014) are difficult to prevent.

With respect to such operational failures a considerable amount of research has been conducted for obstacle detection and collision avoidance (Kruse et al., 2002; Oh et al., 2008; Passarella et al., 2011; Uribe et al., 2012), all of which consider local train safety and do not include spatial data management. In contrast, land-based Mobile Mapping Systems (MMS) may be a more valuable and comprehensive alternative to localised solutions, while potential real-time applications including train control and automation, obstacle detection, and infrastructure condition monitoring would be beneficial to the development of next generation underground railway systems. However, the current MMS georeferencing solution, a Position and Orientation System (POS), has an underlying problem: that of Global Navigation Satellite System (GNSS) outage, which is ubiquitous in underground railway tunnels.

While some generic measures have been developed to mitigate the GNSS outage problem, POS performance still depends greatly on sensor quality and at least partial access to GNSS, the outage problem remains intrinsically unsolved.

To enhance the feasibility of MMS in underground railway environments, a GNSS-free georeferencing solution is required. One solution which can be applied to all designed railway systems, not only those underground, is the Rail-bound Navigation (RBN). A RBN solution augments the conventional POS with the Track Alignment Position (TAP), train control data, and operation patterns, which contributes towards a universal georeferencing and navigation solution that will allow unconstrained development of railway mapping systems.

1.1. Role of Mobile Mapping in Railways

Despite the GNSS outage problem, mobile mapping technology is being embraced in railway engineering. A number of MMS which incorporate laser scanning components, known as Mobile Laser Scanning (MLS) systems, have been customized for railway applications, including rail track and infrastructure surveys, clearance measurement, and tunnel mapping (Morgan, 2009; Leslar et al., 2010; Kremer and Grimm, 2012; Zhu and Hyyppä, 2014).

Post-processing techniques, such as smoothing or indirect spatial-referencing methods, are essential to maintain the overall accuracy. MLS are therefore restricted to railway applications with limited GNSS outages. In cases where the GNSS outages are diminished to a feasible level and MLS is operable in real-time, the technology can be integrated with other railway systems for enhancing railway safety, train operation and management.

1.2. Current Situations for Railway Safety

For railway safety, tunnels and rail tracks are regularly monitored through geotechnical or geodetic methods, including tunnel profile surveys, convergence measurements, settlement monitoring and Automatic Deformation Monitoring Systems (ADMS). Although these methods are relatively reliable and precise, they are only sensitive to changes at specific locations regarding the structural health of tunnels. Accordingly, numerous measurement systems are generally employed for different monitoring tasks. Any unusual change beyond the ambit of measurements cannot be detected.

In general, the structural health of a tunnel is the main concern of typical monitoring works, but minor accidents can also cause serious consequences. Non-structural failures, such as signal failure, train control malfunction, undetected falling objects or obstacles, usually occur more frequently than structural failures but are equally likely to cause service delay, equipment damage or even train collision and derailment ("Island Line Closed …", 2012; Ngo, 2013; Lau, 2014).

1.3. Potential of MLS in Underground Railways

In view of that, MLS provides a dynamic solution to extend the monitoring systems to the entire tunnel sections, which includes measurements to trackside equipment, rail tracks and overhead power cables with high-density spatial details. Through real-time or near real-time processing, tunnel condition monitoring as well as obstacle detection are potential applications supporting train control and safety. If MLS were installed on some, or all of the trains, the spatial database of a tunnel system would be constantly updated in the course of normal train services. Accordingly, periodic comparison of acquired data provides a measure to indicate any unusual condition,

which would facilitate risk management and minimize the potential of accidents or service interruptions.

Regarding the nature of system failure, some problems such as signal failure and train control malfunction are seldom avoidable. Under such circumstances, a MLS system can provide an alternative train localization solution, which is self-contained and independent of the train signalling system. In case of signal failure, it may maintain the train service by aiding manual train operation through train-borne localisation and collision avoidance.

1.4. Research Direction: Rail-bound Navigation

An increasing volume of research is being devoted to point cloud (the raw product of MLS and other imaging technologies) processing and segmentation, track detection, and relevant analysis, which has encouraged the use of MLS systems in railway-related tasks (Yang and Fang, 2014; Soni et al., 2014; Elberink and Khoshelham, 2015; Jwa and Sonh, 2015; Soni et al., 2015). However, few studies have been conducted to evaluate the use of MLS in underground railway systems (Boavida et al., 2012; Gonçalves et al., 2012). In addition, the integration of MLS and railway systems has received little attention.

Hung et al. (2015) have introduced the concept of Underground Railway Laser Scanning (URLS) which integrates MLS and railways and is aimed at supporting real-time train operation and safety via tunnel condition monitoring, hazard detection, train localisation and control automation. To achieve a viable URLS, a number of subsystems require further research in order to narrow the gap between system conceptualisation and implementation.

One of the primary subsystems, TAP, utilises the engineered track alignment data to support nominal train localisation. The combination of TAP and Inertial Navigation System (INS) replaces the typical POS in a GNSS-free environment thus allowing for a full-time, real-time implementation of an URLS. The integration of INS and TAP forms the concept of RBN which is the research direction of this thesis.

1.5. Research Objectives

The following objectives are established to encapsulate the research directions of this thesis.

1.5.1. Formulating the RBN Solution

Despite recent advancements in GNSS-related technologies, there are still limitations to conventional GNSS-free operation of POS-based (INS/GNSS) navigation and positioning. For underground railway applications, a GNSS-free solution is required. Accordingly, the primary objective of this thesis is to formulate a RBN solution by integrating an INS with TAP. The necessary components of RBN and practical considerations relating to such a solution are presented and discussed.

1.5.2. Validating the RBN Solution

Following on from the RBN formulation, the secondary objectives of this thesis is to validate a prototype RBN system through a series of model-based and real world experiments. The performance and stability of the RBN system are examined through a cycle of repeated data collection and system optimisation. Through the validation, RBN can be further developed into a working prototype and introduced as an alternative train navigation system and, finally, used to the further development of the URLS concept.

1.6. Thesis Outline

This thesis is organised in sequence for the formation of RBN solution and the evaluation of system performance. To enhance the overall clarity, the structural outline of the thesis is summarised here.

Chapter 1: Introduction – the advancement and deficiencies of conventional MMS are introduced. The research motivation in developing MLS systems towards an URLS solution originated from the potential benefits after solving georeferencing problems, which formulates the research direction of this thesis: RBN formulation.

Chapter 2: Literature Review – the history of mobile mapping development is concisely summarised in terms of the fundamentals and limitations of direct georeferencing (DG). The current DG solutions and their deficiencies are then reviewed and discussed, followed by the conceptualisation of RBN.

Chapter 3: Track Alignment Positioning – introduces the required concepts and mathematical models that replace the GNSS component in a traditional POS. TAP is generalised and summarised in this chapter, which is considered with necessary assumptions for TAP implementation.

Chapter 4: Rail-bound Navigation – the INS/TAP integration is elaborated with relevant components and considerations, which formulates the core of RBN solution for the system development and implementation.

Chapter 5: System Design and Implementation – the research approach and experimental design, as well as the preliminary navigation results, are explained in this chapter. The important findings are also summarised for further discussion.

Chapter 6: Result Analysis and Discussion – this chapter interprets and explains the results and findings with necessary considerations. Several potential applications are suggested with respect to the evaluated findings and capability of solution.

Chapter 7: Conclusions and Recommendations – the analysing results and major findings are summarised relative to the research objectives in this chapter. In addition, the limitations and contributions of the research are concisely reviewed, followed by several recommendations for future research.

Appendix 1: Inertial Navigation Basis – provides supplementary knowledge of inertial navigation system design which is required for the development of RBN solution. It consists of an overview of inertial sensors, followed by a summary of INS mechanisation, system initialisation and system error control.

Appendix 2: INS Error Models – regarding the inertial navigation basis in Appendix, the kinematic equations and error models of INS are explained and summarised for the system error control process.

Appendix 3: Kalman Filter Basis – the fundamental principles of Kalman filtering and relevant filtering techniques are introduced, which support the establishment of INS/TAP and its error control process.

1.7. Preliminary Research Restrictions

Throughout the four-year research, the research direction and content had been continually realigned to reflect several critical changes in project conditions. To refine the research focus, the preliminary research limitations are summarised in this following sections before moving to next chapter.

1.7.1. Instrumental Restrictions

At the initial research stage, a commercial MMS was available for experiment, which would minimise the time and cost required for a comprehensive URLS implementation and analysis. This is important for investigating the actual performance and necessary optimisation through data collection in railway systems. Unfortunately, the MMS became unavailable at the validation stage of the research. Accordingly, the research direction was revised to focus on the core URLS system component: RBN. The MMS was replaced by a low-cost Inertial Measurement Unit (IMU) for data collection and analysis, while the spatial data acquisition such as laser scanning or photogrammetric measurement was dropped from this research.

1.7.2. Formal Access to Underground Railway and Train Control Data

At the initial stages of this research, access to Hong Kong's MTR facilities was available. Later, following the change of person-in-charge, that access was withdrawn. As a result, the experimental component was performed with minimal installation (carrying the IMU and control unit as luggage) for data collection and without train control data – a less than optimum scenario. The limitations of the data acquisition will be presented in Chapters 5 and 6.

Chapter 2: Direct Georeferencing

In this chapter, the history of mobile mapping development is concisely reviewed and is followed by the fundamentals and limitations of the DG solution – the INS/GNSS integration. The research gaps are then identified through a review and discussion of current solutions to the innate DG problems in underground railway environment, which lead to the formulation of research direction for this thesis – the RBN solution.

2.1. History of Mobile Mapping Technology

The principal configuration of mobile mapping is formulated by a direct georeferencing solution and spatial measurement systems, which originated from Airborne Laser Scanning (ALS) systems during the mid-1970s. The first system was developed by the National Aeronautics and Space Administration (NASA) for hydrographical, military, bathymetry and forestry applications (Hyyppä et al., 2009; Hyyppä, 2011), and consisted of a Global Positioning System (GPS) device, an IMU and a Light Detection And Ranging (LiDAR) device. The first commercial ALS became available in 1994 for topographic mapping (Hyyppä et al., 2009; Hyyppä, 2011). The development and principles of ALS are comprehensively reviewed by Bufton (1989), Baltsavias (1999a), Baltsavias (1999b), Baltsavias (1999c), Wehr and Lohr (1999), Wever and Lindenberger (1999), and Friess (2006).

The DG concept was extended to land-based solutions called MMS during early the 1990s. The first operational MMS, GPSVan^{TM}, was developed at Ohio State University in 1991 (Goad, 1991; Novak, 1991; He and Novak, 1992; He et al., 1994; Novak and Bossler, 1995; Bossler and Toth, 1996), and employed digital cameras and video cameras for data acquisition and a code-only GPS receiver, two

gyroscopes and an odometer for DG. At the meanwhile, the University of Calgary was involved in the development of the VISAT system for highway mapping applications (Schwarz et al., 1993; El-Sheimy et al., 1995; El-Sheimy, 1996; El-Sheimy and Schwarz, 1999; Grejner-Brzezinska et al., 2004).

The advent of compact LiDAR devices lead to MLS systems which became available in the late-1990s. Since then an increasing number of MMS were developed worldwide and have been extensively reviewed (Tao, 2000; Grejner-Brzezinska, 2001; Ellum and El-Sheimy, 2002; Barber et al., 2008; Petrie and Toth, 2008; Toth, 2009; Ussyshkin, 2009; Petrie, 2010; Puente et al., 2011; Puente et al., 2013).

The design of MMS have been generalised into several components corresponding to a collection of navigation systems, mapping sensors and relevant mathematical models including INS mechanisation, INS/GNSS integration, and data georeferencing (Grejner-Brzezinska et al., 2002; Schwarz and El-Sheimy, 2004; El-Sheimy, 2005).

2.2. Concept of Direct Georeferencing

The concept of DG is the backbone of mobile mapping technology as it provides direct measurements of position and attitude of the system sensors, including cameras and LiDAR devices, without the use of ground controls. This concept is fundamentally developed from an aided INS solution providing a time-tagged navigation trajectory with high-rate three-dimensional position and attitude updates.

Most MMS rely on the integration of INS and GNSS subsystems into a POS for their DG solution. The INS is capable of high accuracy short-term position and orientation, while GNSS provides long-term error control through a filtering process.

2.2.1. Inertial Navigation System

In general, an INS determines its position and attitude through the integration of measurements from one or more IMUs which usually consist of a group of accelerometers and gyroscopes to sense the inertial linear acceleration and angular velocity in three mutually perpendicular directions. The position difference between two observation epochs can be derived from the double integration of linear acceleration as following:

$$\Delta p = \int v(\tau) d\tau + \int \int a(\tau) d\tau \, d\tau \tag{2.1}$$

where Δp is the position difference; $v(\tau)$ and $a(\tau)$ are the velocity and acceleration of the system.

The design of an IMU platform can be fundamentally classified into two categories: gimballed gyro-stabilised systems and strap-down systems. The former design compensates the physical rotations of the carrier vehicle relative to the inner platform (where the accelerometers attached) through the gimbal, while latter design maintains the system attitude by high-rate numerical integration. These days, the former design is seldom applied to current systems on account of manufacture and maintenance difficulties. The change of platform attitude for a strap-down system is maintained by the integration of angular velocity as following:

$$\Delta \theta = \int \omega(\tau) d\tau \tag{2.2}$$

where $\Delta \theta$ is the angular difference; $\omega(\tau)$ is the angular velocity of the system.

Although an INS generally provides high update rates (e.g. 100 Hz to 1000 Hz) and precise changes of position and attitude, its use for dead reckoning navigation suffers

from the problems of integration drifts and reduce the long-term navigation accuracy. Consequently, an INS usually requires high accuracy sensors such as Ring Laser Gyroscopes (RLG) for pure inertial navigation, which was generally impractical in the early stages of development on account of their size and cost (Mostafa, 2001).

The advancement of inertial sensing technology has widened the range of performance and compactness such that IMUs are recently classified into different grades, including navigation grade, tactical grade, industrial grade and consumer grade, with different ranges of performance, size, weight and cost. The fundamentals of IMU hardware and data processing have been broadly reviewed in many publications such as Lawrence (1998), Titterton and Weston (2004), Grewal et al. (2007), Groves (2008) and Aggarwal et al. (2010).

2.2.2. Global Navigation Satellite System

The GNSS is an integrated satellite positioning system, including the United States' GPS, the Russian GLObal NAvigation Satellite System (GLONASS), the European Galileo and the Chinese BeiDou (Farrell and Barth, 1999; Grewal et al., 2007; Farrell, 2008; Groves, 2008), which provides position and velocity measurements at relatively lower rates (e.g. $1Hz$ to $10Hz$) and less precise than a typical INS. However, unlike INS, the long-term navigation accuracy of GNSS can be maintained without error accumulation.

2.2.3. Position and Orientation System

Because of the complementary characteristics of INS and GNSS, integrated solution have been developed using a Kalman filter to provide a smooth and bounded navigation solution. Figure 2.1 and Figure 2.2 show the configurations of Linearised Kalman Filter (LKF) and Extended Kalman Filter (EKF), which are the fundamental

approaches employed for INS/GNSS integration. The aiding sources, such as GNSS and speed measurement data, are applied for navigation correction.

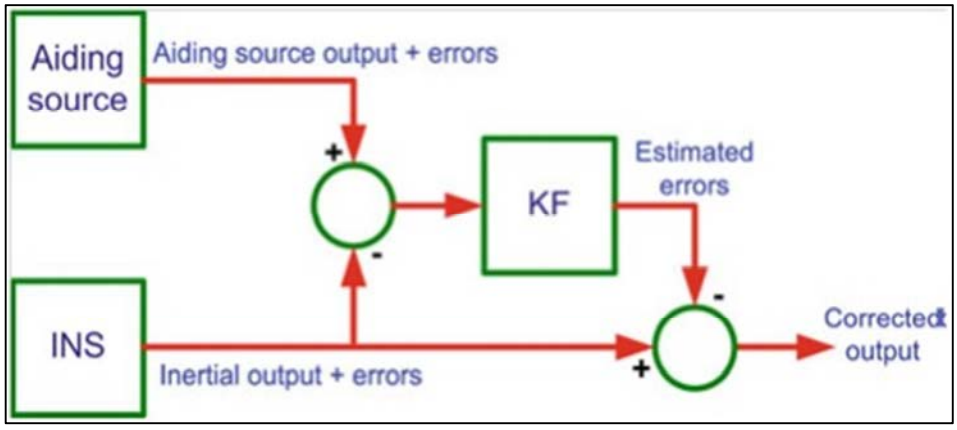

Figure 2.1: Block diagram of Linearised Kalman Filter (Noureldin et al., 2013)

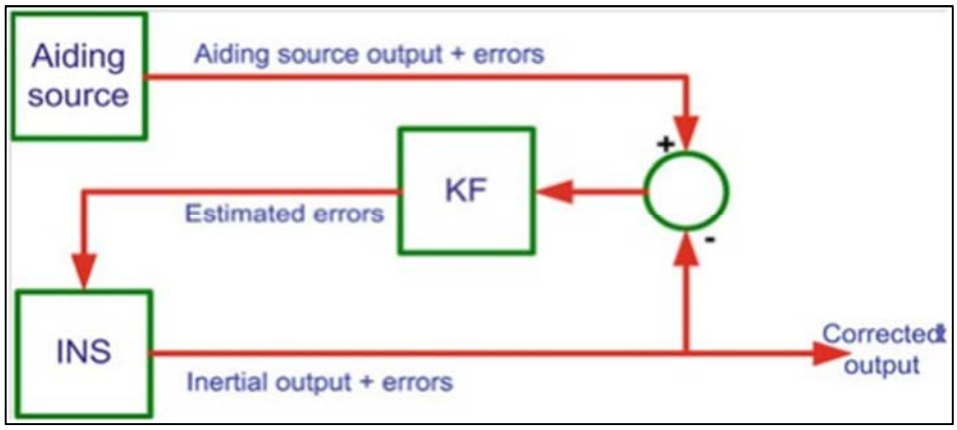

Figure 2.2: Block diagram of Extended Kalman Filter (Noureldin et al., 2013)

Through the integration of INS and GNSS, the DG system can be implemented by configuring with relatively inexpensive inertial sensors, such as Fibre-Optic Gyroscopes (FOG) and recently the Micro-Electro-Mechanical System (MEMS) sensors, which are more practicable for commercial applications.

Finally, integrated INS/GNSS systems were developed into a comprehensive solution for supporting global navigation, a POS, and supports DG for many mobile mapping technologies (Farrell and Barth, 1999; Bekir, 2007; Grewal et al., 2007; Farrell, 2008; Groves, 2008; Aggarwal et al., 2010).

2.3. Deficiencies of Typical POS

The navigation and mapping data collected by a MMS are time synchronised for DG which is performed by a series of coordinate frame transformations. The mapping data, such as images and/or LiDAR points or profiles, is recorded in the sensor frame (a localised coordinate frame for quantifying the spatial measurements) and then transformed into the body frame (a localised coordinate frame for a collection of measurements) with pre-calibrated sensor offsets and rotations. Then comes the transformation between the body frame and the reference mapping frame (a global coordinate frame for representing the data) which is defined and maintained by the POS. Consequently, the mapping data is directly georeferenced from the sensor frame to the mapping frame through a series of transformations (Schwarz and El-Sheimy, 2004; El-Sheimy, 2005; El-Sheimy, 2008) of the form shown in eqn. 2.3.

$$\mathbf{r}_i^m = \mathbf{r}_{\mathrm{b}}^m(t) + \mathbf{C}_b^m(t)\left(\mathbf{C}_s^b \mathbf{r}_i^s + \mathbf{a}_s^b\right) \tag{2.3}$$

where $\mathbf{r}_i^m$ is the measurement vector expressed in the mapping frame; $\mathbf{r}_{\mathrm{b}}^m(t)$ and $\mathbf{C}_b^m(t)$ are the time-varying translation and rotation for transforming the measurement from the body frame to the mapping frame respectively, which are maintained by the POS; $\mathbf{C}_s^b$ is the rotation transforming the measurement vector $\mathbf{r}_i^s$ from the sensor frame to the body frame; $\mathbf{a}_s^b$ is the offset of sensor with respect to the body frame.

2.3.1. Edge of Data Accuracy

According to the DG equation (eqn. 2.3), the mapping data is transformed into the mapping frame through the position and attitude estimated from the POS. The

absolute data accuracy is therefore constrained by the mapping accuracy and georeferencing accuracy.

Photogrammetric measurement is a primary mapping data source for land-based MMS, which has been recently improved by image processing techniques and digital imaging technology in terms of sensor size, resolution and sensitivity. In addition, the overall mapping accuracy is further enhanced by LiDAR devices which provide direct point measurements with precision of millimetre to centimetre levels (Kaartinen et al., 2012).

Numerous studies of georeferencing accuracy have indicated that MMS, in general, can achieve an accuracy of centimetre level under good GNSS conditions (Haala et al., 2008; Hyyppä, 2011; Kaartinen et al., 2012; Puente et al., 2013; Toschi et al., 2015). However, under degraded GNSS conditions the georeferencing errors can accumulate and reach metre level (Haala et al., 2008). Accordingly, the overall accuracy of MMS is typically dominated by the performance of the navigation solution (Hassan et al., 2006a; Ussyshkin and Boba, 2008; Ussyshkin, 2009; Puente et al., 2011).

2.3.2. GNSS Dependence

During GNSS outage, the POS is maintained by pure inertial navigation with a minimum of external controls such as velocity measurement updates. When frequent or extended GNSS outages are expected, navigation-grade or tactical-grade IMUs may be required for configuring the POS. Such IMUs provide a short-term navigation accuracy of millimetre to centimetre levels within a period of a few minutes, but the long-term accuracy would rapidly degrade by the accumulated integration of sensor and navigation errors (Boavida et al., 2012).

Several integration techniques, including uncoupled, loosely coupled, tightly coupled and deeply or ultra-tightly coupled, which have been discussed by Farrell and Barth (1999), Titterton and Weston (2004), Grewal et al. (2007) and Groves (2008), are employed by various POS for improving the navigation accuracy under degraded GNSS conditions. The level of integration architecture, however, has no effect to the overall accuracy for total GNSS outage (Chu and Chiang, 2012).

The accuracy of a POS depends greatly on the GNSS condition which causes uncertainty to the POS performance. In an underground or other GNSS-denied environment, a POS is actually an incomplete navigation solution. Alternative measures are required for controlling the growth of navigation errors, which are necessary for a POS to be developed into a GNSS-free solution.

2.4. General Solutions to GNSS-denied Environment

The loss of data accuracy due to GNSS outage is critical to the operation of a typical POS. Several solutions have been introduced to overcome the problems and are concisely summarised by Hung et al. (2015). In the case of a GNSS-denied environment, some of the measures which may be employed are reviewed and discussed for formulating the strategies of a GNSS-free navigation and georeferencing solution. Six of them are outlined in the following sections.

2.4.1. Optimal Smoothing Algorithm

An optimal smoothing algorithm, such as backward smoothing, two-filter smoothing and Rauch-Tung-Striebel smoothing (Nassar and Schwarz, 2002; Nassar et al., 2005; Liu et al., 2010) is a post-mission technique widely used to estimate INS errors by combining and smoothing the forward and backward Kalman filter (Mostafa et al., 2001; Thies, 2011; Chu and Chiang, 2012).

The smoothing is usually applied for bridging the gap of GNSS outage, which can halve the period of INS drift during the outage and reduce the position error by a factor of four (Groves, 2008). The data accuracy can be maintained at the sub-decimetre level by combining with other methods for long periods of GNSS outage (Boavida et al., 2012). Figure 2.3 illustrates the effect of optimal smoothing with forward and backward Kalman filtering.

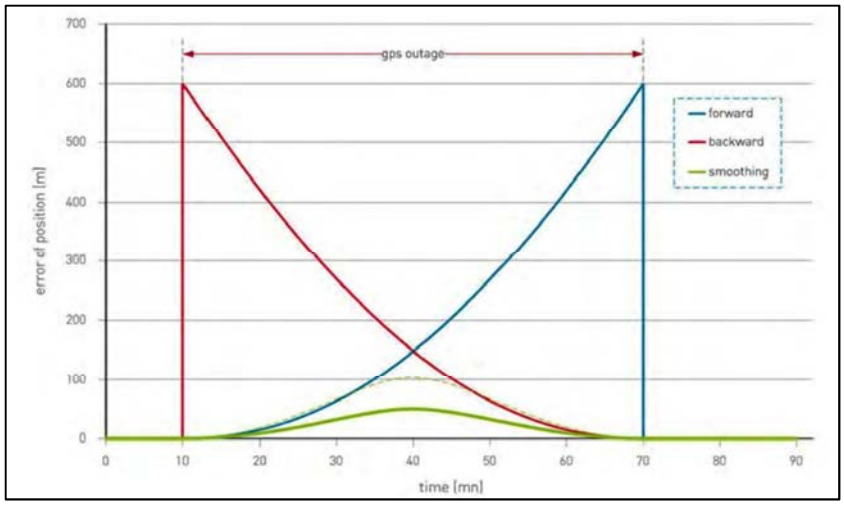

Figure 2.3: Combined forward and backward Kalman Filter (Thies, 2011)

The smoothing technique requires appropriate initialisation and finalisation which are typically realised by GNSS. In a GNSS-denied environment, this technique can bridge the gap between intermittent Coordinate Updates (CUPT) and improve the overall data accuracy. Since optimal smoothing is a post-processing technique, it cannot be applied for formulating a real-time navigation and georeferencing solution.

2.4.2. Independent Velocity Updates

For pure inertial navigation, position errors are accumulated from the double integration of acceleration errors, the integration of velocity errors, and the current position errors. To reduce the error accumulation, external sources of speed measurements are usually employed for Velocity Updates (VUPT).

For land-based applications, a POS is usually equipped with wheel-mounted odometers or Distance Measuring Indicators (DMI) to provide absolute speed measurement for VUPT and Zero Velocity Updates (ZUPT) (Schwarz and El-Sheimy, 2004; El-Sheimy, 2005; Groves, 2008; Petrie, 2010; Hyyppä, 2011; Puente et al., 2011). An odometer or DMI is sufficient to reduce the accumulation of position and velocity errors and is irreplaceable for supporting the inertial navigation.

Although the odometers and DMI can significantly control the velocity errors and vastly improve the growth of position errors through VUPT, the absolute position and attitude errors are still accumulated.

2.4.3. Landmark Updates

The Landmark Update (LMU) is an indirect spatial-referencing solution for correcting vehicle position via measurements to landmarks (Imanishi et al., 2011; Klein and Filin, 2011) extracted, identified and matched with control features from photogrammetric or LiDAR measurements. The quality of this solution depends on the control coordinate accuracy, the spatial measurements, and the LMU intervals.

LMUs are widely employed for maintaining the overall data accuracy during GNSS outage, which is an implementation of CUPT for bounding the navigation errors through mapping data. The LMU approach is a potential georeferencing solution for GNSS-denied environment, however a significant investment in time and cost is usually required for control installation and/or independent survey.

2.4.4. Photogrammetric Bridging

Photogrammetric measurement is a conventional technique for reconstructing three-dimensional data from two-dimensional images, which can be applied to bridge the spatial gap of GNSS outage through relative orientation (Bayoud et al., 2004;

Roncella et al., 2005; Hassan et al., 2006a; Hassan et al., 2006b). After system initialisation, the POS maintains the camera exterior orientation parameters (EOP) for direct georeferencing without ground controls via photogrammetric block triangulation (Tao, 2000; Grejner-Brzezinska, 2001; Ellum and El-Sheimy, 2002). Conversely, in the absence of a complete POS solution, photogrammetric bridging is capable of providing independent EOPs for INS error estimation during GNSS outage.

As photogrammetric bridging is a vision-based solution which does not require additional survey to control features, it can be employed for bridging the gap between intermittent CUPTs. The overall georeferencing accuracy can be improved but is still diminished with time on account of its dead reckoning nature. Since this solution requires photographic measurement, the performance is further restricted by environmental conditions, including lighting (which is invariably very poor in tunnels) and vehicle speed.

2.4.5. Localised Tunnel Projection

Since an INS is usually capable of high precision within certain duration of time depending on the IMU quality, the relative precision within a segment of point cloud data is sufficiently high for describing the mapping object. In tunnel surveys, the tunnel geometry can serve as a nominal constraint for adjusting the navigation trajectory and localising the mapping data (Gonçalves et. al., 2012). Point cloud segmentation is done for independent trajectory adjustment with tunnel geometry, while the entire tunnel is divided into different sections for storage and analysis.

The tunnel projection can facilitate the representation of relative measurement results, which is capable of operation in GNSS-denied railways. In accordance, this solution

provides a localised spatial-referencing such that the absolute data accuracy is not considered. The absolute position and accuracy, however, may be necessary for some applications.

2.4.6. Simultaneous Localisation and Mapping

The technique of Simultaneous Localisation and Mapping (SLAM) was firstly introduced in the 1980s and is currently adopted for real-time robotic and autonomous vehicle applications through simultaneously mapping the environment and refining the system's location from the mapping data (Bailey and Durrant-Whyte, 2006; Durrant-Whyte and Bailey, 2006).

The system localisation is usually maintained by a dead reckoning solution and supports the DG of mapping data, while any identifiable landmark would be extracted and matched with previous mapping data record for improving localisation. The performance of SLAM, however, depends greatly on the geometry of the mapping environment and the ability to form closed loops within the environment.

An increasing amount of research has been applied to the development of MMS with SLAM processing for indoor or outdoor applications, with the performance of such systems demonstrated by Zhao et al. (2008), Suzuki et al. (2010), Elseberg et al. (2012), Elseberg et al. (2013), Zlot and Bosse (2014), Nüchter et al. (2015) and Tsai et al. (2015). However, the overall performance is restricted by various factors, such as the accuracy of localisation, the availability of landmarks, the landmark identification and matching algorithms.

2.5. Direct Georeferencing in Underground Railways

For railway applications, while the POS is usually configured with high performance inertial sensors to overcome the problems of intermittent GNSS signal degradation or

outage, the loss of data accuracy cannot be prevented from long-term GNSS outage. This is particularly significant for underground railways. Alternative control methods, such as system initialisation and alignment, GNSS-free close-loop adjustment, on-site misalignment calibration, back-up solution for INS, GNSS replacement and navigation error control, are crucial considerations for a DG solution to underground railway environment.

In view of that, mobile mapping technologies are seldom applied for daily and real-time underground railway applications due to the need to post-process solutions thus hampering the potential development of MMS in railway systems. Whereas a number of commercial systems with high performance inertial sensor and specific processing software are designed for railways, a complete GNSS-free direct georeferencing solution for railways is currently not available. Formulating a solution to this problem will be extremely valuable to the management of underground railway systems and the provision of safe, reliable and efficient transportation services.

2.6. Concept of Rail-bound Navigation

The concept of RBN was introduced in Hung et al. (2015) as a DG and navigation solution for underground railway systems and forms the backbone of the URLS solution.

In railway systems, train motion is normally bounded and constrained by the physical track, while train localisation is conventionally reduced to and maintained by one-dimensional distance relative to the track alignment. Through a generalised TAP solution, the attitude as well as the position of the train can be retrieved, while their errors are generally bounded. Accordingly, the TAP solution is considered to be an

alternative to the use of GNSS, and when integrated with an INS forms the primary architecture of RBN.

Hung et al. (2015) present a generic architecture for and outlines several issues related to the development of an URLS system. Figure 2.4 illustrates the architecture and the core components of the URLS and identifies five key research directions: (1) speed data fusion; (2) RBN; (3) indirect trajectory refinement; (4) position updates through trackside landmark correlation; and (5) precise stationary positioning.

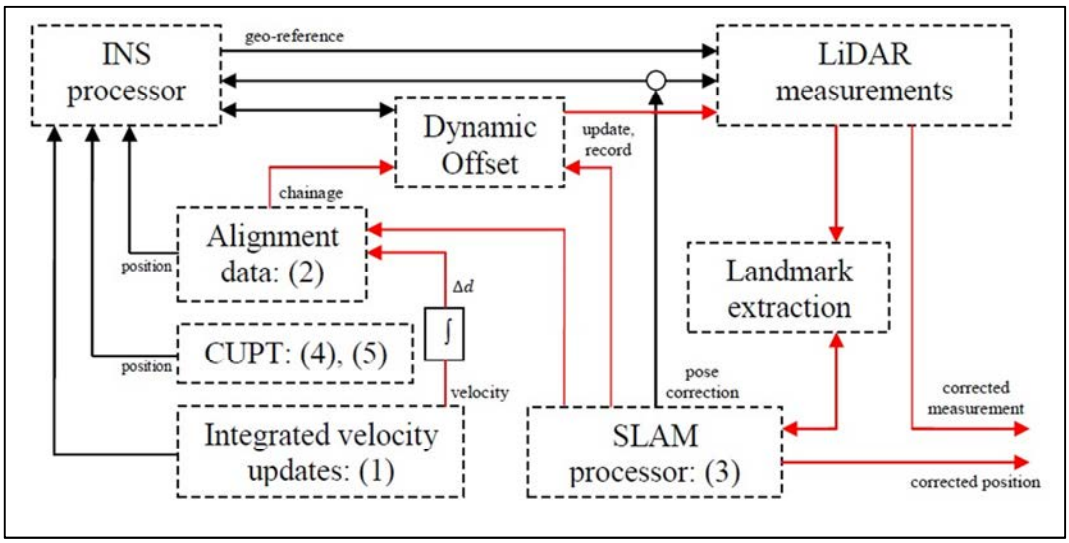

Figure 2.4: Underground Railway Laser Scanning (Hung et al., 2015)

While the RBN is primarily considered for establishing the DG solution of a URLS system, it can also operate as an independent and self-contained system for train navigation. In addition, other potential railway applications such as precise train speed measurement, train control and motion monitoring, and train operation record, are valuable for aiding the development of advanced train control systems. Consequently, the development and analysis of RBN solution constitute the research direction of this thesis, which will be elaborated in Chapter 3 (track alignment positioning) and Chapter 4 (rail-bound navigation).

Chapter 3: Track Alignment Positioning

In the previous chapter, the fundamentals and deficiencies of general DG solution were reviewed, and an alternative DG solution in railway environment, rail-bound navigation, was introduced. Prior to the establishment of solution, the basis of TAP is presented and discussed in this chapter.

To facilitate the RBN development, an overview of TAP is firstly presented. This is then followed by the formulation of essential components, including horizontal and vertical alignment models, after which the necessary assumptions and considerations are discussed and summarised for further implementation.

3.1. Overview of Track Alignment Positioning

In railway environments, train localisation is conventionally reduced to one-dimensional navigation with the rail track alignment and denoted by chainage. The chainage, or station, is the horizontal distance referenced to a specific point along a continuous alignment. Through the track geometry, the three-dimensional position of the point can be retrieved from the chainage and the track alignment data.

The TAP process is a generalised computation introduced to facilitate the extraction of three-dimensional position from the engineering track alignment data for positioning purposes. Figure 3.1 illustrates the overall structure of a TAP process. The chainage is externally determined to extract the sectional alignment parameters. The parameters and relevant errors are defined for TAP implementation with generalised horizontal and vertical alignment functions. Consequently, the relevant position, attitude and standard errors are estimated from the TAP solution, which are utilised for the system initialisation and the error control of RBN.

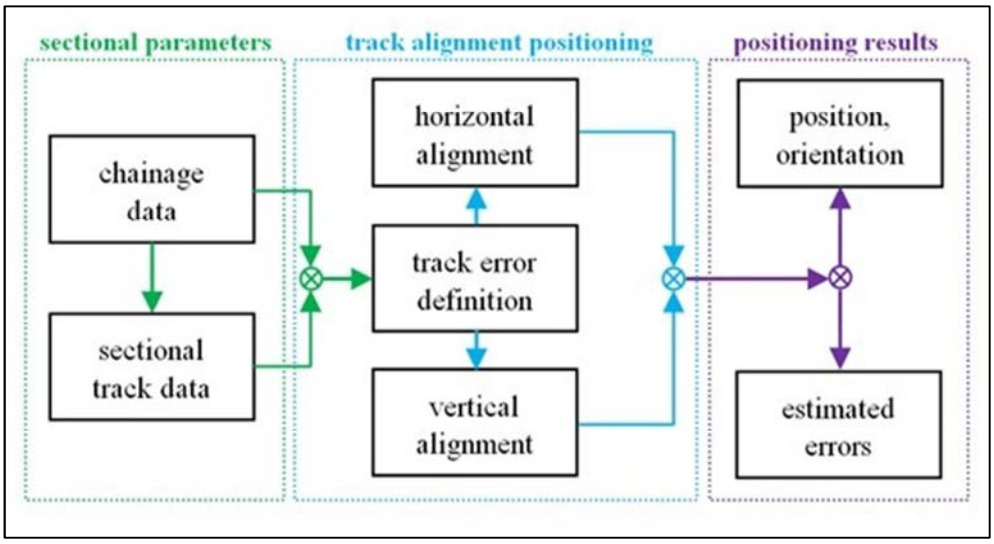

Figure 3.1: Structure of track alignment positioning

3.1.1. Track Alignment Geometry

The track alignment geometry is a primary engineering component for track design, which is the centre line defined for the construction and maintenance of rail track position. In general, the track geometry is described by the horizontal and vertical alignments.

A horizontal alignment is the continuous definition of the horizontal position of a railway line. It comprises interconnected sections of horizontal curves and straight lines. The curves are primarily defined by the radii of curvature and the transition lengths. The curve design parameters are usually considered with respect to the topography, train speed and safety criteria. The horizontal track geometry, including straights, circular curves and transition curves, is usually described by corresponding mathematical models and parameters. Consequently, the horizontal position of any point along the alignment can be retrieved.

A vertical alignment is defined by the level and gradient which indicate the vertical position and the longitudinal slope of the track respectively. It can be parameterised

in several ways, such as parabolic function and vertical circular curve, to describe the level and gradient of any point along the track alignment.

3.1.2. Track-level Frame

A localised track-level frame (*t*-frame) is established to facilitate the TAP computation, which is a resolving frame centring at a point along the track alignment and oriented with the tangential heading of the track. Consequently, the transformation from the *n*-frame to the *t*-frame can be described by eqn. 3.1.

$$\mathbf{C}_n^t = \begin{bmatrix} \cos\psi_t & \sin\psi_t & 0 \\ -\sin\psi_t & \cos\psi_t & 0 \\ 0 & 0 & 1 \end{bmatrix} \tag{3.1}$$

where ψ_t is the track heading derived from TAP.

This frame is primarily defined for resolving and georeferencing the local section of track geometry, which is also employed for resolving the navigation results relative to the track, including the train velocity and lateral train vibration.

3.1.3. Track-body Alignment Frame

In addition, a track-body alignment frame (*a*-frame) is introduced to describe the physical track body attitude with respect to the *t*-frame. This frame is established from the TAP derived attitude including the roll and pitch angles, which provides additional track attitude control from the *t*-frame. The transformation from the *t*-frame to the *a*-frame is shown in eqn. 3.2.

$$\mathbf{C}_t^a = \begin{bmatrix} 1 & 0 & 0 \\ 0 & \cos\phi_t & \sin\phi_t \\ 0 & -\sin\phi_t & \cos\phi_t \end{bmatrix} \begin{bmatrix} \cos\theta_t & 0 & -\sin\theta_t \\ 0 & 1 & 0 \\ \sin\theta_t & 0 & \cos\theta_t \end{bmatrix} \tag{3.2}$$

where ϕ_t and θ_t are the track roll and pitch angles derived from TAP.

An elementary condition for the INS/TAP integration is defined by the transformation between the sensor *b*-frame and the *a*-frame is expressed by a misalignment (eqn. 3.3), which will be further elaborated in chapter 5.

$$\mathbf{C}_b^n = \mathbf{C}_t^n \mathbf{C}_a^t \mathbf{C}_b^a \tag{3.3}$$

where $\mathbf{C}_b^a$ is the misalignment between the b-frame and the a-frame, which comprises constant and dynamic components.

3.2. Chainage Estimation

The horizontal chainage is a primary parameter required to retrieve the track geometry and position of a point, which is externally determined for acquiring the positioning results with TAP process. In a railway system, train localisation can be maintained by integrating speed measurements from tachometer and periodically initialised for position error control.

The chainage can be determined from an initial value and one-dimensional displacement which is primarily integrated from the train speed measurement over time (eqn. 3.4).

$$L(t_1) = L(t_0) + \hat{v}\,\Delta t \tag{3.4}$$

where $L(t_1)$ and $L(t_0)$ are the horizontal chainages at time t_1 and t_0 respectively; $\Delta t = t_1 - t_0$ is the sampling time interval; $\hat{v}$ is the train speed measurement.

For measurement data fusion, a Kalman filter can be applied to model the train motion, while the external measurements, such as chainage re-initialisation and speed data, can be utilised for measurement updates. The corresponding continuous-time system model for one-dimensional train motion is presented in eqn. 3.5.

$$\begin{bmatrix} \dot{p} \\ \dot{v} \\ \dot{a} \end{bmatrix} = \begin{bmatrix} 0 & 1 & 0 \\ 0 & 0 & 1 \\ 0 & 0 & 0 \end{bmatrix} \begin{bmatrix} p \\ v \\ a \end{bmatrix} + \begin{bmatrix} 0 \\ 0 \\ 1 \end{bmatrix} w_a \quad (3.5)$$

where p, v and a are the position or chainage L, velocity, and acceleration respectively; $w_a$is a zero-mean white noise random process.

This system model assumes that the train acceleration is approximately constant and is governed by a random process. The change in acceleration is not modelled but estimated from periodic measurement updates, such as train speed measurement updates. The relevant issues and estimation errors are further discussed in section 3.5.1.

3.3. Horizontal Track Geometry

The horizontal alignment mainly comprises straight and curve sections. Each section is defined by a reference station, described by its horizontal position and forward direction. The position of a point can be generalised into a function of chainage for the local position computation (eqn. 3.6), followed by a transformation of local position (eqn. 3.7). The position for the horizontal alignment is defined in grid coordinates which are usually expressed in a localised frame through map projection.

$$(N_0, E_0, \psi_0, x_i, y_i, \phi_i) = f(L_i) \quad (3.6)$$

where $f(\cdot)$ is a function of horizontal alignment geometry; L_i is the chainage difference from the reference station to point i; N_0, E_0 and ψ_0 are the grid northing, easting and tangential track heading at the reference station respectively; x_i, y_i and ϕ_i are the local coordinates and the intersection angle at point i (the angular change of heading at point *i* relative to the heading of reference station).

$$\begin{bmatrix} N_i \\ E_i \\ \psi_i \end{bmatrix} = \begin{bmatrix} N_0 \\ E_0 \\ \psi_0 \end{bmatrix} + \begin{bmatrix} \cos\psi_0 & -\sin\psi_0 & 0 \\ \sin\psi_0 & \cos\psi_0 & 0 \\ 0 & 0 & 1 \end{bmatrix} \begin{bmatrix} x_i \\ y_i \\ \phi_i \end{bmatrix} \quad (3.7)$$

The horizontal grid coordinates (N_i and E_i) are acquired from a two-dimensional transformation of local coordinates (x_i and y_i) in the coordinate system defined with respect to the sectional reference station, while the tangential heading, ψ_i, is propagated with the intersection angle, ϕ_i.

Figure 3.2 shows the definition of point i in the alignment section with respect to the track-level coordinate system, which describes the transformation in eqn. 3.7. The parameters for the local track geometry, the transformed coordinates and the reference station coordinates are coloured in red, blue and green respectively.

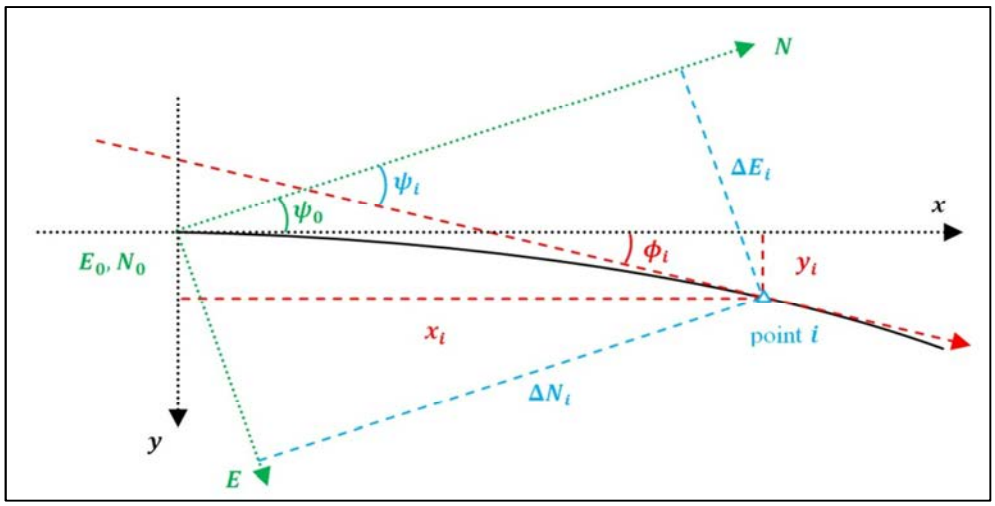

Figure 3.2: Definition of a point's horizontal position in a track alignment

The local coordinates and intersection angle at a point is derived from the horizontal track geometry, including spiral and circular sections. For straight lines, x_i refers to the horizontal length which is the chainage difference from the reference station, while y_i and ϕ_i are assumed to be zero values. The partial derivatives of the functional model given in eqn. 3.7 are derived for error propagation, which are expressed in eqn. 3.8.

$$\begin{bmatrix}\delta N_i\\ \delta E_i\\ \delta\psi_i\end{bmatrix} = \begin{bmatrix}1 & 0 & -y_i\cos\psi_0 - x_i\sin\psi_0\\ 0 & 1 & -y_i\sin\psi_0 + x_i\cos\psi_0\\ 0 & 0 & 1\end{bmatrix}\begin{bmatrix}\delta N_0\\ \delta E_0\\ \delta\psi_0\end{bmatrix} + \begin{bmatrix}\cos\psi_0 & -\sin\psi_0 & 0\\ \sin\psi_0 & \cos\psi_0 & 0\\ 0 & 0 & 1\end{bmatrix}\begin{bmatrix}\delta x_i\\ \delta y_i\\ \delta\phi_i\end{bmatrix} \quad (3.8)$$

For railway track alignment, horizontal curves can be grouped into four types (Ponnuswamy, 2012): circular curve; compound curve; reverse curve; and transition curve. The last three are grouped into a class known as transition curves. The geometries of these two classes are outlined in the following sections.

3.3.1. Circular Curve

For the design of a track alignment, a circular curve (or simple curve) constitutes the fundamental horizontal curve, which is defined by a constant radius of curvature. To maximise a train's operational safety, circular curves are designed with relatively large radii according to the design speed of the alignment.

A circular curve converges at a centre defined by a radius along the y axis of the track-level frame which is established at the sectional reference station. Figure 3.3 shows the definition of a point on a circular curve with respect to the various coordinate systems. The corresponding parameters are coloured with the same convention described in Figure 3.2.

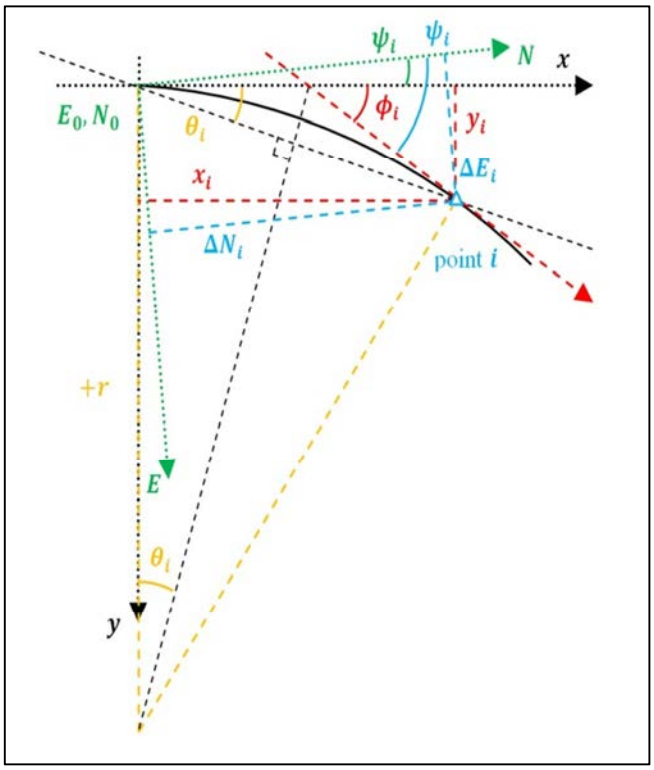

Figure 3.3: Definition of a point's horizontal position on a circular curve

The local coordinates and the intersection angle at point i are derived from the radius of curvature and the arc length which is the chainage difference from the reference station. The functional model for a circular curve is described by eqn. 3.9, while the sign of radius (positive or negative) determines the side of the curve (right or left).

$$\begin{bmatrix} x_i \\ y_i \\ \phi_i \end{bmatrix} = \begin{bmatrix} 2\left(r_0 \sin\frac{\phi_i}{2}\right)\left(\sin\frac{\phi_i}{2}\right) \\ 2\left(r_0 \sin\frac{\phi_i}{2}\right)\left(\sin\frac{\phi_i}{2}\right) \\ \frac{L_i}{r_0} \end{bmatrix} = \begin{bmatrix} r_0 \sin\frac{L_i}{r_0} \\ r_0 - r_0 \cos\frac{L_i}{r_0} \\ \frac{L_i}{r_0} \end{bmatrix} \tag{3.9}$$

where r_0 is the radius of curvature defined at the sectional reference station.

Eqn. 3.9 indicates the functional model to determine the local coordinates and intersection angle which are linearised with respect to the chainage and track parameters in eqn. 3.10.

$$\begin{bmatrix} \delta x_i \\ \delta y_i \\ \delta \phi_i \end{bmatrix} = \begin{bmatrix} \cos\frac{L_i}{r_0} & \sin\frac{L_i}{r_0} - \frac{L_i}{r_0}\cos\frac{L_i}{r_0} & 0 \\ \sin\frac{L_i}{r_0} & 1 - \cos\frac{L_i}{r_0} - \frac{L_i}{r_0}\sin\frac{L_i}{r_0} & 0 \\ \frac{1}{r_0} & -\frac{L_i}{r_0^2} & 0 \end{bmatrix} \begin{bmatrix} \delta L_i \\ \delta r_0 \\ \delta L_0 \end{bmatrix} \tag{3.10}$$

where L_0 is the horizontal length of the sectional reference station.

The linearised functional relationship between horizontal position and tangential track heading at point i and the principal parameters for the circular curve definition can be derived by substituting eqn. 3.10 into eqn. 3.8.

3.3.2. Transition Curve

In addition to circular curve, a transition curve is introduced to the track alignment with the consideration of train safety and passenger comfort in railway. A train is subjected to a centrifugal force when moving over a curve track section. The centrifugal force is directly proportional to the weight and square of velocity and is inversely proportional to the radius of curvature, which is shown in eqn. 3.11. The train motion would cause discomfort to occupants and increase the load of train axles and rail track when entering into or leaving from sections with different radii or between straight and curve sections.

$$F_c = \frac{mv^2}{r} \tag{3.11}$$

where F_c is the centrifugal force, m is the mass of train, v is the train velocity, r is the radius of curvature.

The purpose of the transition curve is to provide a consistent change of centrifugal acceleration as the train enters or leaves sections with different radii of curvature. In general, a transition curve can be defined by a spiral curve, a cubic parabola, or Bernoulli's lemniscate (Ponnuswamy, 2012) with the spiral curve commonly adopted for transition curve design. It is fundamentally defined as a linear change of curvature from infinite to definite radii with the condition stated in eqn. 3.12.

$$\begin{aligned} k &= r_i L_i \\ &= r_0 L_0 \end{aligned} \tag{3.12}$$

where k is a constant for curve design.

The clothoid spiral has its curvature increasing with distance from the origin. A point on the defined curve can be expressed in Cartesian coordinates through Fresnel integrals (Kiencke and Nielsen, 2000) which can be approximated by the power series expansion of cosine and sine integration. The coordinates and spiral intersection angle are defined in eqn. 3.13. Since the first order expansion is sufficiently accurate for the approximation, the higher order terms are removed for simplicity. The functional model is linearised into eqn. 3.14.

$$\begin{aligned} \begin{bmatrix} x_i \\ y_i \\ \phi_i \end{bmatrix} &= \begin{bmatrix} \sum_{n=0}^{\infty} (-1)^n \dfrac{L_i^{4n+1}}{(2n)!\,(4n+1)(2r_0L_0)^{2n}} \\ \sum_{n=0}^{\infty} (-1)^n \dfrac{L_i^{4n+3}}{(2n+1)!\,(4n+3)(2r_0L_0)^{2n+1}} \\ \dfrac{L_i^2}{2r_0L_0} \end{bmatrix} \\ &\approx \begin{bmatrix} L_i - \dfrac{{L_i}^5}{40(r_0L_0)^2} \\ \dfrac{L_i^3}{6r_0L_0} - \dfrac{L_i^7}{336(r_0L_0)^3} \\ \dfrac{L_i^2}{2r_0L_0} \end{bmatrix} \end{aligned} \tag{3.13}$$

$$\begin{bmatrix}\delta x_i \\ \delta y_i \\ \delta \phi_i\end{bmatrix} = \begin{bmatrix} 1 - \frac{L_i^4}{8\, r_0^2 L_0^2} & \frac{L_i^5}{20\, r_0^3 L_0^2} & \frac{L_i^5}{20\, r_0^2 L_0^3} \\ \frac{L_i^2}{2\, r_0 L_0} - \frac{L_i^6}{48\, r_0^3 L_0^3} & -\frac{L_i^3}{6\, r_0^2 L_0} + \frac{L_i^7}{112\, r_0^4 L_0^3} & -\frac{L_i^3}{6\, r_0 L_0^2} + \frac{L_i^7}{112\, r_0^3 L_0^4} \\ \frac{L_i}{r_0 L_0} & -\frac{L_i^2}{2\, r_0^2 L_0} & -\frac{L_i^2}{2\, r_0 L_0^2} \end{bmatrix} \begin{bmatrix}\delta L_i \\ \delta r_0 \\ \delta L_0\end{bmatrix} \quad (3.14)$$

The linearised functional relationship between horizontal position and tangential heading at point i and the principal parameters for the spiral curve definition is derived by substituting eqn. 3.14 into eqn. 3.8.

3.3.3. Rail Cant: Roll Angle

For a curve section, the centrifugal force of a train, which has been quantified in eqn. 3.11, is inversely proportional to the radius of curvature. Therefore, the inner wheels of the train would experience a greater magnitude of centrifugal force than that of the outer wheels. To maintain the railway safety, cant, or superelevation, is a vital element of a track alignment and characterised by a height difference between the inner and outer rails. It introduces an additional overturning force to compensate for the excessive centrifugal force, which minimises the risk of derailment or train overturn on a curved section as illustrated in Figure 3.4.

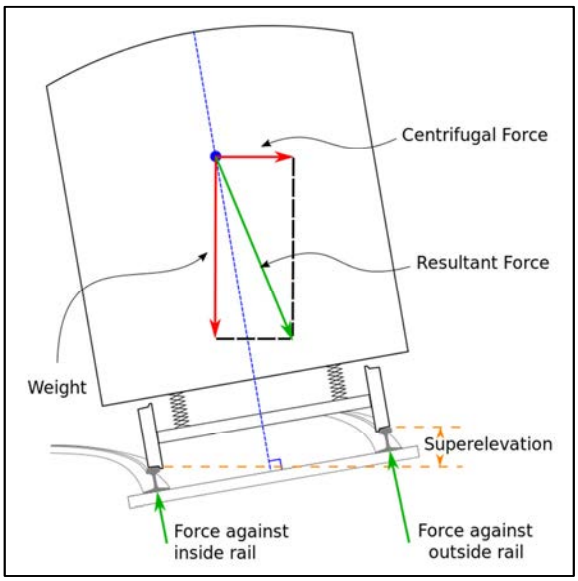

Figure 3.4: The rail cant and centrifugal force (Cant deficiency, n.d.)

Through the rail cant, an excessive centrifugal force is resolved from the weight of train, which compensates the difference of forces against the inner and outer rails. In general, the cant value is designed with the average train speed and radius of curvature. However, this is not the purpose of RBN implementation such that the cant values obtained from the track alignment data is accepted for TAP computation.

From the track alignment, a constant cant is derived for a circular section and a zero cant is assigned to a straight section or curve with large radius at low train speed. Since the spiral curve maintains a consistent change of centrifugal acceleration, the cant within a spiral section can be linearly interpolated from the neighbouring sections. The interpolation of cant and its error equation are derived in eqn. 3.15 and eqn. 3.16 respectively.

$$c_i = c_0 + (c_1 - c_0)\frac{L_i}{L_0} \tag{3.15}$$

where c_i is the height difference between inner and outer rails at point i, c_0 and c_1 are the cants of previous and next sections respectively.

$$\delta c_i = \begin{bmatrix} \frac{(c_1 - c_0)}{L_0} & \frac{-L_i(c_1 - c_0)}{L_0^2} & \frac{L_0 - L_i}{L_0} & \frac{L_i}{L_0} \end{bmatrix} \begin{bmatrix} \delta L_i \\ \delta L_0 \\ \delta c_0 \\ \delta c_1 \end{bmatrix} \tag{3.16}$$

While the rail cant is typically defined as a height difference between rail tracks, it can be alternatively expressed as an angular value as shown in eqn. 3.17.

$$\theta_c = \sin^{-1}\frac{c_i}{w} \tag{3.17}$$

where θ_c is the angular value of rail cant, which represents the roll angle of the rail track (and must be taken into account in RBN); w is the standard width of the rail track. The error equation of the roll angle is derived in eqn. 3.18.

$$\delta\theta_c = \frac{1}{\sqrt{w^2 - c_i^2}} \begin{bmatrix} \frac{(c_1 - c_0)}{L_0} & \frac{-L_i(c_1 - c_0)}{L_0^2} & \frac{L_0 - L_i}{L_0} & \frac{L_i}{L_0} \end{bmatrix} \begin{bmatrix} \delta L_i \\ \delta L_0 \\ \delta c_0 \\ \delta c_1 \end{bmatrix} + \frac{-c_i}{w\sqrt{w^2 - c_i^2}} \delta w \quad (3.18)$$

3.4. Vertical Track Geometry

Whereas the horizontal alignment is defined by the sections of straights, spirals, and circular curves on account of safety and comfort, the vertical alignment is relatively less complicated. Vertical alignment is primarily defined by the reference stations with height and gradient, which are connected by vertical curves with constant rate of gradient change. Therefore, vertical alignment can be defined by a series of circular curves with constant radii of curvature, which can be simplified into a parabolic function.

3.4.1. Parabolic Function

The vertical curves can be expressed by parabolic functions or second-order polynomial, which are applied for generalising the vertical curve modelling through eqn. 3.19.

$$y = a_2 x^2 + a_1 x + a_0 \quad (3.19)$$

where x refers to the horizontal chainage difference; y is the height at a point given by x. Regarding eqn. 3.19, the coefficients of the parabolic function can be directly derived from its derivatives and the vertical curve parameters through eqn. 3.20.

$$\begin{bmatrix} y|_{x=0} \\ \partial y/\partial x\,|_{x=0} \\ \partial^2 y/\partial x^2 \end{bmatrix} = \begin{bmatrix} a_0 \\ a_1 \\ 2a_2 \end{bmatrix} = \begin{bmatrix} h_0 \\ g_0 \\ (g_1 - g_0)/L_0 \end{bmatrix} \quad (3.20)$$

where h_0 is the height defined at the reference station; g_0 and g_1 are the gradients defined at the neighbouring reference stations. The constant vertical offset a_0 is the height at the reference station $x = 0$; The rate a_1 is defined by the gradient at the reference station $x = 0$. In addition, the second derivative of y with respect to x corresponds to the rate of gradient which is expressed by the change of gradients over horizontal length.

3.4.2. Height and Gradient

From the parabolic definition, the height and gradient at a given chainage are generalised into eqn. 3.21 with the corresponding error equations expressed in eqn. 3.22.

$$\begin{bmatrix} h_i \\ g_i \end{bmatrix} = \begin{bmatrix} \left(\frac{g_1 - g_0}{2L_0}\right) L_i^2 + g_0 L_i + h_0 \\ \left(\frac{g_1 - g_0}{L_0}\right) L_i + g_0 \end{bmatrix} \tag{3.21}$$

where h_i and g_i are the height and gradient derived at point i.

$$\begin{bmatrix} \delta h_i \\ \delta g_i \end{bmatrix} = \begin{bmatrix} \left(\frac{g_1 - g_0}{L_0}\right) L_i + g_0 & \left(\frac{g_0 - g_1}{2L_0^2}\right) L_i^2 & \frac{2L_0 L_i - L_i^2}{2L_0} & \frac{L_i^2}{2L_0} & 1 \\ \frac{g_1 - g_0}{L_0} & \left(\frac{g_0 - g_1}{L_0^2}\right) L_i & \frac{L_0 - L_i}{L_0} & \frac{L_i}{L_0} & 0 \end{bmatrix} \begin{bmatrix} \delta L_i \\ \delta L_0 \\ \delta g_0 \\ \delta g_1 \\ \delta h_0 \end{bmatrix} \tag{3.22}$$

3.4.3. Rail Gradient: Pitch Angle

A typical track alignment generally characterises the gradient by the height difference over a unit distance. Alternatively, the gradient can be expressed in angular units through eqn. 3.23.

$$\theta_g = \tan^{-1} g_i \tag{3.23}$$

where θ_g is the angular gradient, which represents the pitch angle of the rail track. The linear error equation of the angular gradient is illustrated in eqn. 3.24.

$$\delta\theta_g = \frac{1}{1+g_i^2}\begin{bmatrix}\frac{g_1-g_0}{L_0} & \left(\frac{g_0-g_1}{L_0^2}\right)L_i & \frac{L_0-L_i}{L_0} & \frac{L_i}{L_0} & 0\end{bmatrix}\begin{bmatrix}\delta L_i\\ \delta L_0\\ \delta g_0\\ \delta g_1\\ \delta h_0\end{bmatrix} \tag{3.24}$$

3.5. Summary and Preliminary Discussion

The horizontal and vertical alignments constitute the basis of TAP which comprises a series of functions of chainage and alignment parameters. The grid position ($E_i \quad N_i \quad h_i$) and attitude ($\theta_c \quad \theta_g \quad \psi_i$) at any point along the track centre line can be retrieved for RBN implementation. Although the TAP solution is theoretically available for supporting the nominal position and attitude of a train, several practical issues are considered prior to implementation and integration with INS.

3.5.1. Deficiency of Chainage Estimation

Accurate chainage estimation is fundamental to extract accurate TAP results. In section 3.2, a Kalman filter approach is introduced to model the one-dimensional train motion, which is periodically updated by chainage re-initialisation or speed measurement.

Typical speed data obtained from a tachometer corresponds to three-dimensional train motion, which is integrated into overestimated chainage on account of unresolved vertical motion. The definition of *a*-frame provides an alternative solution to resolve the speed into horizontal and vertical components. From an integrated INS/TAP solution, the velocity is primarily resolved into horizontal and vertical components through the mechanisation in the navigation frame. Therefore, the

chainage can be integrated directly from the horizontal displacement from the navigation results. The chainage update methods for RBN implementation and relevant problems are discussed in Chapter 4.

3.5.2. Longitudinal Uncertainty

Through the pre-defined track alignment data, the TAP results provide a lateral constraint to the RBN solution, while the longitudinal errors require additional awareness. Through interacting with the train control system, alternative speed and position data are advocated to retain a direct longitudinal error control.

According to the preliminary RBN results of Hung et. al. (2016), the longitudinal position errors would introduce further impacts, such as attitude errors, to the overall navigation performance since the TAP results are determined from the chainage. Regarding a highly dynamic environment, the track attitudes change rapidly at small curves implying that a small chainage error would introduce considerable track attitude errors. Therefore, the additional impacts of longitudinal errors are directly proportional to the dynamics of track. In railway environment, the variation of track attitude is relatively small to maintain the train safety. The attitude error control is therefore presumed to be accurate to some extent. The actual impacts of chainage errors regarding the track attitudes would be further analysed in Chapter 5.

3.5.3. Track Data Uncertainty

The track geometry is defined by track parameters from engineering design or as-built record, which do not exactly describe the physical track conditions on account of track defects and periodic track maintenance. In addition, a train would not completely follow the physical track due to the effects of vibrations, centrifugal forces, and suspension systems. The reduced track data solely provides a nominal

reference for train positioning. The physical track defect and train motion remain doubtful.

Hung et al. (2015) has introduced a dual-IMU architecture for handling the physical track defect and train motion by separate IMUs. The reference IMU maintains the position and attitude of the reference train axle, which is integrated with TAP and improves the physical track measurement from the track data. The physical track defect and train motion are therefore decomposed for improving the error control.

In this thesis, the role of reference IMU is alternative replaced by appropriate stochastic control, which simplifies the hardware requirements and sensor error control. Further details are discussed in Chapter 4 for RBN system design and implementation.

Chapter 4: Rail-bound Navigation

In Chapters 3, the fundamentals of TAP was introduced and its role in the design of a RBN solution was outlined.

In this chapter, the definitions of coordinate frames and mathematical preliminaries are firstly summarised to facilitate the mathematical representation in later sections. The structure of RBN is then introduced and followed by the essential components such as system initialisation, chainage updates, constant and dynamic misalignment control, and the navigation error control. Prior to the system implementation, preliminary assumptions and practical issues are discussed.

4.1. General Coordinate Frames

The RBN solution quantifies the physical motion (position and attitude) through the maintenance of coordinate frames and their relationships. In general, several coordinate frames, including the body frame, the Earth frame and the navigation frame, are involved in the mechanisation of an INS for RBN implementation.

4.1.1. Body Frame

The body frame (*b*-frame), or the vehicle frame, is an orthogonal coordinate frame fixed to the body of carrier vehicle and aligned with its roll, pitch and yaw (or heading) axes. For simplicity, the *x*, *y* and *z* axes are usually established by and coincident with the IMU sensor axes, thus the inertial motion, such as linear accelerations and angular velocities, are measured in this frame. In addition, the body frame is an essential representation for an INS that the position and attitude of the reference object is described through the transformation between the body frame and another reference coordinate frame.

4.1.2. Inertial Frame

The inertial frame (*i*-frame) or the Earth-Centred Inertial (ECI) frame is a stationary coordinate frame fixed to the stars, which is centred to Earth and has its *z* axis coincident with Earth's polar axis. The *i*-frame is a reference frame in which Newton's Laws of Motion are valid, so it is essential to an INS that the inertial motions are defined and sensed relative to this frame.

4.1.3. Earth Frame

The Earth frame (*e*-frame), or the Earth-centred Earth-fixed (ECEF) frame, is a global coordinate frame centred to Earth and employed for near-Earth applications. Figure 4.1 illustrates the axis definition of the *e*-frame relative to the Earth model. The *z* axis (Z_e) is coincident with the polar axis and is positive in the direction of the North Pole; the *x* axis (X_e) intersects at the Greenwich meridian and the equatorial plane; and the *y* axis (Y_e) is defined in the equatorial plane and orthogonal to the *x*-*z* plane.

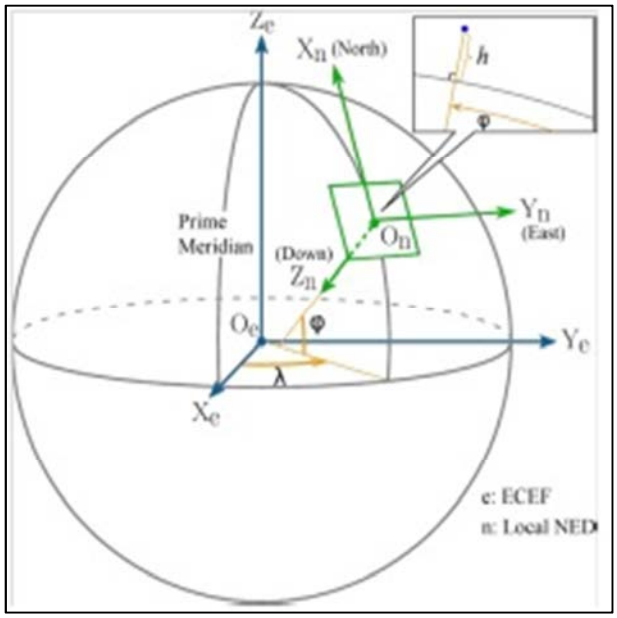

Figure 4.1: ECEF and local-level NED coordinate systems (Cai et al., 2011)

4.1.4. Navigation Frame

The navigation frame (*n*-frame), or the local-level frame, is a local geographic coordinate frame centred to the body position relative to Earth's surface. For north-east-down (NED) axes implementation, the *x*-*y* plane is tangent to the ellipsoidal surface of the Earth model with the *x* axis (X_n) and *y* axis (Y_n) pointing to the north and east directions respectively, while the *z* axis (Z_n) is normal to the ellipsoidal surface and points downward as shown in Figure 4.1. In this frame, the position is usually expressed in curvilinear coordinates (latitude, longitude and height) relative to an Earth model.

4.1.5. Relationships between Coordinate Frames

An INS usually represents the navigation results relative to the *e*-frame or the *n*-frame for land-based applications. The navigation results, such as position, velocity and attitude, describe the transformation of the body frame relative to a reference frame at a given epoch. The relationship between the *b*-frame and the reference frame is established through initialisation process and is maintained by the inertial motion sensed in the *b*-frame relative to the stationary *i*-frame that constituting the foundation of inertial navigation.

The *e*-frame is a non-stationary frame describing the physical Earth, which rotates at a constant rotation rate about the *z* axis relative to the inertial frame. The relationship between the *e*-frame and the *i*-frame can be described by a transformation given in eqn. 4.1 (Noureldin et al., 2013). Accordingly, the mechanisation equations of INS in the *e*-frame involves a compensation of Earth rotation rate between the *e*-frame and the *i*-frame.

$$\mathbf{C}_i^e = \begin{bmatrix} \cos\omega_{ie}\Delta T & \sin\omega_{ie}\Delta T & 0 \\ -\sin\omega_{ie}\Delta T & \cos\omega_{ie}\Delta T & 0 \\ 0 & 0 & 1 \end{bmatrix} \tag{4.1}$$

where $\mathbf{C}_i^e$ is the transformation from the *i*-frame to the *e*-frame; ω_{ie} is the Earth rotation rate; ΔT is the time difference from the initial epoch when the *e*-frame aligns with the *i*-frame.

Since the *n*-frame is locally defined by the global position which is referenced to the *e*-frame, the transformation between the *e*-frame and the *n*-frame (eqn. 4.2) can be established by a series of transformation with latitude and longitude through the relationship illustrated in Figure 4.1.

$$\begin{aligned} \mathbf{C}_e^n &= \begin{bmatrix} -\sin\varphi & 0 & \cos\varphi \\ 0 & 1 & 0 \\ -\cos\varphi & 0 & -\sin\varphi \end{bmatrix} \begin{bmatrix} \cos\lambda & \sin\lambda & 0 \\ -\sin\lambda & \cos\lambda & 0 \\ 0 & 0 & 1 \end{bmatrix} \\ &= \begin{bmatrix} -\sin\varphi\cos\lambda & -\sin\varphi\sin\lambda & \cos\varphi \\ -\sin\lambda & \cos\lambda & 0 \\ -\cos\varphi\cos\lambda & -\cos\varphi\sin\lambda & -\sin\varphi \end{bmatrix} \end{aligned} \tag{4.2}$$

where $\mathbf{C}_e^n$ is the transformation from the *e*-frame to the *n*-frame; φ and λ are the latitude and longitude respectively.

The mechanisation of INS in the *n*-frame therefore involves a further compensation of a turn rate (or transport rate) of the *n*-frame relative to the *e*-frame. The turn rate is governed by the change in global position as derived in eqn. 4.3.

$$\begin{aligned} \boldsymbol{\omega}_{en}^n &= \begin{bmatrix} \dfrac{v_e}{R_N + h} & -\dfrac{v_n}{R_M + h} & -\dfrac{v_e}{(R_N + h)\cos\varphi}\sin\varphi \end{bmatrix} \\ &= [\dot{\lambda}\cos\varphi \quad -\dot{\varphi} \quad -\dot{\lambda}\sin\varphi] \end{aligned} \tag{4.3}$$

where $\boldsymbol{\omega}_{en}^n$ is the turn rate of the *n*-frame relative to the *e*-frame, which is represented in the *n*-frame; v_n and v_e are the Earth-relative velocity in north and east directions respectively; R_M and R_N are the radii of curvature in the direction of meridian and

prime vertical respectively Grewal et al. (2007); h is the height; $\dot{\varphi} = \frac{v_n}{R_M+h}$ and $\dot{\lambda} = \frac{v_e}{(R_N+h)\cos\varphi}$ are the rate of changes in latitude and longitude respectively.

An INS is usually mechanised in the *n*-frame because this coordinate frame provides resolving axes in horizontal and vertical for more convenient representation and interaction. However, it is well-known that a singularity problem exists for near-pole navigation. An alternative coordinate frame, the Wander-Azimuth frame, is broadly suggested for resolving the heading from the navigation frame with an additional Wander angle to maintain the computation stability (Titterton and Weston, 2004; Bekir, 2007; Groves, 2008).

4.2. Mathematical Preliminaries

The convention of mathematical equations and symbols involved throughout this thesis are summarised in this section, which aims at enhancing the readability and understanding of corresponding mathematical representations.

4.2.1. General Transformation and its Representation

In this thesis, the angular relationship between two coordinate frames is represented by a rotation matrix $\mathbf{C}_p^q$ which indicates a transformation from the *p*-frame to the *q*-frame. For three-dimensional space, the rotation matrix comprises three rotations with respect to the three orthogonal axes (*x*, *y* and *z* axes) which can be multiplied in different sequences.

The convention of Euler rotation sequence *x*-*y*-*z* is accepted for the computation in this thesis. The formulation of a transformation matrix from the *b*-frame to the *n*-frame is illustrated in eqn. 4.4 which is derived for the *n*-frame *n*-*e*-*d* axes corresponding to the *b*-frame *x*-*y*-*z* axes (or *r*-*p*-*h* axes).

$$\mathbf{C}_b^n = \begin{bmatrix} \cos\psi & -\sin\psi & 0 \\ \sin\psi & \cos\psi & 0 \\ 0 & 0 & 1 \end{bmatrix} \begin{bmatrix} \cos\theta & 0 & \sin\theta \\ 0 & 1 & 0 \\ -\sin\theta & 0 & \cos\theta \end{bmatrix} \begin{bmatrix} 1 & 0 & 0 \\ 0 & \cos\phi & -\sin\phi \\ 0 & \sin\phi & \cos\phi \end{bmatrix}$$
$$= \begin{bmatrix} \cos\theta\cos\psi & -\cos\phi\sin\psi + \sin\phi\sin\theta\cos\psi & \sin\phi\sin\psi + \cos\phi\sin\theta\cos \\ \cos\theta\sin\psi & \cos\phi\cos\psi + \sin\phi\sin\theta\sin\psi & -\sin\phi\cos\psi + \cos\phi\sin\theta\sin \\ -\sin\theta & \sin\phi\cos\theta & \cos\phi\cos\theta \end{bmatrix} \quad (4.4)$$

where $\mathbf{C}_b^n$ is a direction cosine matrix (DCM) regarding the transformation from the *b*-frame to the *n*-frame; ϕ, θ and ψ are the Euler rotation angles roll, pitch and heading respectively. For small rotation angles, the DCM can be reduced to the form of eqn. 4.5 through the approximations of sine and cosine functions.

$$\begin{aligned} \mathbf{C}_b^n &\approx \begin{bmatrix} 1 & -\psi & \theta \\ \psi & 1 & -\phi \\ -\theta & \phi & 1 \end{bmatrix} \\ &= \begin{bmatrix} 1 & 0 & 0 \\ 0 & 1 & 0 \\ 0 & 0 & 1 \end{bmatrix} - \begin{bmatrix} 0 & \psi & -\theta \\ -\psi & 0 & \phi \\ \theta & -\phi & 0 \end{bmatrix} \\ &= \mathbf{I} - \mathbf{\Psi} \end{aligned} \quad (4.5)$$

where $\mathbf{\Psi}$ is the skew-symmetric matrix for small Euler angles $-\phi$, $-\theta$ and $-\psi$. In addition, it indicates that the order of rotation can be neglected for small angle approximation, which is a valid assumption for the implementation of inertial navigation due to high update rates.

The rotation matrix can be parameterised by different methods, including DCM, quaternion, rotation vector and Euler angles which involves corresponding problems (Titterton and Weston, 2004; Bekir, 2007; Grewal et al., 2007; Farrell, 2008; Noureldin et al., 2013). Although the quaternion method is generally considered as the most effective way for parameterisation and integration of rotation matrices, the attitude representation and relevant equations are expressed with the form of DCM to maintain the overall readability.

4.2.2. Curvilinear Transformation

The *n*-frame mechanisation of an INS usually represents the position in curvilinear coordinates (latitude, longitude and height), while the changes in position, velocity and attitude are expressed with respect to, for example, *n-e-d* axes. Accordingly, a transformation, which is illustrated in eqn. 4.6, is required to convert linear values, such as displacement and velocity, into a curvilinear coordinate system for position integration.

$$\mathbf{D} = \begin{bmatrix} \frac{1}{R_M + h} & 0 & 0 \\ 0 & \frac{1}{(R_N + h)\cos\varphi} & 0 \\ 0 & 0 & -1 \end{bmatrix} \tag{4.6}$$

where **D** is the transformation of the linear magnitude from *n-e-d* resolving axes to the curvilinear magnitude.

4.2.3. Gravity Model

The navigation solution of an INS is primarily maintained by the linear displacement and angular rotation integrated from the inertial acceleration and angular velocity respectively. The accelerometers, however, also sense Earth's gravity acceleration, which requires appropriate gravity compensation. In this thesis, a World Geodetic System (WGS) 84 ellipsoidal gravity model, which is known as the Somigliana model (Groves, 2013), is applied to estimate the normal gravity acceleration at given latitude and height (eqn. 4.7).

$$g_0 = g_e \left[\frac{1 + k \sin^2 \varphi}{\sqrt{1 - e^2 \sin^2 \varphi}} \right] \tag{4.7}$$

where g_0 is the normal gravity acceleration; $g_e = 9.7803253359\ \mathrm{ms}^{-2}$ is the normal gravity constant; $k = 0.001931853$ is a formula constant; e is the eccentricity of the Earth model. The normal gravity acceleration, which is modelled at the ellipsoidal surface, is further corrected with the height through eqn. 4.8 (Groves, 2013):

$$g = g_0 \left\{ 1 - \frac{2}{R_0} \left[1 + f(1 - 2\sin^2 \varphi) + \frac{\omega_{ie}^2 R_0^2 R_1}{\mu} \right] h + \frac{3}{R_0^2} h^2 \right\} \tag{4.8}$$

where g is the magnitude of gravity acceleration; R_0 and R_1 are the semi-major and semi-minor axes of the Earth model; $\mu = 3.98604418 \times 10^{14} m^3 s^{-2}$ is Earth's gravitational constant.

4.2.4. Specific Notations

For the mechanisation of an INS, the relationships, such as acceleration and rotation, of one frame relative to another frame require appropriate representation. For example, the angular velocity $\boldsymbol{\omega}_{ib}^{e}$, describes the rate of rotation of the *b*-frame relative to the *i*-frame, which is expressed in the *e*-frame. In addition, the skew-symmetric representation of $\boldsymbol{\omega}_{ib}^{e}$ is given by $\boldsymbol{\Omega}_{ib}^{e}$.

The vector of angular velocity can be transformed from one frame to another frame by multiplying a corresponding rotation matrix to the vector. Eqn. 4.9 illustrated a transformation of $\boldsymbol{\omega}_{ib}^{e}$ from the Earth frame to the navigation frame, while the transformation for the skew-symmetric form of the vector is given in Eqn. 4.10.

$$\boldsymbol{\omega}_{ib}^{n} = \mathbf{C}_{e}^{n} \boldsymbol{\omega}_{ib}^{e} \tag{4.9}$$

$$\boldsymbol{\Omega}_{ib}^{n} = \mathbf{C}_{e}^{n} \boldsymbol{\Omega}_{ib}^{e} \mathbf{C}_{n}^{e} \tag{4.10}$$

The convention of notation (subscript and superscript) is also applied to the representation of accelerometer measurement $\mathbf{f}_{ib}^{b}$ that describes the acceleration of the b-frame relative to the i-frame which expressed in the b-frame.

4.2.5. General Notations for Vectors and Matrices

In this thesis, a vector, such as position, velocity and gravity, is generally depicted in bold lowercase letter, while a matrix is represented by bold uppercase letter. Any superscript indicates the coordinate frame in which the vector is given.

For simplicity, specific meanings are represented by assigning relevant accents or symbols to the vectors or matrices. For examples, $\dot{\boldsymbol{x}}$, $\delta\boldsymbol{x}$, $\tilde{\boldsymbol{x}}$, and $\hat{\boldsymbol{x}}$ are generally referred to the time derivative, error, measurement, and estimate of $\boldsymbol{x}$ respectively, while other accents or symbols are involved if necessary. In addition, the subscript of a symbol is retained for specific purposes with individual explanations.

4.3. Overview of Rail-bound Navigation

In railway environment, TAP is suggested in this thesis to directly replace the role of GNSS with the track constraints. Through the INS/TAP integration, the RBN solution is established to measure the train dynamics and overcome the problems of navigation uncertainties by alternative measures. To facilitate RBN development, the measures to potential error control problems are firstly summarised in this section.

4.3.1. INS/TAP Integration

To retain the system generality, the typical navigation system and error models are adopted for the mechanisation of INS in this thesis (refers to Appendix 1). The INS/TAP integration is initially established by an EKF through a loosely coupled configuration. Figure 4.2 illustrates the structure of INS/TAP integration that the INS

and TAP are processed in series through the chainage updates. Both the INS and TAP navigation results are passed to the filter to estimate the navigation and sensor errors which then feedback to the INS.

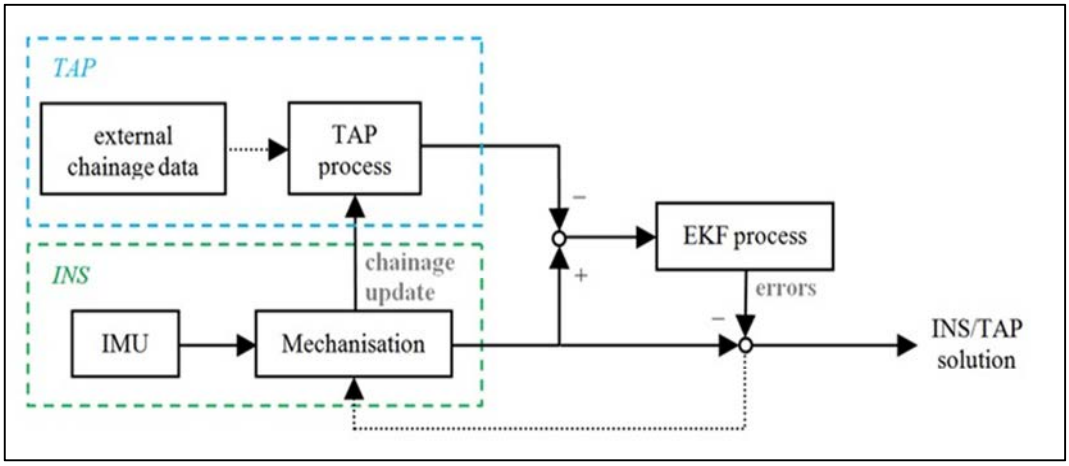

Figure 4.2: INS/TAP integration through an extended Kalman filter

The loosely coupled configuration is suggested to simplify the relationship between INS and TAP processes, which provides a practical solution to analyse the overall performance and discover any potential problem. In addition, the loosely coupled configuration also facilitate further development by maintaining the individual integrity of both the INS and TAP components. Tightly coupled configuration is therefore not recommended in this thesis.

4.3.2. Rail-bound Navigation Structure

The RBN solution is the implementation of a navigation system established from the fundamental INS/TAP integration, which consists of a series of error control in addition to the INS/TAP integration. This solution is primarily designed for maximising the ability of an INS with loosened hardware requirements. Additional measures are involved to resolve the practical issues and develop towards a comprehensive solution.

For a typical POS, the inertial sensors and GNSS receivers are installed at a rigid body that the lever-arm is considered constant. In contrast, the train body where the inertial sensors are attached at undergoes independent motion with the track reference through the flexible bogies. Consequently, the lever-arm and boresight misalignment between the INS and TAP results are not defined as constant. Alternative measures are necessary to further compensate and control the excessive discrepancies. In addition, the RBN solution requires further integration with the railway system. The relevant issues, including system initialisation and its transition, chainage maintenance, navigation error control and feedback, and system misalignment control, are individually discussed in later sections.

Figure 4.3 illustrates an overview of RBN structure, which is modified from the preliminary configuration introduced by Hung et al. (2016). The system is initialised by an external chainage or position of reference. While the nominal position and attitude are determined through the TAP solution, the system roll and pitch are estimated by inertial measurements. The position, velocity, attitude and misalignment between the system body and track reference, are then initialised.

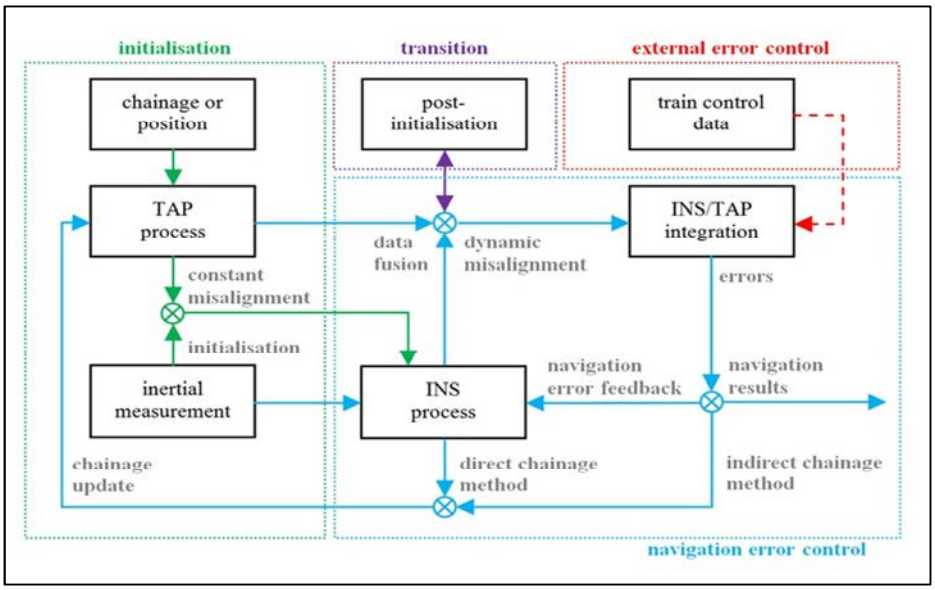

Figure 4.3: An overview of rail-bound navigation structure

While the navigation system is maintained by high rate INS process, the chainage is propagated at a lower rate through direct or indirect methods which are discussed in section 4.5. In the meanwhile, the system is undergoing a transition phase, which requires a post-initialisation (fine alignment) for the refinement of constant misalignment.

The RBN solution is basically a self-contained navigation solution that the navigation errors are continuously constrained by the TAP results. In addition, it is capable of utilising available sources of data, such as train control data, mapping data or interactive operational records for future development.

4.4. Rail-bound Navigation Initialisation

Through the TAP results, the initial position, velocity of navigation system can be directly determined from the chainage of reference, while the system alignment is performed by the accelerometer measurements. The constant misalignment between the TAP derived train attitudes and the INS derived system attitudes are also determined during the initialisation phase.

4.4.1. Position and Velocity Initialisation

The initial position of the system body can be estimated by the linear displacement relative to the track alignment reference, which is expressed in eqn. 4.11.

$$\mathbf{r}_b^n = \mathbf{r}_a^n + \mathbf{DC}_a^n \mathbf{r}_{ab}^a \tag{4.11}$$

where $\mathbf{r}_b^n$ is the position of the *b*-frame origin expressed in the *n*-frame; $\mathbf{r}_a^n$ is the TAP derived position of track reference in the *n*-frame; $\mathbf{C}_a^n$ is the TAP derived transformation from the *a*-frame to the *n*-frame, which is determined with the

reference chainage; $\mathbf{r}_{ab}^{a}$ is the constant displacement of the *b*-frame relative to the *a*-frame origin (the front bogie).

For stationary initialisation, the initial velocity is simply zero in all axes. In case that the stationary initialisation period is insufficient, the system velocity errors, as well as position errors, would grow rapidly because of the poor system alignment. Regarding the rail-bound nature, any external speed data measured in the track direction can be applied for non-stationary velocity initialisation (eqn. 4.12).

$$\hat{\mathbf{v}}_{eb}^{n} = \mathbf{C}_{a}^{n}\hat{\mathbf{v}}_{eb}^{a} \tag{4.12}$$

where $\hat{\mathbf{v}}_{eb}^{a} = [\hat{v}_x \quad 0 \quad 0]^T$ is the Earth-relative velocity defined in the *a*-frame; $\hat{v}_x$ is the one-dimensional velocity measured in the direction of track body.

4.4.2. Track-to-Train Transition

For the system alignment process, the roll and pitch angles are estimated through the self-levelling method, while the heading is approximated from the TAP derived track heading. However, the track heading and the train heading are slightly different on account of the track curvature and the rigidity of train car, which is simplified and illustrated in Figure 4.4.

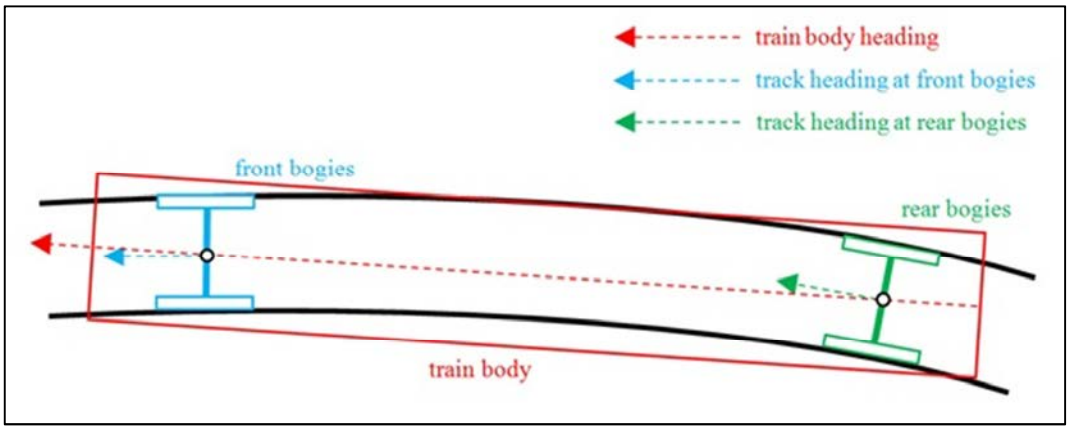

Figure 4.4: Heading difference between train body and track

The train heading, and also the roll and pitch angles, are generally bounded by the track attitudes derived at the front and rear bogies, which introduce additional transition effects to the train attitudes. Regarding the rail track linearity, the nominal train attitudes can be simply estimated from the average of the front and rear TAP results with negligible effect. From the reference chainage of the front bogies, the chainage at rear bogies can be approximated through eqn. 4.13.

$$\begin{aligned} L_r &\approx L_f - \frac{1}{2}\left(2R_f \sin^{-1}\frac{\Delta s}{2R_f} + 2R_r \sin^{-1}\frac{\Delta s}{2R_r}\right) \\ &= L_f - R_f \sin^{-1}\frac{\Delta s}{2R_f} - R_r \sin^{-1}\frac{\Delta s}{2R_r} \end{aligned} \tag{4.13}$$

where L_r and L_f are the chainage at rear and front bogies respectively; R_r and R_f are the radii of curvature estimated at rear and front bogies; and Δs is the constant separation between front and rear reference bogies.

In eqn. 4.13, the chainage difference is approximated by the nature of circular curve. As the distance between bogies is sufficiently short with respect to the radii of the curve, the difference between spiral curve and circular curve is assumed negligible. Therefore, the chainage difference can be computed on a circular curve, which is estimated by the average with the radii at the front and rear bogies. In railway environment, the general curve radius exceeds $300m$ for safety issues such that the estimated correction to bogie separation is only millimetre-level at a bogie separation of $15m$. As a result, the approximation of rear bogie chainage is sufficiently accurate.

4.4.3. Train-to-Body Misalignment

Through the estimated chainages at the front and rear reference bogies, the train attitudes can be determined from the TAP results. The attitude differences between the estimated train body (without dynamic motion) and the system body are

described by a misalignment term. Additional error terms are introduced to the transformation as illustrated in eqn. 4.14.

$$\begin{aligned} \mathbf{C}_b^n &= \mathbf{C}_t^n \mathbf{C}_a^t \mathbf{C}_b^a \\ \delta\hat{\mathbf{C}}_n^n \hat{\mathbf{C}}_b^n &= \mathbf{C}_a^n \hat{\mathbf{C}}_b^a \delta\hat{\mathbf{C}}_b^b \end{aligned} \tag{4.14}$$

where $\delta\hat{\mathbf{C}}_n^n$ is the attitude errors associating with $\hat{\mathbf{C}}_b^n$ which is estimated from an INS; $\delta\hat{\mathbf{C}}_b^b$ is the misalignment matrix (or the dynamic misalignment matrix) associating with $\hat{\mathbf{C}}_b^a$ which is estimated from INS/TAP integration. To determine the constant misalignment, eqn. 4.14 is rearranged into eqn. 4.15, while the dynamic misalignment term is dropped for the stationary initialisation.

$$\begin{aligned} \hat{\mathbf{C}}_b^a &\approx \mathbf{C}_t^a \mathbf{C}_n^t \delta\hat{\mathbf{C}}_n^n \hat{\mathbf{C}}_b^n \\ &= \mathbf{C}_n^a \delta\hat{\mathbf{C}}_n^n \hat{\mathbf{C}}_b^n \end{aligned} \tag{4.15}$$

It presumes that the *b*-frame heading is aligned with the *t*-frame or *a*-frame heading. An additional heading misalignment is introduced and remains unsolved in the term $\delta\hat{\mathbf{C}}_b^b$ which is dropped in the stationary initialisation process. The heading misalignment is further estimated and compensated by further processes.

4.5. RBN Chainage Updates

Through the stationary initialisation, the train localisation is maintained by relevant chainage updating methods. In Chapter 3, a Kalman filter solution is suggested to model the one-dimensional train motion, which requires external data such as chainage or speed for navigation updates. For RBN, the chainage can be internally maintained by the INS, which are generalised into direct and indirect methods.

4.5.1. Direct Chainage Integration

Since the navigation system is mechanised in the *n*-frame, the horizontal displacement is resolved from the navigation results at high-rate. Therefore, the chainage can be directly integrated from the INS navigation results (eqn. 4.16).

$$L(t_1) \quad = L(t_0) + \sqrt{\Delta\hat{N}^2 + \Delta\hat{E}^2} \tag{4.16}$$

where $L(t_1)$ and $L(t_0)$ are the horizontal chainages at time t_1 and t_0 respectively; $\Delta\hat{N}$ and $\Delta\hat{E}$ are the estimated horizontal displacement in northing and easting directions, which are estimated by the INS. The relevant error equation is linearised and represented in eqn. 4.17, which provides a measure for chainage error propagation through the INS process noise.

$$\delta L(t_1) \quad = \begin{bmatrix} \dfrac{\Delta\hat{N}}{\sqrt{\Delta\hat{N}^2 + \Delta\hat{E}^2}} & \dfrac{\Delta\hat{E}}{\sqrt{\Delta\hat{N}^2 + \Delta\hat{E}^2}} & 1 \end{bmatrix} \begin{bmatrix} \delta\Delta\hat{N} \\ \delta\Delta\hat{E} \\ \delta L(t_0) \end{bmatrix} \tag{4.17}$$

The direct chainage integration is derived from the INS process such that the covariance of $\Delta\hat{N}$ and $\Delta\hat{E}$ can be determined and transformed from the process noise covariance of the INS. For the implementation at lower rates, such as $10Hz$ or lower, the chainage increment can be estimated from the summation of displacement over a period of time as illustrated in eqn. 4.18.

$$\begin{aligned} L(t_k) \quad &= L(t_0) + \sqrt{\left[\sum_{\tau=1}^{k} \Delta\hat{N}(t_\tau)\right]^2 + \left[\sum_{\tau=1}^{k} \Delta\hat{E}(t_\tau)\right]^2} \\ &= L(t_0) + \sqrt{\Delta\bar{N}^2 + \Delta\bar{E}^2} \end{aligned} \tag{4.18}$$

where $\Delta\widehat{N}(t_\tau)$ and $\Delta\widehat{E}(t_\tau)$ are the horizontal displacement in northing and easting directions at time t_τ; $\Delta\overline{N}$ and $\Delta\overline{E}$ are the summation of horizontal displacement in north and east directions.

4.5.2. Indirect Chainage Estimation

An alternative chainage estimation is indirectly acquired through the TAP solution, which can be performed at a relatively lower rate (e.g. $2Hz$). By neglecting the change of heading at the chainage update rate, the current TAP results, including the chainage, position and attitude, are initially employed to resolve the position difference into chainage difference at the track direction (eqn. 4.19).

$$L(t_1) \quad = L_0 + [\cos\psi_0 \quad \sin\psi_0]\begin{bmatrix}\widehat{N} - N_0\\ \widehat{E} - E_0\end{bmatrix} \tag{4.19}$$

where N_0, E_0 and ψ_0 are the initial horizontal grid coordinates and track heading derived from TAP solution with initial chainage L_0; $\widehat{N}$ and $\widehat{E}$ are the horizontal grid coordinates estimated from the INS. Regarding the misalignment error, the term ψ_0 is alternatively replaced by the INS derived heading $\hat{\psi}$ through the condition $\mathbf{C}_n^t = (\mathbf{C}_b^n\mathbf{C}_a^b\mathbf{C}_t^a)^T$, which involves the covariance of the misalignment error. The corresponding error equation for indirect chainage estimation is derived and summarised in eqn. 4.20.

$$\delta L_t \quad = [\cos\hat{\psi} \quad \sin\hat{\psi} \quad \Delta E\cos\hat{\psi} - \Delta N\sin\hat{\psi}]\begin{bmatrix}\delta\widehat{N}\\ \delta\widehat{E}\\ \delta\hat{\psi}\end{bmatrix} \tag{4.20}$$

where $\Delta N = \widehat{N} - N_0$ and $\Delta E = \widehat{E} - E_0$ are the grid coordinate differences.

The current chainage is updated for computing the track position and heading through the TAP solution. To minimise the approximation errors, an iterative process can be performed for low rate implementation as illustrated in Figure 4.5.

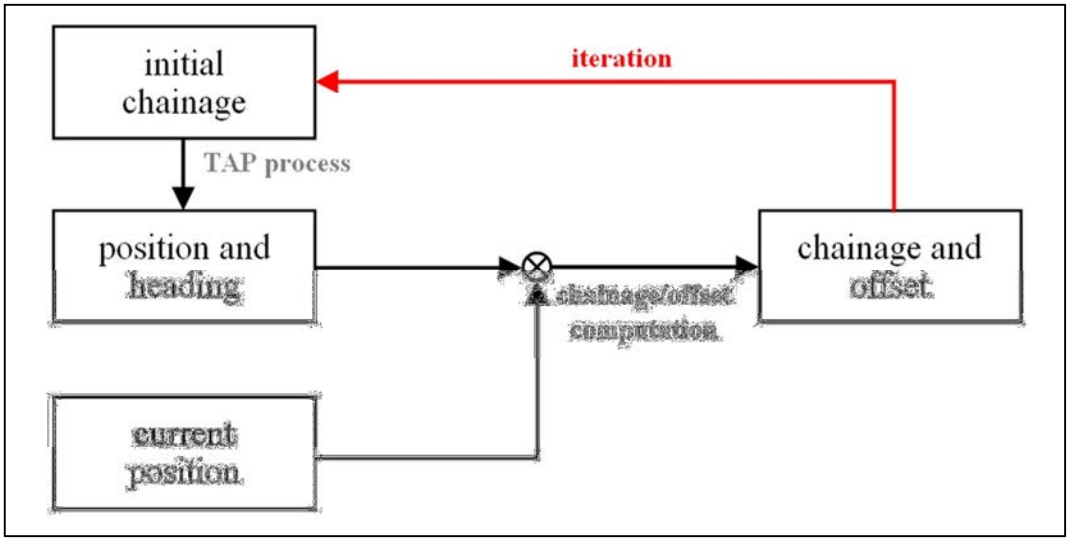

Figure 4.5: Indirect chainage estimation procedures

4.5.3. Potential Chainage Errors

Since the TAP results are determined from the chainage, accurate chainage estimation is important to the RBN error control process. The direct and indirect chainage estimation methods, however, introduce relevant problems to their practical performance.

The direct method is independent of the track alignment, which is applicable to large heading errors. The integrated chainage, however, is generally overestimated on account of the uncompensated lateral train motion. In contrast, the indirect method resolves the train displacement into longitudinal and lateral components with respect to the track alignment. The chainage is theoretically accurate for small heading misalignment, which would be underestimated regarding an inaccurate projection of horizontal displacement onto the track alignment for large heading error.

Since the direct and indirect methods are considered to be complementary, they can be integrated with the Kalman filter solution for chainage updates through appropriate weight control. The practical accuracy of chainage estimation, however, requires further optimisation such as relative weight control and heading misalignment correction.

4.6. Fine Alignment for Rail-bound Navigation

Following the stationary initialisation, the misalignment between TAP derived train heading and system heading is neglected, such that the integrated INS/TAP relationship is not completely established. Consequently, the fine alignment process is required to update the constant misalignment and accomplish full system initialisation.

4.6.1. Constant Misalignment Approximation

Since an extended Kalman filter is employed for the data fusion of the RBN implementation, the navigation errors are estimated from the differences between INS and TAP results through the correlation established from the system and stochastic model. The impact of undetermined heading error can be minimised by an additional heading uncertainty through the initial system and measurement covariance.

Through the filtering process, the attitude correction is estimated from the integrated INS/TAP solution. The heading correction to the *b*-frame is resolved into the constant misalignment term by eqn. 4.5, while the dynamic misalignment is neglected until the fine alignment process is terminated.

4.6.2. Chainage Error Control

During the fine alignment phase, the heading error is progressively compensated through the filtering process, which is primarily determined from the correlation established in the system model. The accuracy of chainage is therefore essential to sustain the correctness of navigation updates.

In section 4.5, the direct and indirect methods are suggested for the chainage maintenance, which are considered to be complementary in nature. Accordingly, both methods can be integrated through the Kalman filter solution and compensated for their corresponding problems. Eqn. 4.21 illustrates a measurement model for chainage updates with multiple sources of chainage data.

$$\mathbf{z}_L = \begin{bmatrix} -1 & 0 & 0 \\ \vdots & \vdots & \vdots \\ -1 & 0 & 0 \end{bmatrix} \begin{bmatrix} p \\ v \\ a \end{bmatrix} + \mathbf{v}_L \tag{4.21}$$

where $\mathbf{z}_L = \begin{bmatrix} \hat{L}_1 - p \\ \vdots \\ \hat{L}_n - p \end{bmatrix}$ is the innovation of chainage measurement; $\hat{L}_i$ is the input corresponding to the estimated chainage for source $i = 1,2, \dots, n$; $\mathbf{v}_L$ is a $n \times 1$ vector of residuals with respect to L_i ; $\mathbf{C}_L = \begin{bmatrix} \sigma_1^2 & \cdots & 0 \\ \vdots & \ddots & \vdots \\ 0 & \cdots & \sigma_n^2 \end{bmatrix}$ is the covariance matrix describing the measurement noises.

For the purposes of concept validation, it is assumed that the direct method is sufficiently accurate during the fine alignment phase. In contrast, the indirect method is not beneficial to the chainage estimation when the heading error is unknown. Therefore, the indirect method is removed during the fine alignment phase.

4.6.3. Adaptive Covariance Estimation

The measurement updates of filtering process require appropriate estimation of process and measurement covariance. While the TAP derived results are partially dependent on the navigation system, the covariance estimation for position is invalid before finalising the heading misalignment estimation. The Innovation-based Adaptive Estimation (IAE) can be applied for alternative noise estimation through the innovation statistics (Groves, 2008). The innovation covariance can be estimated from the moving average of innovation of residual sequence (Almagbile et al., 2010) shown in eqn. 4.22. The TAP noise can then be derived from eqn. 4.23 with the estimated innovation covariance.

$$\mathbf{C}_{\delta\mathbf{z}} = \frac{1}{n}\sum_{k=1}^{n} \delta\mathbf{z}_k \delta\mathbf{z}_k^T \tag{4.22}$$

where $\mathbf{C}_{\delta\mathbf{z}}$ is the innovation covariance; n is the number of data; $\delta\mathbf{z}_k$ is the innovation at given epoch k.

$$\mathbf{R} = \mathbf{C}_{\delta\mathbf{z}} - \mathbf{H}\mathbf{P}_x\mathbf{H}^T \tag{4.23}$$

where $\mathbf{R}$ is the TAP estimated covariance; $\mathbf{H}$ is the design matrix; $\mathbf{P}_x$ is the propagated state covariance.

4.6.4. Transition of Fine Alignment Phase

The transition of the fine alignment phase is determined by the condition of INS/TAP convergence with bounded navigation errors. Prior to the convergence, the INS and TAP are incorrectly integrated on account of the heading and chainage errors. Therefore, the transition of the fine alignment phase can be denoted by passing a hypothesis test with Student's *t* distribution at a given confidence level α. The

observed testing value is computed from eqn. 4.24. Given the conditions, H_0: the navigation parameter is consistent with the TAP estimated precision, against H_1: the navigation parameter is not consistent with the TAP estimated precision.

$$T = \frac{\delta\bar{\mathbf{z}}}{\sigma/\sqrt{n}} \tag{4.24}$$

where T is the observed value for Student's t test; $\delta\bar{\mathbf{z}} = \frac{1}{n}\sum_{k=1}^{n}\delta\mathbf{z}_k$ is the sampling innovation/residual; σ is the TAP derived standard deviation.

In case of poorly initialised INS/TAP condition, the sampling innovation/residual would be significantly larger than the expected standard deviation, which rejects the null hypothesis in favour of the alternative. If the sampling innovation/residual is consistent with the TAP-estimated precision, the observed testing value would fall out the critical region defined by the relevant test statistic value. Consequently, the initialisation process is considered to be completed.

It is expected that the sampling residuals would converge to a certain level after a period of time, while the TAP estimated covariance would progressively increase as shown in Figure 4.6.

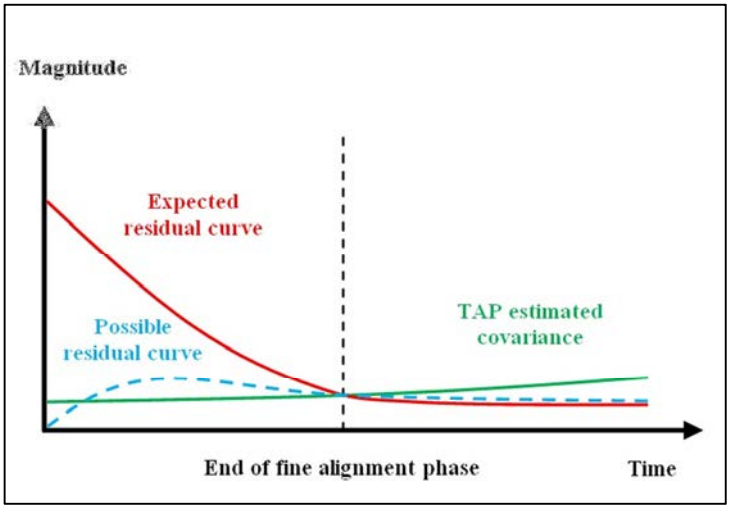

Figure 4.6: Expected characteristics of initial residual and covariance

While a large initial sampling residual is expected, the TAP estimated precision should be high enough to fail the null hypothesis. However, the actual results may not follow the expected outcome if the misalignment is not sufficiently large. In addition, the changes of position and attitude, as well as the magnitude of sampling residuals, would be small at low speed. It is highly possible that the fine alignment phase is immediately terminated at the beginning of the fine alignment phase. In addition, the actual curve of initial residuals may differ from the expectation, such that the hypothesis test is not always feasible. Alternatively, the transition of the fine alignment phase can be determined by a threshold of time, which is more practicable and reliable.

4.7. Navigation Error Control

After the system initialisation, the system navigation is primarily maintained by the INS process. To constrain the growth of navigation errors, the navigation error control is performed at a low rate (e.g. $2Hz$), which is implemented by the measurement updates of Kalman filtering process. The measurement updates, including the coordinate updates, velocity updates and attitude updates, can be merely executed with the TAP results.

4.7.1. Coordinate Updates

The CUPT method is the fundamental solution to integrate the INS and TAP results. The relevant equation of position error is summarised in eqn. 4.25, which represents the innovation of the corresponding measurement model. The corresponding covariance of TAP estimated position is elaborated in eqn. 4.26 by assuming the error sources are independent.

$$\delta \boldsymbol{z}_{\mathrm{r}} = \mathbf{r}_a^n + \mathbf{DC}_a^n \mathbf{r}_{ab}^a - \hat{\mathbf{r}}_b^n$$

$$
\begin{aligned}
&\approx \mathbf{r}_a^n + \mathbf{D}\mathbf{C}_b^n\left(\hat{\mathbf{C}}_b^a \delta\hat{\mathbf{C}}_b^b\right)^T \mathbf{r}_{ab}^a - \hat{\mathbf{r}}_b^n \\
&= \mathbf{r}_a^n + \mathbf{D}\mathbf{C}_b^n \delta\hat{\mathbf{C}}_b^{b\,T} \hat{\mathbf{C}}_a^b \mathbf{r}_{ab}^a - \hat{\mathbf{r}}_b^n
\end{aligned} \tag{4.25}
$$

where $\delta \boldsymbol{z}_{\mathrm{r}}$ is the innovation of position error; $\hat{\mathbf{r}}_{ab}^a$ and $\delta\hat{\mathbf{r}}_{ab}^a$ are the estimated positional offset of the *b*-frame relative to the *a*-frame and its errors respectively.

$$
\begin{aligned}
\mathbf{r}_{\mathrm{TAP}} &= \mathbf{r}_a^n + \mathbf{D}\mathbf{C}_b^n \delta\hat{\mathbf{C}}_b^{b\,T} \hat{\mathbf{C}}_a^b \mathbf{r}_{ab}^a \\
\delta\mathbf{r}_{\mathrm{TAP}} &= \mathbf{D}\delta\mathbf{r}_a^n + \mathbf{D}\mathbf{C}_b^n \left[\hat{\mathbf{C}}_a^b \mathbf{r}_{ab}^a\right]_\times \delta\Delta_b^b + \mathbf{D}\mathbf{C}_b^n \delta\hat{\mathbf{C}}_b^{b\,T} \hat{\mathbf{C}}_a^b \delta\mathbf{r}_{ab}^b \\
&\approx \mathbf{D}\delta\mathbf{r}_a^n + \mathbf{D}\mathbf{C}_b^n \left[\mathbf{r}_{ab}^b\right]_\times \delta\Delta_b^b + \mathbf{D}\mathbf{C}_a^n \delta\mathbf{r}_{ab}^a \\
\mathbf{P}(\mathbf{r}_{\mathrm{TAP}}) &= \mathbf{D}\left[\mathbf{P}(\mathbf{r}_a^n) + \mathbf{C}_b^n \left[\mathbf{r}_{ab}^b\right]_\times \mathbf{P}(\Delta_b^b)\left(\mathbf{C}_b^n \left[\mathbf{r}_{ab}^b\right]_\times\right)^T + \mathbf{C}_a^n \mathbf{P}(\mathbf{r}_{ab}^a)\mathbf{C}_a^{n\,T}\right]\mathbf{D}^T \\
&= \mathbf{D}\left[\mathbf{P}(\mathbf{r}_a^n) + \mathbf{C}_b^n \left[\mathbf{r}_{ab}^b\right]_\times \mathbf{P}(\Delta_b^b)\left[\mathbf{r}_{ba}^b\right]_\times \mathbf{C}_n^b + \mathbf{C}_a^n \mathbf{P}(\mathbf{r}_{ab}^a)\mathbf{C}_n^a\right]\mathbf{D}
\end{aligned} \tag{4.26}
$$

where $\mathbf{r}_{\mathrm{TAP}}$ is the TAP estimated system position; $\left[\hat{\mathbf{C}}_a^b \mathbf{r}_{ab}^a\right]_\times = \left[\mathbf{r}_{ab}^b\right]_\times$ is the skew-symmetric matrix of $\mathbf{r}_{ab}^b$; Δ_b^b is the vector of dynamic misalignment; $\mathbf{P}(\cdot)$ is the covariance of corresponding elements.

4.7.2. Velocity Updates

In case that external speed, such as tachometer or train control data, is available for data fusion, VUPT can also be applied for measurement updates. The innovation of velocity error and the corresponding covariance are shown in eqn. 4.27 and eqn. 4.28 respectively.

$$
\delta\boldsymbol{z}_{\mathrm{v}} = \mathbf{C}_a^n \begin{bmatrix} \hat{v}_x \\ 0 \\ 0 \end{bmatrix} - \hat{\mathbf{v}}_{\mathrm{e}}^n \tag{4.27}
$$

where $\delta\boldsymbol{z}_{\mathrm{v}}$ is the innovation of velocity error; $\hat{v}_x$ is the speed data; $\hat{\mathbf{v}}_{\mathrm{e}}^n$ is the Earth-relative velocity predicted from the INS.

$$
\mathbf{v}_{\mathrm{REF}} = \mathbf{C}_a^n \begin{bmatrix} \hat{v}_x \\ 0 \\ 0 \end{bmatrix}
$$

$$
\begin{aligned}
&\approx \mathbf{C}_b^n \delta\hat{\mathbf{C}}_b^{b^T} \hat{\mathbf{C}}_a^b \mathbf{v}_{eb}^a \\
\delta\mathbf{v}_{\mathrm{REF}} &= \mathbf{C}_b^n \left[\hat{\mathbf{C}}_a^b \mathbf{v}_{eb}^a\right]_\times \delta\Delta_b^b + \mathbf{C}_b^n \delta\hat{\mathbf{C}}_b^{b^T} \hat{\mathbf{C}}_a^b \delta\mathbf{v}_{eb}^a \\
&\approx \mathbf{C}_b^n \left[\mathbf{v}_{eb}^b\right]_\times \delta\Delta_b^b + \mathbf{C}_a^n \delta\mathbf{v}_{eb}^a \\
\mathbf{P}(\mathbf{v}_{\mathrm{REF}}) &= \mathbf{C}_b^n \left[\mathbf{v}_{eb}^b\right]_\times \mathbf{P}(\Delta_b^b) \left(\mathbf{C}_b^n \left[\mathbf{v}_{eb}^b\right]_\times\right)^T + \mathbf{C}_a^n \mathbf{P}(\mathbf{v}_{eb}^a) \mathbf{C}_a^{n^T} \\
&= \mathbf{C}_b^n \left[\mathbf{v}_{eb}^b\right]_\times \mathbf{P}(\Delta_b^b) \left[\mathbf{v}_{be}^b\right]_\times \mathbf{C}_n^b + \mathbf{C}_a^n \mathbf{P}(\mathbf{v}_{eb}^a) \mathbf{C}_n^a
\end{aligned} \tag{4.28}
$$

where $\mathbf{v}_{\mathrm{REF}}$ is the estimated train velocity from reference data; $\mathbf{v}_{eb}^a = [\hat{v}_x \quad 0 \quad 0]^T$ is the Earth-relative velocity defined in the *a*-frame; $\left[\hat{\mathbf{C}}_a^b \mathbf{v}_{eb}^a\right]_\times = \left[\mathbf{v}_{eb}^b\right]_\times$ is the skew-symmetric matrix of $\mathbf{v}_{eb}^b$.

The RBN solution can perform an internal VUPT from the INS estimated velocity. The norm of velocity vector $\hat{v}_x = \|\hat{\mathbf{v}}_{\mathrm{e}}^n\|$ represents the train speed in three-dimensional space, while the TAP derived attitudes $\mathbf{C}_a^n$ provide a nominal constraint of rail-bound motion. It is noted that the performance of internal VUPT depends on the accuracy of roll and pitch angles so this approach may not provide sufficient improvement if the system is poorly levelled.

4.7.3. Attitude Error Control

One of the characteristics of RBN solution is that a direct attitude error control is available from the TAP results. The rail-bound nature would provide an additional constraint to the system attitude errors, as well as the accumulation of velocity and position errors, which is particularly critical to the navigation systems established by low-cost inertial sensors. The attitude errors which are elaborated in eqn. 4.14 can be rearranged as follows:

$$
\begin{aligned}
\delta\hat{\mathbf{C}}_n^n &= \mathbf{C}_t^n \mathbf{C}_a^t \mathbf{C}_b^a \delta\hat{\mathbf{C}}_b^b \hat{\mathbf{C}}_n^b \approx \mathbf{I} - \Psi_n \\
\left[\delta\mathbf{z}_\rho\right]_\times &= \Psi_n \\
&= \mathbf{I} - \delta\hat{\mathbf{C}}_n^n \\
&\approx \mathbf{I} - \mathbf{C}_a^n \hat{\mathbf{C}}_b^a \delta\hat{\mathbf{C}}_b^b \hat{\mathbf{C}}_n^b
\end{aligned} \tag{4.29}
$$

where $\left[\delta \boldsymbol{z}_{\rho}\right]_{\times}$ is the skew matrix of attitude innovation; Ψ_n is the skew matrix of attitude errors $\boldsymbol{\rho}$. The corresponding covariance of TAP estimated system attitudes is elaborated in eqn. 4.30.

$$\begin{aligned} \delta\Delta_{TAP} &\approx \delta\Delta_a^n + \mathbf{C}_a^n \hat{\mathbf{C}}_b^a \delta\Delta_b^b \\ \mathbf{P}(\Delta_{TAP}) &= \mathbf{P}(\Delta_a^n) + \mathbf{C}_a^n \hat{\mathbf{C}}_b^a \mathbf{P}\left(\Delta_b^b\right)\left(\mathbf{C}_a^n \hat{\mathbf{C}}_b^a\right)^T \\ &\approx \mathbf{P}(\Delta_a^n) + \hat{\mathbf{C}}_b^n \mathbf{P}\left(\Delta_b^b\right)\hat{\mathbf{C}}_n^b \end{aligned} \tag{4.30}$$

where Δ_{TAP} is the vector of TAP estimated attitude errors.

4.7.4. Measurement Error Models

According to Groves (2008), the coupling of attitude errors and gyroscopic biases with the measurements through the lever arm are negligible. The measurement error model of position, velocity and attitude updates is therefore simplified as in eqn. 4.31.

$$\begin{bmatrix} \delta \boldsymbol{z}_{\mathrm{r}} \\ \delta \boldsymbol{z}_{v} \\ \delta \boldsymbol{z}_{\rho} \end{bmatrix} = \begin{bmatrix} -\mathbf{I} & \mathbf{0} & \mathbf{0} & \mathbf{0} & \mathbf{0} \\ \mathbf{0} & -\mathbf{I} & \mathbf{0} & \mathbf{0} & \mathbf{0} \\ \mathbf{0} & \mathbf{0} & -\mathbf{I} & \mathbf{0} & \mathbf{0} \end{bmatrix} \begin{bmatrix} \delta \mathbf{r} \\ \delta \mathbf{v} \\ \boldsymbol{\rho} \\ \delta \mathbf{f}^b \\ \delta \boldsymbol{\omega}_{ib}^b \end{bmatrix} + \begin{bmatrix} \boldsymbol{N}_{\mathrm{r}} \\ \boldsymbol{N}_{v} \\ \boldsymbol{N}_{\rho} \end{bmatrix} \tag{4.31}$$

where $\boldsymbol{N}_r$, $\boldsymbol{N}_v$ and $\boldsymbol{N}_\rho$ are the estimated uncertainties of position, velocity, and attitude errors respectively.

The uncertainties of position, velocity and attitude errors are represented by the measurement covariance matrices elaborated in eqn. 4.26, eqn. 4.28, and eqn. 4.30 respectively. The process of measurement updates can be found in Appendix 3.

To minimise the attitude difference, the navigation system is configured with a closed-loop EKF solution where the navigation and sensor errors would feedback to the system state. The dynamic motion, however, may introduce excessive impacts to

the estimation of the sensor biases, as well as the navigation results, which require further modelling or compensation of dynamic misalignment.

4.8. Dynamic Motion Control

After the system initialisation and fine alignment, the navigation system is theoretically aligned with the track reference through the constant displacement and misalignment. The train motion, however, introduces dynamic displacement and misalignment that the overall performance may be diminished.

The dynamic displacement is defined as the position errors between INS and TAP results resolved in the *a*-frame, while the dynamic misalignment is defined as the additional rotation of the *b*-frame relative to the *a*-frame. The dynamic displacement and misalignment are rearranged in the form of eqn. 4.32.

$$\begin{bmatrix} \delta \mathbf{r}_{ab}^{a} \\ \delta \hat{\mathbf{C}}_{b}^{b} \end{bmatrix} = \begin{bmatrix} \mathbf{C}_{b}^{a} \hat{\mathbf{C}}_{n}^{b} (\mathbf{r}_{b}^{n} - \mathbf{r}_{a}^{n}) - \mathbf{r}_{ab}^{a} \\ \hat{\mathbf{C}}_{a}^{b} \mathbf{C}_{n}^{a} \hat{\mathbf{C}}_{b}^{n} \end{bmatrix} \tag{4.32}$$

The dynamic errors in addition to the constant displacement and misalignment are mainly caused by the physical train motion and vibrations, physical track defects and uncertainties, which are generally time-correlated throughout the train motion. The displacement is assumed to be zero-mean, which is primarily caused by the dynamic misalignment. To provide a position constraint, the dynamic displacement has been dropped from the position innovation as shown in eqn. 4.25, while the dynamic misalignment $\delta \hat{\mathbf{C}}_{b}^{b}$ is retained for the motion dynamics.

The dynamic misalignment control is important to minimise the attitude discrepancies between the actual motion sensed by INS and the nominal motion predicted by TAP. An over constrained solution may be resulted by ignoring the

dynamic misalignment. In contrast, the attitude error control would be ineffective if the dynamic misalignment is not compensated.

4.8.1. Moving Average/ Complementary Filter

The dynamic misalignment is assumed to gradually change with time, while the nominal magnitude can be estimated by moving average or complementary filter techniques. However, the dynamic misalignment and the attitude errors are correlated such that an additional zero-mean assumption is required for the error control.

The moving average and complementary filtering approaches are easily implemented without considering and modelling the error characteristics. The smoothened dynamic misalignment can be applied to compute the position innovation, which is removed from the attitude innovation regarding the zero-mean assumption.

4.8.2. Harmonic Oscillation Model

Since the train motion is rail-bound and smoothened by the train bogies, the dynamic motion conceptually follows a damped harmonic motion. The damped harmonic motion assumes that the change of amplitude, angular frequency, phase shift and offset are constant.

In reality, the train motion does not follow a damped harmonic motion, because external forces are continuously acting on the train. Consequently, the harmonic oscillating patterns can be described by a simple harmonic motion (SHM) within a short period of time (eqn. 4.33).

$$\hat{x} \quad = A\sin(\omega t + \Delta) + B \tag{4.33}$$

where $\hat{x}$ is the estimated magnitude; A is the amplitude; ω is the angular frequency; t is the time reference; Δ is a constant phase shift; B is a constant offset.

Through the characteristics of SHM, the dynamic misalignment can be estimated and modelled into parameters over time. Regarding the zero-mean assumption, the non-zero offset indicates the existence of biases which can be removed if necessary. The estimated dynamic misalignment can be used to compute the position and attitude innovation because the non-zero offset is removed.

4.9. Practical Issues for Implementation

In this chapter, several major issues regarding the implementation of RBN solution have been discussed on the basis of INS/TAP integration and relevant mathematical models, which are primarily developed with the theoretical considerations. In this section, the major components are reviewed and optimised with practical considerations.

4.9.1. Initial Alignment and Sensor Turn-on Biases

During the stationary initialisation, the accelerometer and gyroscope outputs are assumed constant. To enhance the long-term navigation performance, the initial roll and pitch angles, and the sensor turn-on biases should be accurately determined. In general, it can be done by averaging the inertial measurements with a larger number of sample, such that the measurement random noises can be diminished. In practice, the inertial measurements are not absolutely constant due to physical train vibrations and time-correlated sensor bias drifts.

To maintain the validity of initial estimation, a moving average or complementary filter can be applied to update the nominal inertial measurements within a time threshold or number of sample. Therefore, the time-correlated effects can be

sufficiently reduced, while the precision of estimation can be retained at a reasonable level.

Alternatively, the system initialisation can be performed with the EKF solution. The inertial measurements are directly employed for the measurement updates. The measurement error model for initialisation can be established by the functional relationships between the inertial measurements and the system error states as derived in Farrell (2008).

The direct initialisation and EKF measurement update method are examined and compared before the implementation of navigation system. The experimental results will be discussed in next chapter.

4.9.2. Initial Covariance Definition

For general navigation systems, it is common to assume large values for the initial system covariance to emphasise the state uncertainty. The navigation results then progressively converge and are bounded at a certain level of precision through measurement updates. This practice is reasonable because the aiding sources, such as GNSS and odometer, are independent to the navigation system and the propagation of system covariance.

The INS and TAP results, however, are fundamentally correlated regarding the chainage updating methods. Providing large values for the initial system covariance, the position uncertainty would propagate to the chainage covariance and the TAP results. Accordingly, the system covariance would not converge to a reasonable level.

One possible practice is employing a more realistic initial covariance to indicate the actual navigation uncertainty. Since the train position is bounded by the physical

track and the chainage accuracy is considered better than decimetre-level, it is feasible to acquire an accurate position and covariance for initialisation.

Alternatively, the problem can also be handled by adopting a reasonable value for the initial chainage covariance. During the fine alignment phase, the direct method is suggested for chainage maintenance, which requires the INS process noises for the chainage covariance propagation. The covariance of chainage, as well as that of TAP results, are therefore independent to the initial covariance of INS navigation results.

4.9.3. Chainage Propagation and Uncertainty

In section 4.5, the direct and indirect methods are suggested for chainage and covariance propagation. Nevertheless, the covariance propagation for the indirect method is fundamentally dependent on the position uncertainties of the navigation system. A mutual relationship is therefore established between the INS and TAP results, such that the relevant error equation becomes invalid.

For the direct method, chainage is integrated from the INS estimated displacement. Since the accumulated displacement is retrieved from the INS results, the covariance of chainage can be integrated from the INS process noise over the sampling time period. Although the INS and TAP results are still correlated, this method provides a covariance propagation which is independent to the absolute position uncertainties of the navigation system.

To remove the mutual relationship, the direct method is recommended for chainage maintenance. However, it is noted that the actual performance and the theoretical performance of an INS can be different, which may cause additional problems for implementation. By employing low-cost MEMS sensors for navigation, the position uncertainties usually increase rapidly and become invalid for indicating the actual

system performance. Consequently, a simplified covariance propagation model is alternatively established to de-correlate the chainage from the INS process. Regarding the rail-bound nature, a constant rate of error accumulation is assumed and determined from empirical study. The error model shown in eqn. 4.31 is sufficiently accurate for the propagation of chainage covariance under a constrained motion.

$$\delta L(t_1) \quad = [\Delta t \quad 1] \begin{bmatrix} \delta \dot{L} \\ \delta L(t_0) \end{bmatrix} \tag{4.34}$$

where $\delta \dot{L}$ is a constant error rate defined for chainage integration.

While the INS results are progressively corrected through the filtering process, additional chainage error would accumulate with time as shown in Figure 4.7.

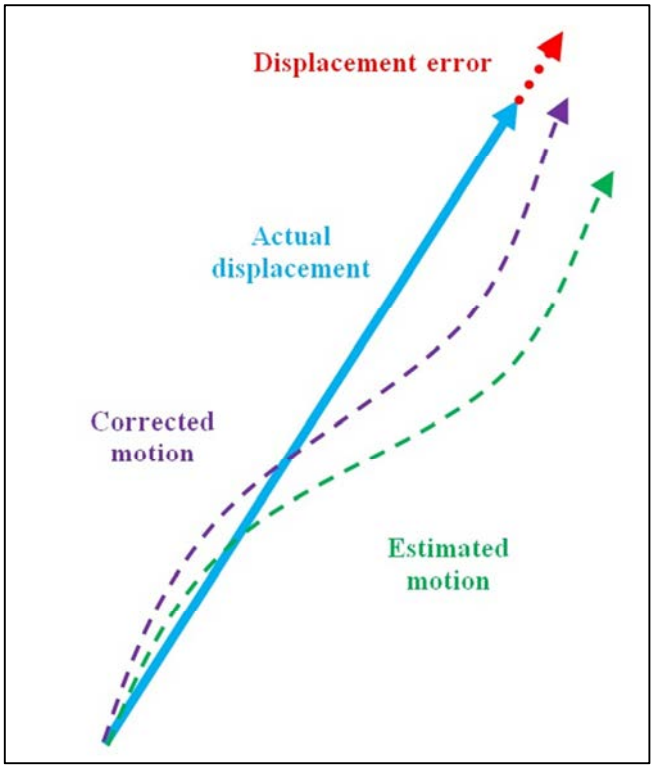

Figure 4.7: Integrated Displacement Error

The chainage is integrated through an individual filter, which is independent to the main navigation system filtering process. As illustrated in Figure 4.7, the compensation of navigation errors may introduce a correction for longitudinal position. A feedback mechanism is therefore required to retrieve the chainage following the correction, such that the propagated position and the chainage would not diverge. The indirect method is suitable for the implementation of the feedback mechanism. Since no additional measurement is provided for longitudinal error control, the chainage covariance remains unchanged for the feedback measure.

4.9.4. Dynamic Motion Uncertainty

It is mentioned in section 4.8 that the dynamic displacement and misalignment are assumed to be zero-mean and characterised by harmonic oscillation. In practice, the dynamic motion is constituted by different sources of forces, such as compensated vibrations and overturning forces at curves. Therefore, it is a resultant motion of harmonic oscillations with multiple frequencies. In addition, the elemental forces are not constant and change with time. It is not practicable to decompose and model all the harmonic oscillations during motion.

The moving average or complementary filter provides an alternative measure to minimise the short-term oscillations caused by train vibrations. The zero-mean assumption, however, is invalid at certain conditions. For example, the train would experience a continuous overturning force when travelling at a curve, such that the dynamic misalignment is not zero-mean and should not be removed.

In section 4.7, the covariance matrices for TAP estimated position, velocity and attitude are derived. The terms $\mathbf{P}\left(\Delta_b^b\right)$ and $\mathbf{P}(\mathbf{r}_{ab}^a)$ are required for covariance propagation, which can be approximated from the sampling sequence of estimated

dynamic displacement and misalignment (eqn. 4.32) by eqn. 4.22. Therefore, the dynamic motion is retained through the navigation error control with the introduction of appropriate uncertainties. The modelling or estimation of dynamic motion is not necessary.

4.9.5. Inertial Navigation Uncertainty

Although the system model and stochastic model have been established for the propagation of INS errors and covariance, the practical performance may vary with the choice of sensors, especially the MEMS IMUs.

In this thesis, the INS is implemented by two consumer-grade MEMS IMUs. By employing the sensor specification, the navigation covariance may not be consistent with the actual performance, such that the relative weight between INS and TAP results cannot be correctly maintained. As a result, an optimal navigation solution would be unachievable.

In general, a MEMS IMU requires additional error analysis for the stochastic modelling, since the actual performance is relatively unstable and different from system specification. For simplicity, the stochastic parameters are empirically defined from the post-process navigation results in this thesis. To verify the feasibility of mentioned solutions, the implementation results of the navigation system and the RBN solution are discussed in Chapter 5.

Chapter 5: System Design and Implementation

In this Chapter, the design of a prototype navigation system including the components, sensor calibration and data processing are presented. The results of testing on a small-scale experiment employing a simple model train are presented along with a concise discussion of the practical restrictions, the potential problems, and the relevant remedial measures are then concisely discussed. Higher level validation of the RBN solution was conducted from sampling data collected in MTR trains. The results of TAP estimation, navigation and RBN solution are enumerated and discussed regarding the eligibility of the solution.

5.1. Prototype System Design and Development

To facilitate the implementation of the RBN solution, a prototype system has been built for data collection. In this section, the navigation system design, relevant components and experimental conditions are presented.

5.1.1. Navigation System Components

As a comprehensive MMS or high performance navigation system (such as navigation or tactical grade sensors) was ultimately not available, a lower grade IMU was used for examining and validating the developed RBN solution. Accordingly, the FreeIMU (Varesano, 2013), a consumer-grade MEMS IMU, has been employed for inertial data collection.

The FreeIMU is configured with a 6-axis gyroscope and accelerometer (MPU6050) and a 3-axis magnetometer (HMC5883L), which is primarily designed for motion sensing and low-cost Attitude and Heading Reference System (AHRS). Although the performance of the FreeIMU may be insufficient to support an inertial navigation

solution, the results can be enhanced by an aided navigation structure, such as the RBN solution.

Figure 5.1 illustrates the structure of the prototype system version 1.0 which was used for a preliminary study (Hung et al., 2016). The FreeIMU is connected to and controlled by an Arduino UNO REV3 processing device for data collection. Both the devices are mounted on a platform constructed by building blocks, which can be attached to a host train for data collection.

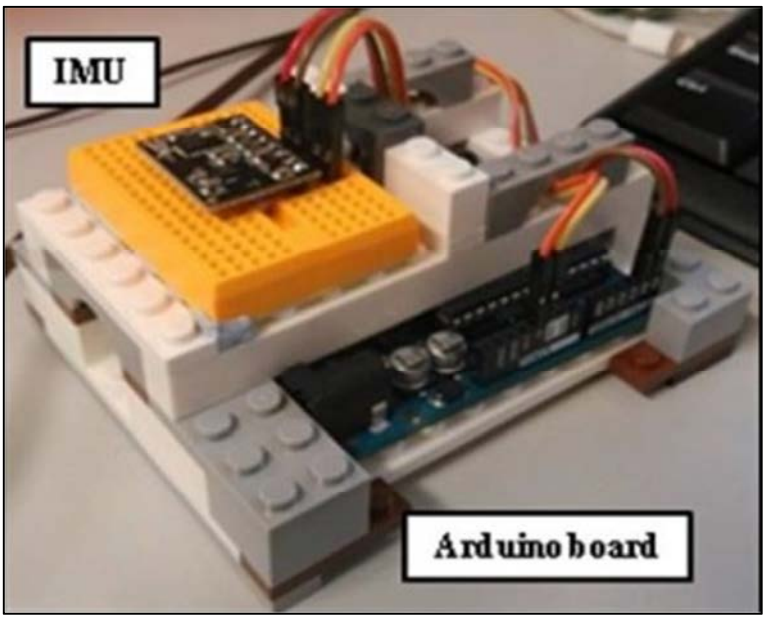

Figure 5.1: The prototype navigation system - version 1.0 (Hung et al., 2016)

5.1.2. Self-calibration Process

The FreeIMU is programmed through an open-source Arduino Software (Ardiuno, 2016) and the corresponding libraries (FreeIMU-Updates, 2016), which governs the sampling of accelerometer, gyroscope and magnetometer outputs. In addition, a self-calibration process (FreeIMU Calibration, 2014) is employed to estimate and compensate the sensor biases and scale errors of accelerometers and magnetometers. The Graphical User Interface (GUI) of the FreeIMU calibration application is shown

in Figure 5.2. The calibrated parameters are uploaded to the FreeIMU through the Arduino processing software.

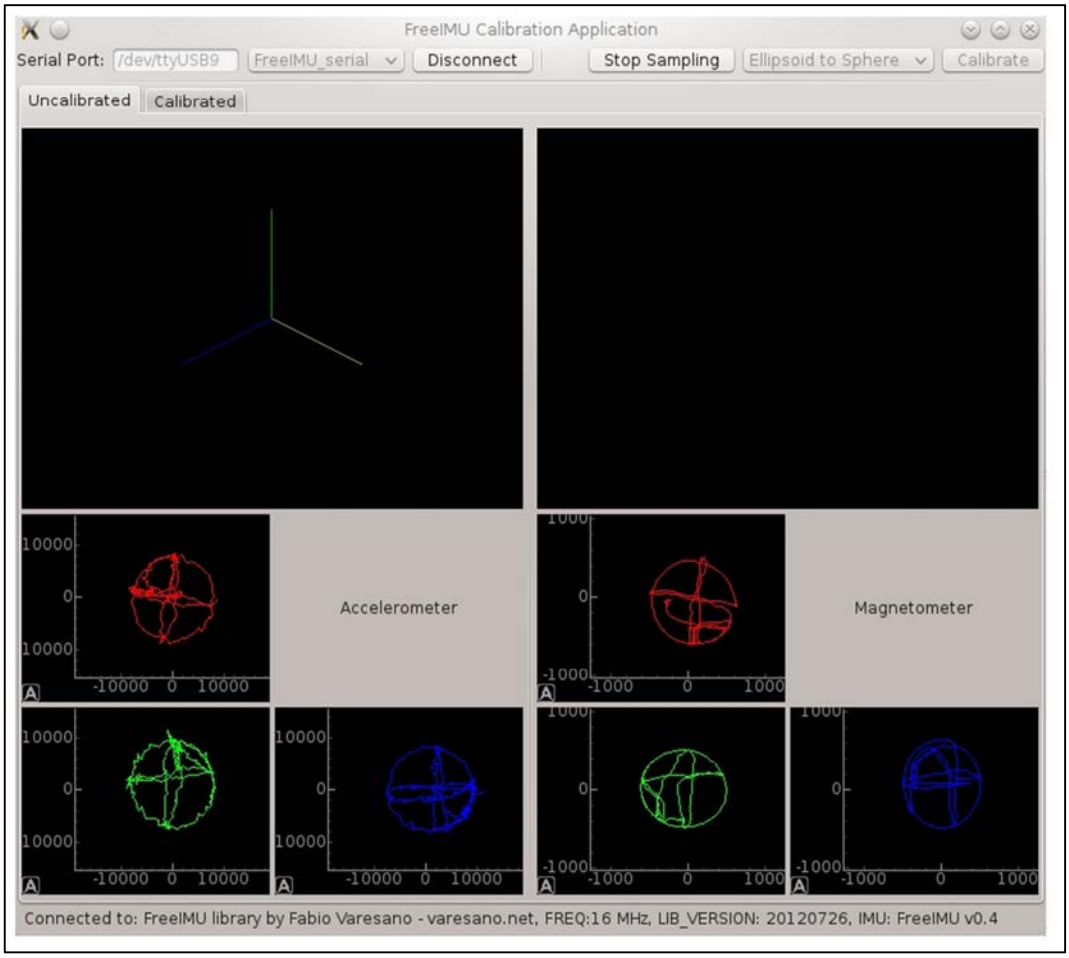

Figure 5.2: The GUI of FreeIMU calibration (FreeIMU Calibration, 2014)

5.1.3. Data Sampling and Processing

Following the sensor calibration, the measurement data are sampled at a frequency of $125Hz$ and collected by a freeware *Processing* (Processing, n.d.). Since the FreeIMU is the only source of measurement device, additional time synchronisation is not considered in this prototype system.

The prototype navigation system is developed in a Matrix Laboratory (MATLAB) environment with an INS toolkit ("The Toolkit", 2010) for the INS mechanisation. The track alignment data, time references, and IMU sampling data are imported and

processed after data collection. In this thesis, the validation of solution is the primary objective for system implementation. The practical problems relating to real-time processing are not considered.

5.2. Preliminary Experiment with Simulated Motion

A preliminary experiment with a small-scale railway model and motorised model train was conducted to implement the RBN solution and examine its performance (Hung et al., 2016). The results and findings are concisely reviewed and summarised in this section.

5.2.1. Track Design and Settings

A small-scale track model which has dimensions of around $1000mm$ by $700mm$ with a gauge width of $42mm$ was employed to simulate the rail-bound motion of a train. The track model was set on a levelled surface such that the track alignment was compiled without longitudinal gradient or cant. The track was an enclosed loop comprising straight and circular sections as shown in Figure 5.3.

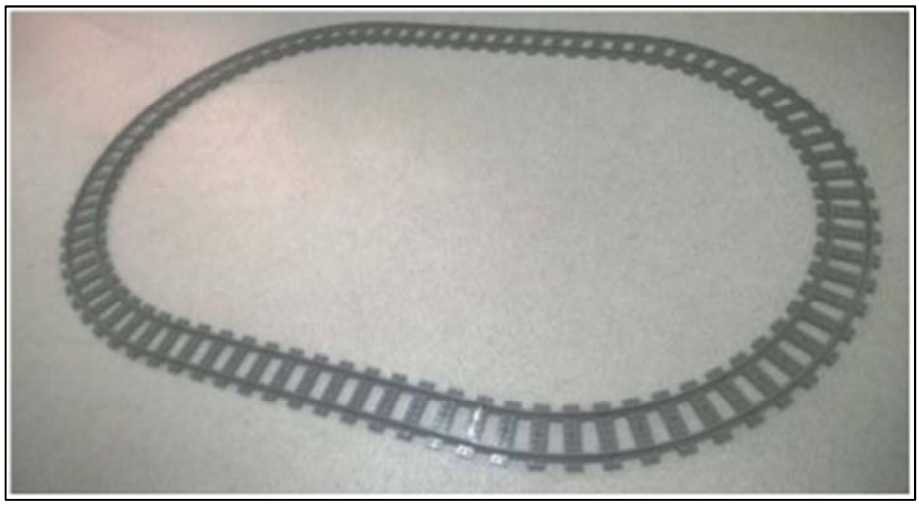

Figure 5.3: The physical track model (straight and circular sections)

The motorised model train shown in Figure 5.4 was used to simulate the train motion for the prototype system. The model train consisted of a battery, a motor unit, and a rigid train body connected to front and rear rotatable bogies. The FreeIMU device was directly attached to the upper train body.

Figure 5.4: The motorised model train

Rail-bound train motion data was collected for two loops of the track over a period of about $15s$. The train was stationary for around $3s$ for initialisation and finalisation. The power of the train was manually controlled.

The navigation system was mechanised in an arbitrary grid coordinate frame and the global effects to inertial measurements are assumed negligible. In addition, the RBN solution was implemented by a complementary filter for direct navigation error control (eqn. 5.1) which was simplified to facilitate the study.

$$\bar{z} \quad = G(s)\hat{z}_{\mathrm{INS}} + [1 - G(s)]\hat{z}_{\mathrm{TAP}} \tag{5.1}$$

where $\bar{z}$ is the compensated result; $\hat{z}_{\mathrm{INS}}$ and $\hat{z}_{\mathrm{TAP}}$ are the navigation results estimated from INS and TAP respectively; $G(s)$ and $[1 - G(s)]$ are the low-pass and high-pass filters respectively.

5.2.2. Preliminary Results and Finding

The motion data captured by the FreeIMU device are shown in Figure 5.5 (Hung et al., 2016). The acceleration (from about $18s$ to $22s$) and deceleration (from about $30s$ to $34s$) of the train's motion cannot be clearly identified. In contrast, the linear and circular motion are clearly indicated by the gyroscope outputs. The periodic chainage at the front bogie can be determined to compile a speed profile and estimate the accuracy of position and attitude.

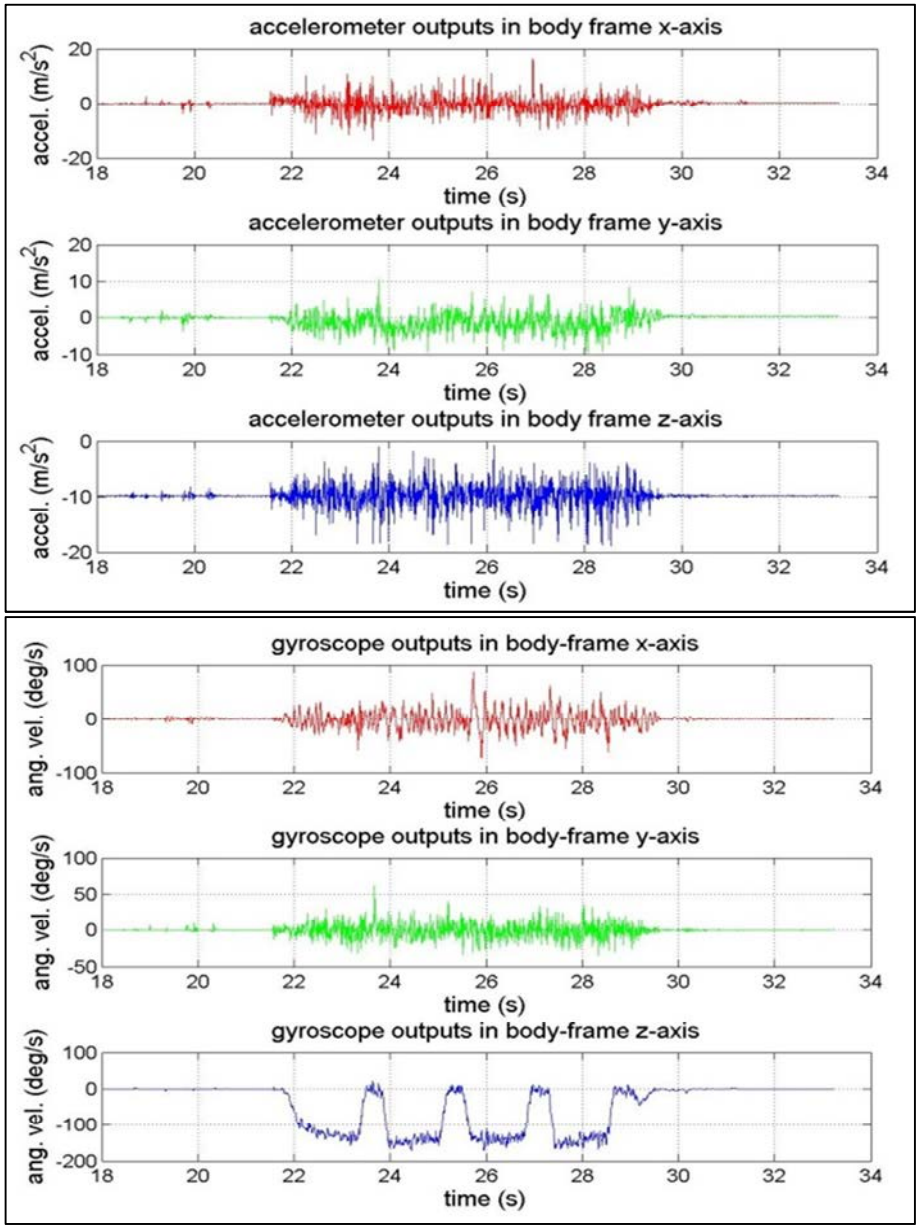

Figure 5.5: Accelerometer (Up) and gyroscope (Down) data in the *b*-frame

Through the recognised chainage reference, the position and attitude errors have been estimated by TAP solution. The position and attitude errors for the pure inertial navigation and the RBN solution from Hung et al. (2016) are presented in summary form in Figure 5.6. The INS and RBN errors are coloured in red and green respectively and are plotted with respect to the sectional boundaries in series.

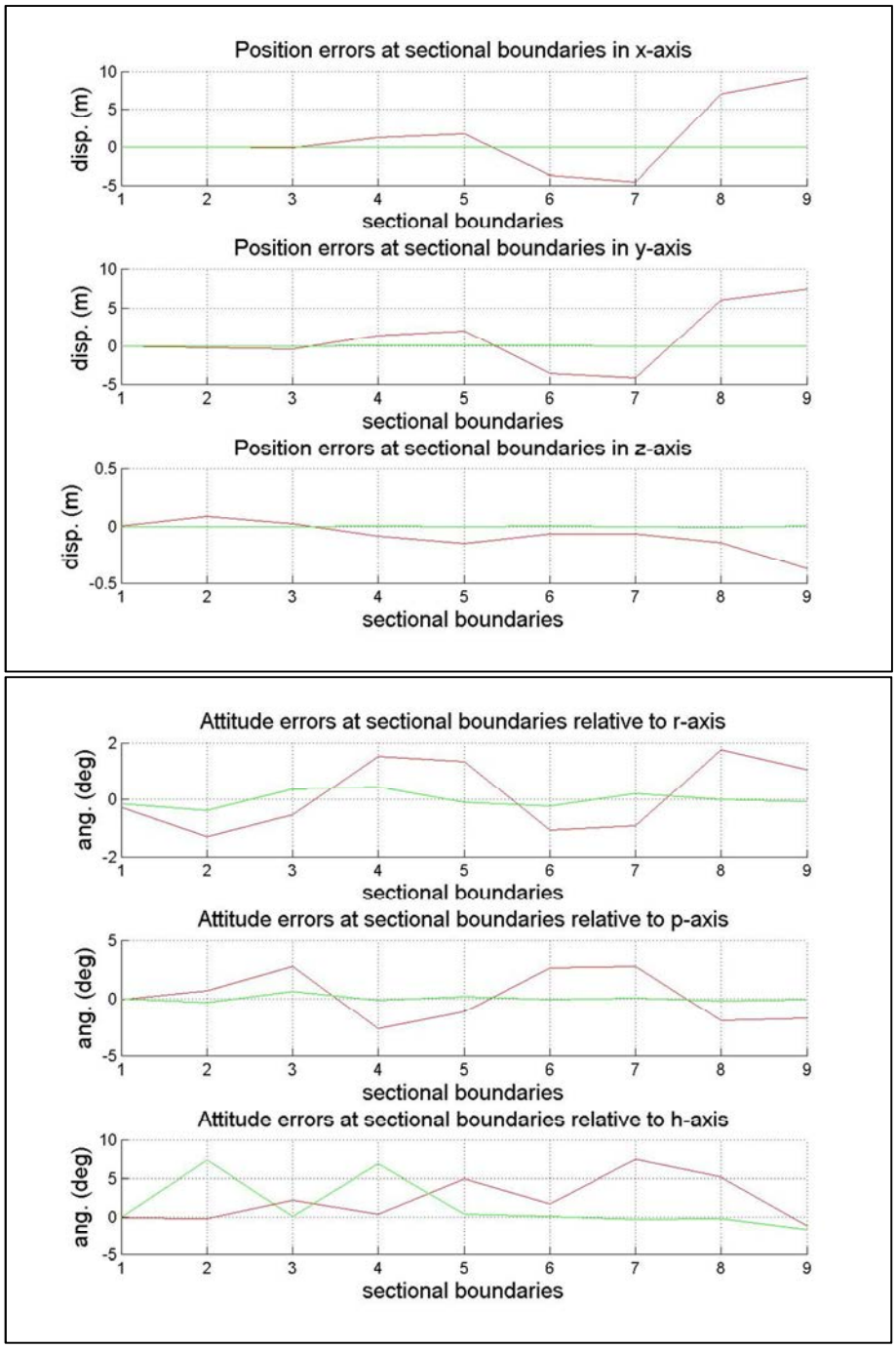

Figure 5.6: Position (Up) and attitude (Down) errors at sectional boundaries

The horizontal and vertical position errors of INS are rapidly accumulated and reach metre-level and decimetre-level respectively, which are too large to describe the nominal train motion to the extent that the navigation results are completely unacceptable. It was found that the excessive position errors are mainly integrated from the velocity errors caused by poor system alignment.

Through the RBN solution, the position errors were reduced significantly to centimetre-level in both horizontal and vertical directions. The improvement is mainly caused by the enhanced attitude and velocity, while the longitudinal position accuracy is especially important to retrieve correct TAP results for error control. In this experiment, the longitudinal position error is mainly constrained by the nominal speed data. The attitude control further diminished the growth of velocity errors caused by incorrectly resolved gravity acceleration.

The dynamic misalignment is not considered in this experiment such that the differences between the navigation results and TAP estimated results are uncertain. As a result, the loss of dynamic motion can be observed after applying the RBN solution.

5.2.3. Summary of Preliminary Experimental Results

From the results of simulated rail-bound motion, the simplified RBN solution produced a considerable improvement over the standalone INS result. Because of the following experimental restrictions, the experimental results are insufficient to demonstrate the performance of RBN in real world conditions:

- **Nature of motion**: the acceleration and braking of the model train were poorly controlled such that the signal-to-noise ratio (SNR) has been masked by the

uncompensated high-rate vibrations. Therefore, the actual motion cannot be accurately captured by the inertial sensors.

- **Track design**: the small radius of curvature has introduced additional uncertainties to the solution, which may invalidate the assumption of track-to-train correction. As a result, the real world performance cannot be fully demonstrated through this oversimplified track design.
- **Scale of railway model**: the size of the railway model is too small to represent the reality of railway environment, while the period of motion simulation is insufficient to analyse the long-term improvement. From the experimental study, the actual performance of RBN solution remains uncertain.
- **Simplified implementation**: the RBN solution was implemented by a complementary filter. The navigation error control was directly weighed and applied, while the recalibration of sensor biases and dynamic motion were not considered. The results indicated a loss of motion dynamics which is probably caused by the simplified implementation.

Further experiments were conducted to collect real data in MTR trains during normal service hours, which are designed to overcome the restrictions of preliminary study. The results presented in Section 5.4 sufficiently represent the actual train motion and railway conditions.

5.3. Expected Conditions and Restrictions

In previous chapters, the theoretical models and practical considerations have been discussed for the establishment of RBN solution. Through the simulated rail-bound motion, the performance of proposed solution has illustrated under several experimental restrictions. Prior to further experiments, the expected conditions and restrictions for experimental design are discussed in this section.

5.3.1. Absence of Precise Gravity Information

Although the gravity acceleration has been globally modelled to support near-Earth navigation, the local gravity anomaly would introduce considerable errors in the vertical direction. The gravity anomaly is generally estimated and compensated through a local geoid model. The loss of navigation accuracy in the vertical direction, however, cannot be avoided regarding the excessive gravity errors.

For the prototype navigation system, a local geoid model is absent hence precise gravity compensation is not available. Alternatively, the accelerometer outputs are assumed accurate enough to represent the actual gravity acceleration, such that the gravity anomaly can be empirically determined from the differences between accelerometer outputs and normal gravity acceleration during stationary initialisation. In a real railway environment, the vertical train motion is considerably smoother and better bound by the track alignment than that of the model. While gravity changes slightly with global position, the gravity anomaly can be continuously calibrated by accelerometer outputs through moving average or filtering processes.

5.3.2. Absence of External Reference

It is mentioned in Chapter 1 that the train control data or external reference data, such as position and speed, are not accessible for continuous analysis to the system performance. Therefore, the navigation results are fundamentally analysed during stationary phases.

The chainage error corresponding to the station platform is the primary indicator for examining the reliability of a solution. In addition, the velocity and attitude errors can also be determined from the misclosures at the end of train motion. During the stationary phase, the train speed should be zero in all axes, while the attitudes

estimated from the navigation system should be consistent with the accelerometer derived attitudes. To validate the performance, sufficient time is required to collect data for system initialisation and finalisation.

5.4. Experimental Design for Real Train System

With regard to the expected restrictions, another experiment was organised and performed by a series of data collections in a real world railway environment, which aims to provide more useful conditions for a comprehensive analysis. In this section, the background information of the real world data collection and relevant considerations are presented.

5.4.1. Reference Track Alignment Data

The MTRC is the only corporation that operates railway networks in Hong Kong. To implement the navigation solution, relevant track data are necessary to execute the TAP solution. Thus, a sample dataset was requested to validate the TAP mathematical models in the early stage of research. Due to a confidentiality agreement the data cannot be reproduced here.

The track alignment data of section between Hang Hau (HAH) station and Po Lam (POL) station were provided, which is an extension of Tseung Kwan O (TKO) line. The location of track section is illustrated on the Google Map which is captured and shown in Figure 5.7.

The alignment data have been retrieved from an as-built survey in 2002, while the physical track is maintained relative to the local position.

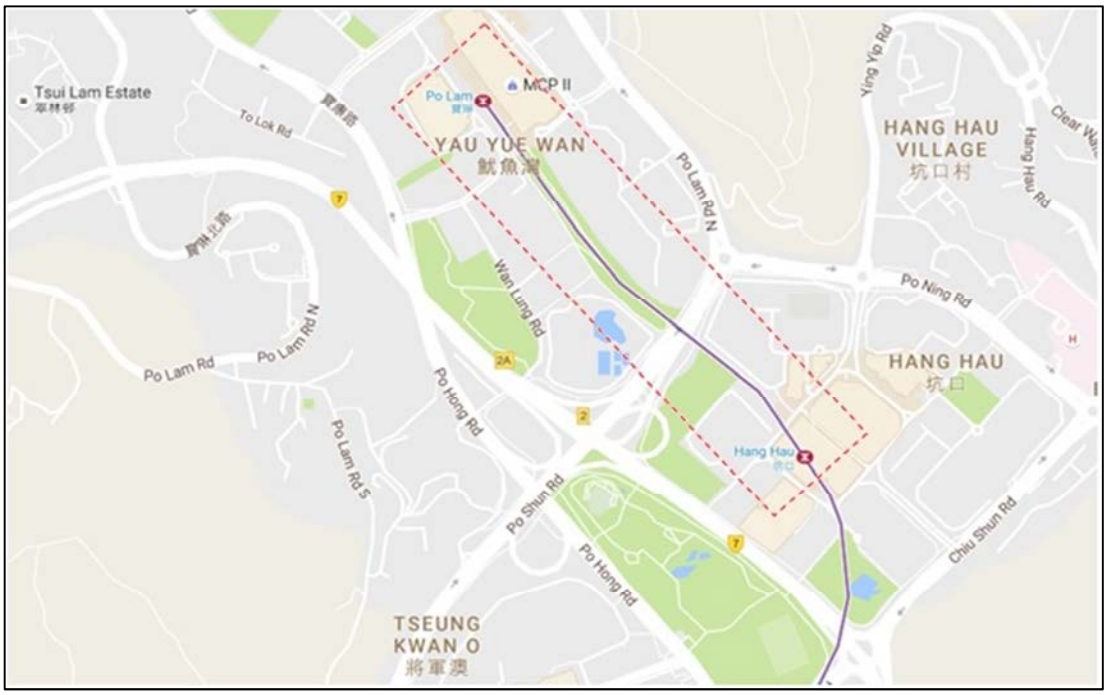

Figure 5.7: Location of HAH to POL track section

The reference chainage of the track alignment is locally defined at the centre of the station platform. The available section of alignment includes the eastbound (from HAH to POL) and westbound (from POL to HAH) track data, which are parameterised into horizontal and vertical alignments of the track centreline according to the models presented in Chapter 4. Both the eastbound and westbound tracks have a horizontal length of $1000m$ and a height difference of $10m$. The tracks overlap near the end of POL station.

The horizontal and vertical alignment are referenced to the HK1980 grid coordinate system and Hong Kong Principal Datum (HKPD) respectively. The relevant datum transformation and projection are defined and explained by the Survey and Mapping Office (SMO) of the Lands Department ("Explanatory Notes…", 1995).

5.4.2. Railway and Train System

In general, the Grade of Automation (GOA) is defined by the International Association of Public Transport (UITP) to classify the automation and the nature of

train operation (“Press Kit Metro…”, n.d.). The current train control system for the TKO line can be classified into GOA3 which supports driverless train operation. Although a train operator is retained for supervising the train, the train acceleration and braking are computer controlled. Consequently, the train motion is relatively smooth and favours the inertial measurements.

For the TKO line, the standard track gauge has a width of $1432mm$. Each trainset is formatted with eight cars, which are configured with three car types: A car, B car and C car. The maximum train speed is around $80\,km/h$ or $22.2\,m/s^2$. The maximum acceleration, service braking and emergency braking are limited to approximately $1.3\,m/s^2$, $1.35\,m/s^2$ and $1.4\,m/s^2$ respectively for safety concerns. The operational restrictions for train speed, acceleration and braking can be compared to the navigation results if necessary.

5.4.3. Data Sampling and Arrangement

To facilitate the data collection procedures, the original devices have been mounted to the platform constructed by building blocks and fixed in a portable box. A second FreeIMU and processing device was attached to the navigation system as shown in Figure 5.8. The additional sensor was configured to collect redundant and independent data for performance analysis in Chapter 6.

Figure 5.8: The prototype navigation system - version 2.0

The FreeIMU devices were connected to a portable computer through universal serial bus for data collation. During the experiment, the box was temporarily attached on the floor of the first train car by blu-tack. To minimise the uncertainties of periodic data collection, the devices have been located at the same position relative to the train (near the first train door on the right head side), as well as the physical track. The relative position between the track reference and the sensor origin was estimated by direct linear measurements of centimetre-level precision.

In general, the experimental data was collected in the night-time to minimise the interference of passengers. The details of experiments are presented in corresponding sections.

5.4.4. Estimation of Reference Chainage

The absolute position of the sensor is retrieved from the initial chainage of track reference and the relative position. The relative displacement between the sensor origin and the reference platform screen door was measured in the track direction, while the chainage of the platform screen door was determined from the

neighbouring chainage plate installed on the tunnel wall at a 10 m interval. The propagation of chainage reference is elaborated in eqn. 5.2.

$$\begin{aligned} L_s &= L_0 + \Delta L_0 + \Delta L_s \\ \delta L_s &= \delta L_0 + \delta \Delta L_0 + \delta \Delta L_s \\ \sigma_{L_s}^2 &= \sigma_{L_0}^2 + \sigma_{\Delta L_0}^2 + \sigma_{\Delta L_s}^2 \end{aligned} \tag{5.2}$$

where L_s is the chainage of sensor; L_0 is the reference chainage at the chainage plate; ΔL_0 is the relative distance between chainage plate and reference platform screen door; ΔL_s is the relative distance between the reference platform screen door to the sensor.

Through the propagation of linear measurements, the initial chainage covariance can be approximately determined. The absolute accuracy of chainage of sensor, however, has been reduced to around few centimetres to a decimetre. To estimate the effects of absolute chainage error, the possible navigation errors of TAP solution would be investigated in section 5.5 before further implementation.

5.5. Examination of Track Alignment Positioning

The eastbound track section from HAH station to POL station is selected for the examination of TAP solution, which would be further employed for the implementation of navigation system and RBN solution.

5.5.1. Characteristics of Track Alignment

The TAP position and attitude of track alignment have been estimated against chainage as shown in Figure 5.9 and Figure 5.10 respectively. The gradual changes in northing and easting grid coordinates indicate the linearity of track alignment, while the track level is progressively increased by nearly $10m$ along the track.

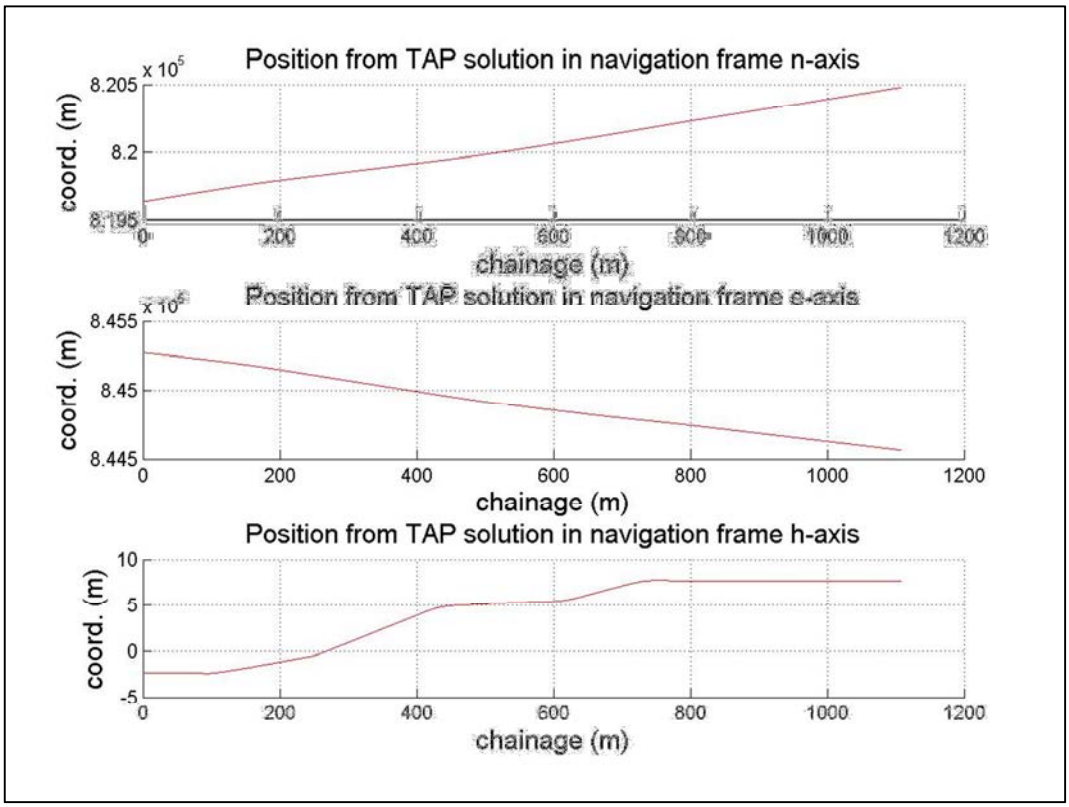

Figure 5.9: The estimated grid coordinates of track against chainage

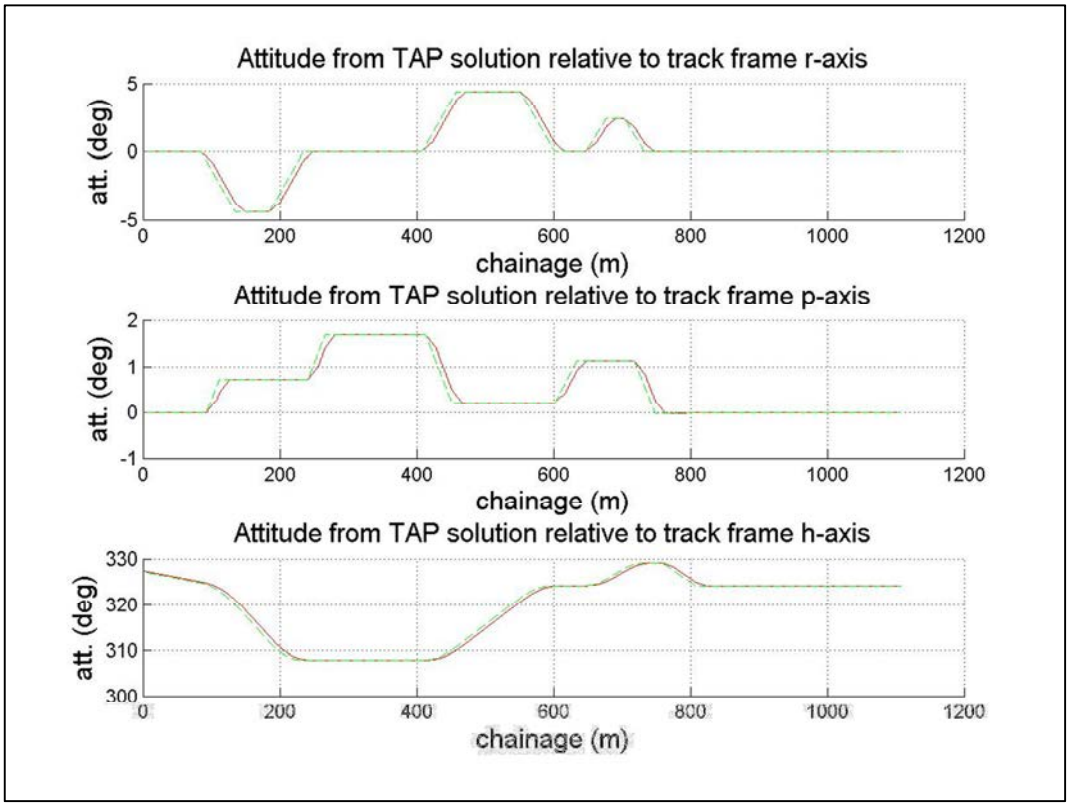

Figure 5.10: The estimated attitudes of track against chainage

According to Figure 5.10, the roll and pitch are bounded by 5° and 2° respectively. The primary attitudes defined at the front bogie are coloured in green, while the train attitudes coloured in red are revised with the track-to-train correction. The rigidity of train and bogies would introduce a transition effect to the train attitudes which would be slightly smoothened from the original track attitudes.

The rate of roll is caused by the linear interpolation of cant within the transition curve sections, which is fundamentally correlated to the heading. For the pitch profile, the rate of pitch is generated by the constant change of gradient such that a correlation between the pitch and the level can be found.

For the heading profile, a constant angular rate indicates a circular curve section. The changes of heading between slopes are generally smoothened by the transition curves, while the track-to-train correction has introduced an excessive transition over the smoothened track heading.

It is found that no transition curve is applied at around chainage of $800m$, which is probably simplified for track alignment design. The removal of transition curve is acceptable because the designed train speed is reduced at the point and crossing area. In addition, the trains have to decelerate when approaching to the station platform. Regarding the reduced train speed, the resultant centrifugal force would be diminished. The cant is therefore removed from the curve section.

5.5.2. Navigation Errors from Chainage Error

In railway system, the chainage is the fundamental variable for train positioning such that the chainage error is a primary consideration for the correctness of TAP results. Through the TAP solution, additional position and attitude errors would be resulted

from the chainage error, while the impacts of chainage error are generally determined by the magnitude of chainage error and the linearity of track alignment.

To investigate the impact of chainage, a constant chainage error is simulated to generate the position and attitude errors which are acquired from the differences between nominal results and biased results. The Root Mean Squared (RMS) position and attitude errors are summarised in Table 5.1 against different magnitudes of chainage error.

Table 5.1: RMS of TAP position and attitude errors

chainage error (m)	RMSE of position (m)			RMSE of attitude (°)		
	x	y	z	r	p	h
0.1	0.100	0.000	0.001	0.0042	0.0013	0.0066
0.5	0.500	0.000	0.007	0.0209	0.0066	0.0332
1.0	1.000	0.001	0.014	0.0417	0.0131	0.0664
10.0	10.000	0.058	0.140	0.4020	0.1235	0.6610

From the results, the RMS position and attitude errors are directly proportional to the chainage error, because the changes of track geometry are generally constant, such as the radius of curvature, cant and gradient. Apart from the chainage, the overall TAP results are generally acceptable when the chainage error reaches $0.5m$. For a chainage error exceeding $1.0m$, the RMS of vertical position errors reach a centimetre-level. The results may not be sufficient to certain applications which require an accurate georeferencing solution. On the other hand, the impacts of attitude errors cannot be directly examined, which would be illustrated from the navigation results in later section. To conclude, a metre-level chainage error would cause a direct impact to the overall performance of navigation system.

5.5.3. Precision of TAP Estimate

In Chapter 4, the mathematical models of TAP have been developed to retrieve the position and attitude from the track alignment data, while the corresponding covariance can be estimated from the chainage uncertainty. To validate the error models, the precision of TAP solution is estimated and compared with the simulated position and attitude errors. Figure 5.11 and Figure 5.12 illustrate the uncertainties of TAP position and attitude respectively, which are expressed in absolute errors and standard deviations. The errors are simulated by a chainage error of $0.1m$, which is also employed to define the standard deviation of chainage for the propagation of TAP position and attitude precision.

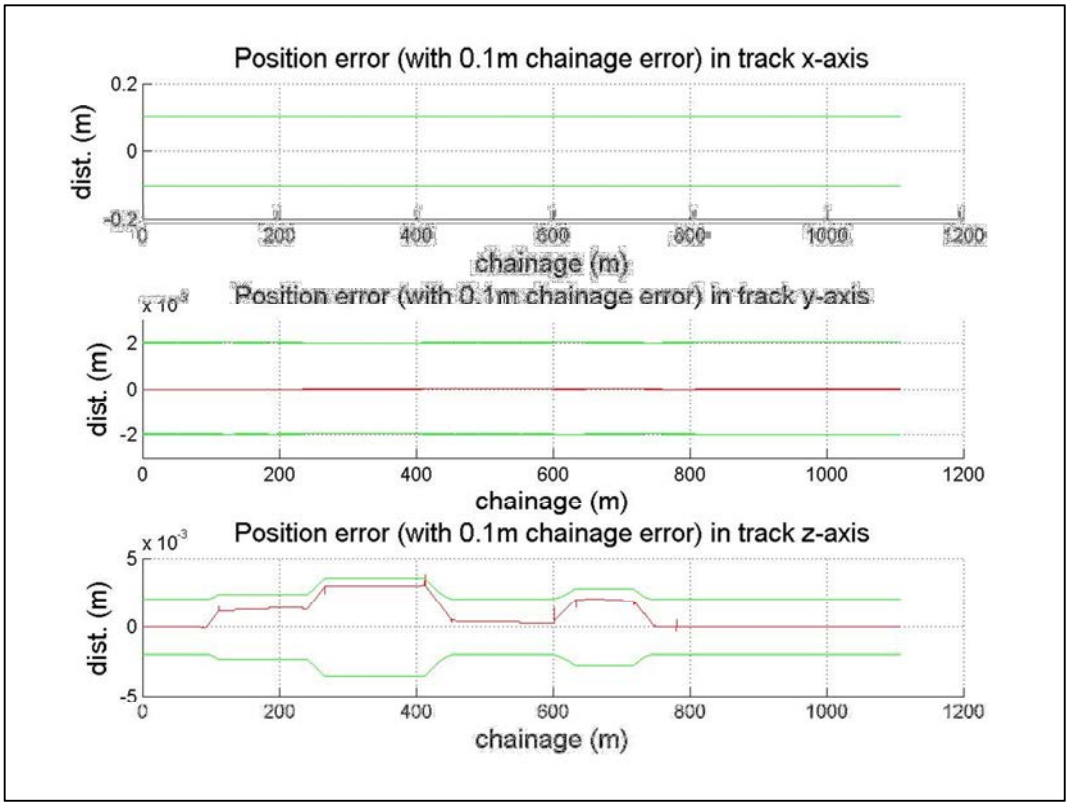

Figure 5.11: The estimated position errors and precision at 0.1 m chainage error

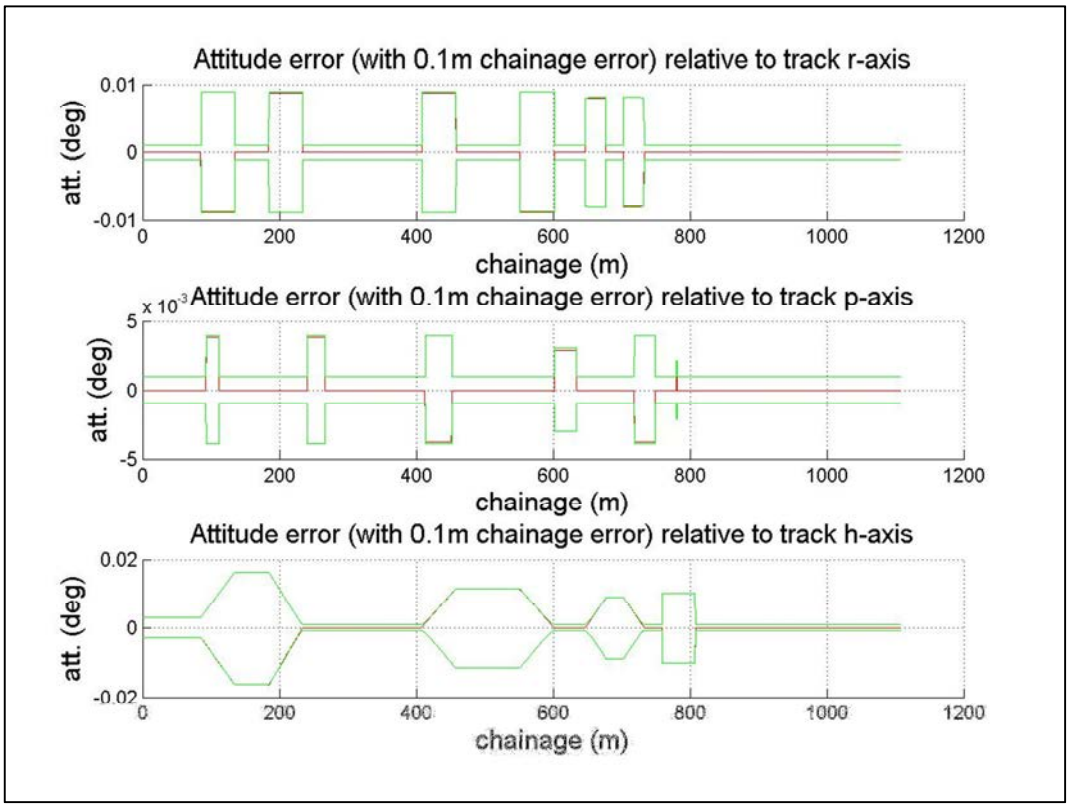

Figure 5.12: The estimated attitude errors and precision at 0.1 m chainage error

The position errors are resolved into the *t*-frame to investigate the lateral impacts. The $0.1m$ longitudinal position error is recovered from the chainage error, which is approximately overlapped with the estimated standard deviation. The lateral position errors are theoretically less than $1mm$ which is negligible. The vertical position errors are relatively larger and bounded at $4mm$. The unusual variations found at the section boundaries are caused by the uncompensated transformation of lateral errors. The estimated roll, pitch and heading errors are bounded by $0.01°$, $0.005°$ and $0.02°$ respectively. Therefore, the initial chainage error of $0.1m$ is sufficiently accurate for the attitude error control to a navigation system.

The estimated standard deviations of position and attitude are propagated from the chainage uncertainty, while the additional uncertainties are constantly defined and introduced to the position and attitude of reference. The track geometry parameters

are assumed to be constant in the solution such that the chainage uncertainty is the only variable for estimation.

The results indicate that the position and attitude errors are bounded by the estimated standard deviations. The estimated precision and the simulated errors are consistent, which imply that the TAP error models are correctly established for the propagation of TAP uncertainties from the reference chainage.

5.5.4. Physical Track Uncertainties

The TAP solution provides constraints to the growth of navigation errors in form of track position and attitude. In case of track deformation, the navigation results would be incorrectly constrained by the track data. To maintain the correctness of track constraint, both the chainage uncertainty and physical track uncertainty are involved in the estimation of reference track covariance.

It is noted that the magnitudes of physical track uncertainty are rather critical to the navigation accuracy when the compensation of absolute track deformation is not available. The actual impacts would be investigated through the implementation of navigation system in Chapter 6.

5.6. Implementation of the Navigation System

In this section, the navigation system is established with inertial data collected by the primary sensor. The TAP solution is employed for the system initialisation, while the navigation is merely maintained by the INS solution for standalone results. In addition, the TAP error control is applied to compute the RBN navigation results for comparison.

5.6.1. Data Collection for Inertial Experiment

The inertial measurement data used in this section was collected on 13/08/2015, which captured the motion of a train operated from HAH station to POL station, including the stationary phases. The train motion was sustained for about $95s$ with a horizontal distance of $1007m$, with the initial and final stationary phases lasting for about $9s$ each. The motion is considered sufficient to indicate the reality and general characteristics of train navigation. The measurement data presented in this section are sampled at a frequency of $10Hz$.

5.6.2. Inertial Measurement Data

For the implementation of the navigation system, the accelerometer and gyroscope biases were estimated and compensated during system initialisation, while the position, velocity and attitude were maintained through the system mechanisation.

The standalone INS and RBN results are coloured in red and green respectively. The accelerometer outputs are compensated for sensor biases and gravity acceleration, which have been levelled as shown in Figure 5.13. The horizontal acceleration should be zero-mean during stationary or non-accelerating motion. The gyroscope outputs are compensated for sensor biases and shown in Figure 5.14, which should be zero-mean during the stationary phases.

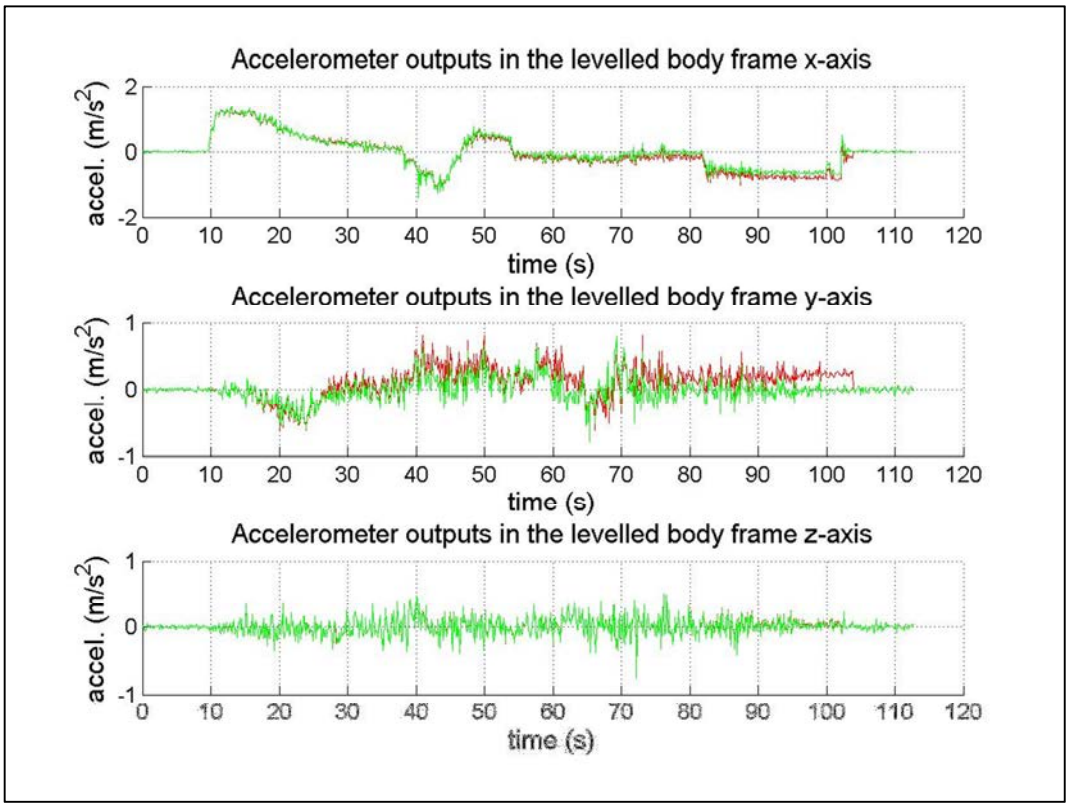

Figure 5.13: Compensated and levelled accelerometer outputs

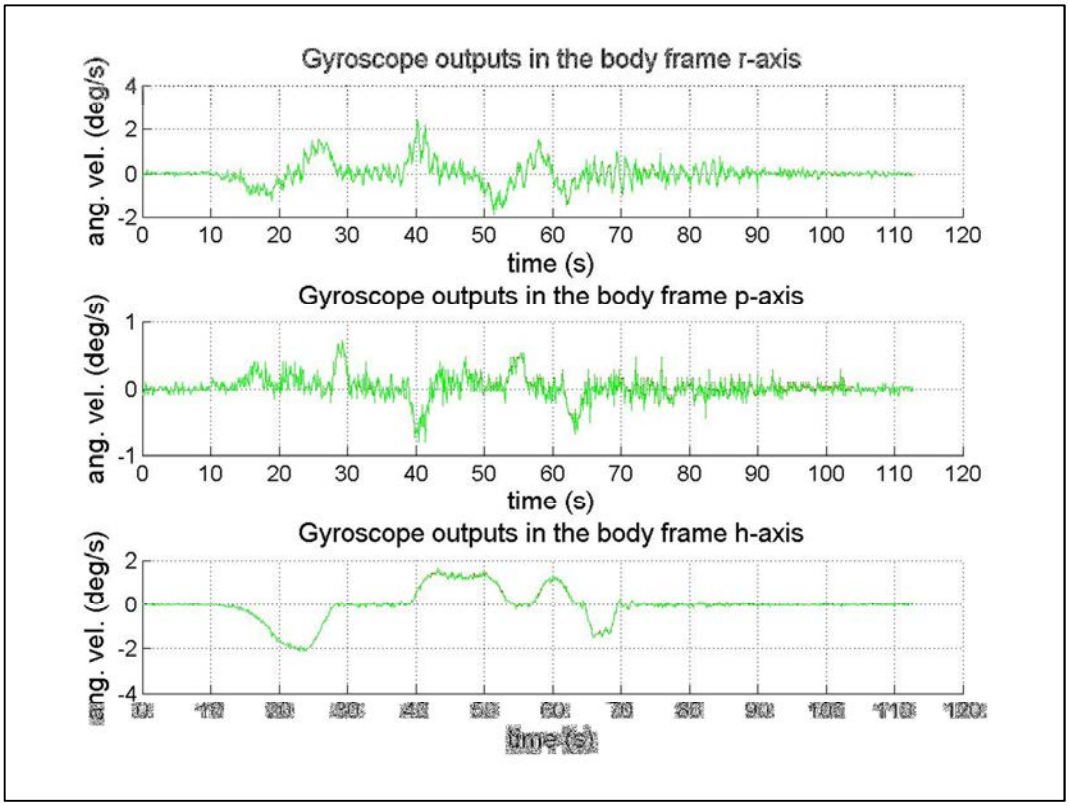

Figure 5.14: Compensated gyroscope outputs

The train acceleration and braking have been well captured by the acceleration in the *x* axis, while the beginning and the termination of train motion are clearly identified. The acceleration in the longitudinal track direction is bounded by the operational restrictions as summarised in section 5.4.2. Through the average of measurements, the acceleration in all axes converged to zero during the initialisation.

The *y* axis is approximately aligned in the lateral track direction. The changes in acceleration are mainly caused by the track-to-train misalignment, such that the train motion is resolved into lateral direction when passing through at curve sections. As a result, a significant correlation between the *y* axis acceleration and *h* axis angular velocity can be observed.

In both the *x* and *y* axes of the INS results, sudden changes can be found at around $104s$, which indicate the misclosures caused by the pitch and roll errors propagated through the navigation system. From the results of RBN solution, the attitude accuracy is considerably enhanced such that the misclosures for the levelled acceleration in *x* and *y* axes are greatly reduced. For the acceleration in the *z* axis, the motion is not clearly captured because the gradient rate is generally small.

From Figure 5.14, the angular velocities are generally bounded by $3°/s$ in all axes, which are much smaller and smoother than that in the preliminary experiment. The angular velocities relative to the *r* axis are mainly caused by the changes of cant in the transition curve sections, while the high-rate variations are caused by the harmonic train oscillations. The oscillations are clearly observable in the *r* axis because the train vibrates in the lateral direction regarding the centrifugal forces. In contrast, the base of train bogies in the longitudinal track direction is sufficiently large to constrain the oscillations in the *p* axis, while the oscillations in the *h* axis are restricted by the track through the train bogies.

In summary, the results indicate that the train motion and its characteristics has been well captured by the inertial measurements. The sensor biases have been approximately compensated during the initialisation, while the transformation is established and maintained to resolve the acceleration into a levelled frame relative to the *b*-frame. Since the time for system initialisation is relatively short, the estimated sensor biases may not be accurate. Through the RBN solution, the impacts of sensor biases have been diminished by continuous navigation error control.

5.6.3. Train Navigation Results

In this section, the attitudes and velocities estimated from the standalone INS and RBN solution are summarised and concisely discussed. The characteristics of train motion and physical rail track which may be significant to the performance of navigation system are preliminarily inspected. Finally, the position errors are illustrated with the reference track position.

The profiles of system roll, pitch and heading are illustrated in Figure 5.15, while the system velocities are summarised in Figure 5.16 to realise the impacts of attitude errors. The INS and RBN results are coloured in red and green respectively.

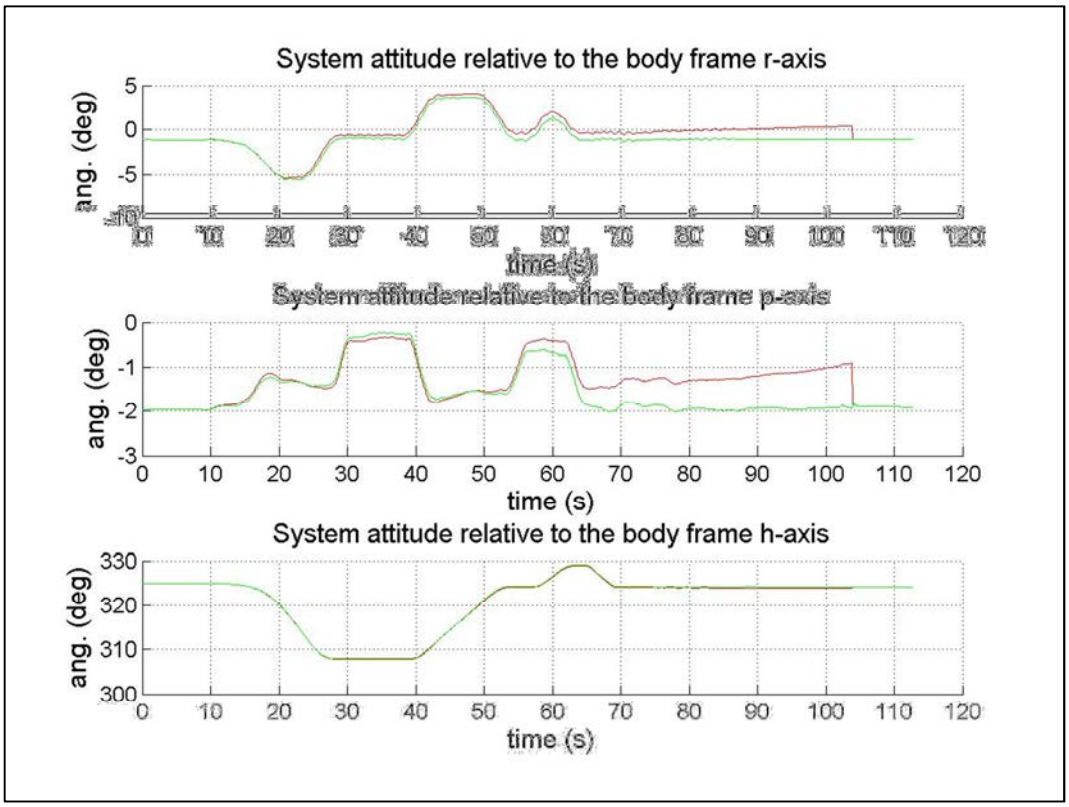

Figure 5.15: INS and RBN derived system attitudes

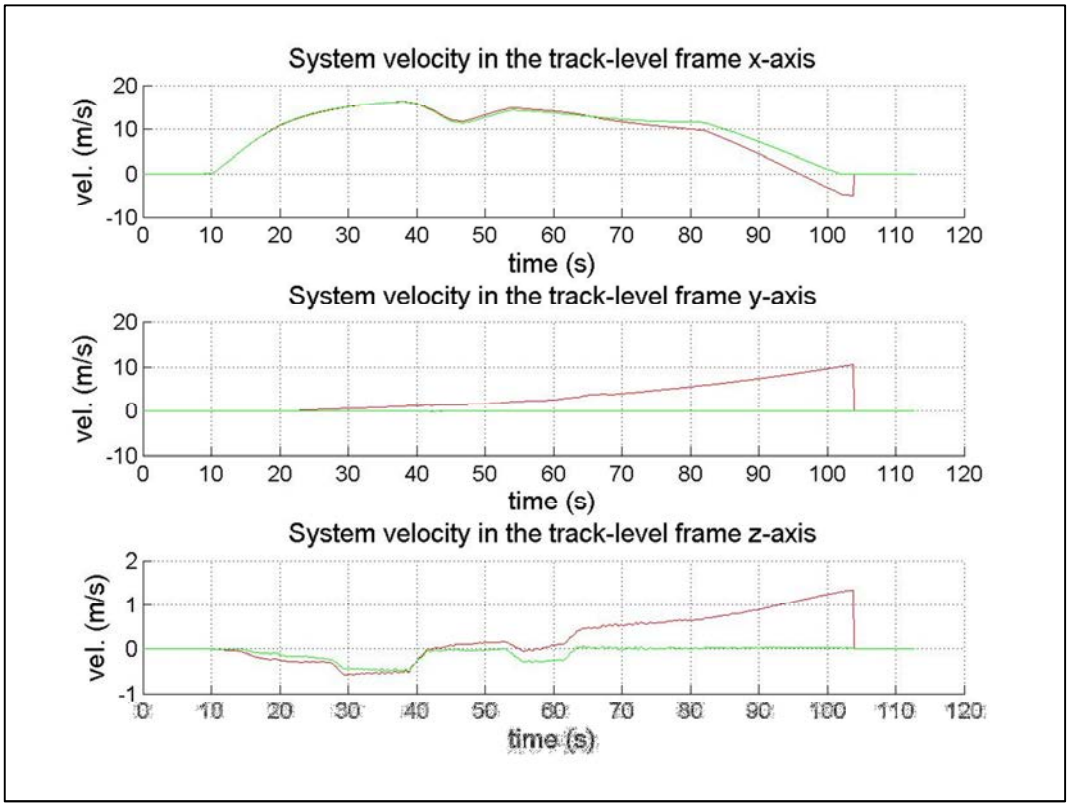

Figure 5.16: INS and RBN derived system velocities

From Figure 5.15, the INS estimated attitudes follow the similar patterns when correlating with that in Figure 5.10. It indicates that the measured train motion is primarily consistent with the theoretical attitudes estimated from the TAP solution. The compensated train vibrations are indicated by the harmonic oscillations in roll and pitch profiles. The magnitude of vibration in the *r* axis is generally larger than that in the *p* axis.

After the train stopped at the POL station platform, the train attitudes are re-initialised from the accelerometers, while the accumulated attitude errors indicate the end of train motion. It is noted that the errors in the *p* axis are considerably larger than that in other axes, which introduce additional velocity and position errors in the longitudinal track direction.

At the end of train motion as shown in Figure 5.16, the INS velocity errors in the *y* and *z* axes exceed $10\,m/s$ and $1\,m/s$ respectively, while that in *x*-axis reaches $5\,m/s$. The sensed gravity acceleration is incorrectly resolved and compensated regarding the excessive roll and pitch errors, which is integrated into velocity errors. In general, the attitude errors may be caused by poor system alignment, uncompensated sensor biases and drifts, unmodelled systematic errors or fault outputs.

Through the RBN solution, the attitude misclosures in all axes have been greatly reduced, while the harmonic oscillations are generally maintained and sufficiently represent the actual train motion. The correctness of system attitudes can be alternatively supported by the greatly reduced velocity errors shown in Figure 5.16.

It can be predicted from the velocity profiles that the horizontal position of INS solution should be considerably large. In contrast, the RBN solution should provide

relatively accurate positioning results in all axes. Figure 5.17 illustrates the horizontal system position and the reference track.

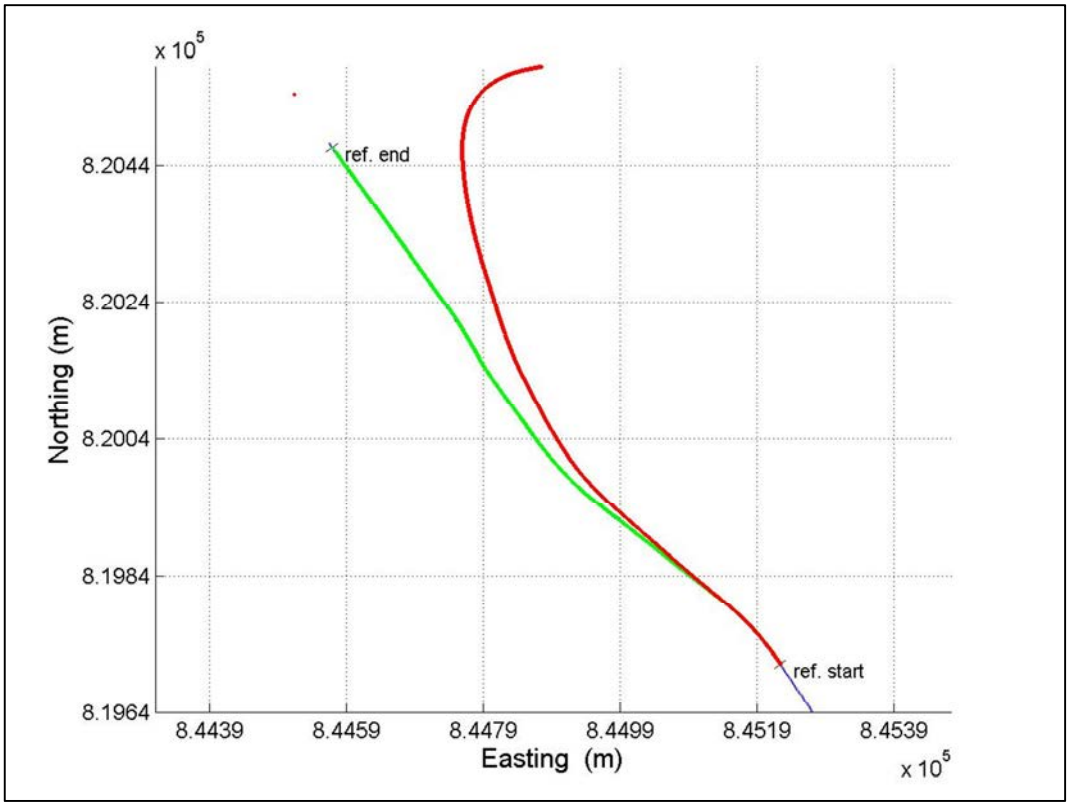

Figure 5.17: The horizontal system position and reference track

The initial reference chainage is around $85.50m$ which was determined from the centre of platform at HAH station. Since the train doors have to be aligned with the corresponding platform screen doors, the relative position of the train with reference to the platform at POL station is the same as that at HAH station. Through the track alignment definition, the corresponding reference chainage at POL station should be $1092.80m$ after the train stopped.

The standalone INS solution has captured the train motion at the first quarter of entire section, while the position errors have been rapidly increased and drifted away from the reference track. According to Figure 5.17, the accumulated horizontal distance reaches $100m$, while the lateral position has drifted for more than $300m$. The position errors are extremely large and cannot be applied to any railway

application. For the RBN results, the chainage error has been greatly reduced from over 100 metre-level to around $-4.6m$. The lateral position is bounded by the reference track. The remaining errors in longitudinal position are still remarkable.

From the navigation results, the patterns of pitch profile have a remarkable distortion, which is probably caused by the physical track defects or nature of train motion. As a result, the pitch errors are not accurately controlled which lead to additional longitudinal position errors.

5.6.4. Summary of Potential and Limitations

Following the comparison, the attitude, velocity and position errors are noticeably reduced by employing the RBN solution, which have initially validated the correctness of the proposed solution. In addition, the implementation in a real world railway system has proved the preliminary discussions regarding the potential and actual performance.

Although the navigation errors are greatly constrained, the position errors are still too large for many railway applications. It is noted that the system simplifications and assumptions may diminish the actual performance. The potential accuracy can be probably improved by further investigation and optimisation, such as physical models for track-to-train transition, dynamic train motion and external train control data. Irrespective of the poor sensor quality and lack of additional control data, the navigation results have nevertheless illustrated the potential of RBN solution.

To further improve and validate the solution, several measures are applied to tackle the potential problems, while the repeatability of result is analysed by redundant measurements, including secondary measurements on the same run and independent runs on the same track section. In addition, the nature of train motion, track

conditions and train operational characteristics are also investigated. The navigation solution is also employed in other track section to examine the consistence of performance.

The possible sources and characteristics of errors should be indicated and verified to examine the actual performance of RBN solution, which are further discussed in Chapter 6.

Chapter 6: Result Analysis and Discussion

In Chapter 5, the TAP solution and the navigation system are briefly examined, while the RBN solution was implemented with the primary sensor outputs. The navigation results of standalone INS and RBN solution were presented. Although a remarkable improvement was shown by employing the RBN solution, the position errors were still notably large.

In this chapter, the possible sources of errors and the characteristics of solution are investigated and verified. The primary and secondary sensors are then employed for the system implementation, such that the navigation results can be compared under the same external conditions, including train motion and track defects. The repeatability of navigation solution is examined through redundant measurements, while the possible systematic errors such as the physical track correction are determined. The proposed navigation solution is then validated by operating the navigation system in independent railway sections.

6.1. Optimisation for Rail-bound Navigation

Although a considerable improvement has been illustrated by the navigation results, the RBN solution requires further optimisation to improve the position accuracy. In this section, the system initialisation, sensor bias recalibration, the track uncertainties and dynamic train motion are analysed and discussed regarding the navigation results for the same track section.

6.1.1. System Initialisation

To investigate the impacts of sampling size to the initialisation results, another set of data was collected on 30/10/2015 with the both stationary phases sustained for about

$35s$. Several methods such as simple average, moving average and EKF have been discussed in Chapter 4 for handling the sensor outputs. Table 6.1 summarises the initial sensor biases and attitudes determined from these different approaches. The moving average method was applied to average the sensor outputs within defined time intervals. To analyse the impacts of different time intervals, the initialisation results computed from the intervals of $0.5s$, $1s$, $5s$, $10s$ and $20s$, are also included. The inconsistent results are coloured in red for comparison.

Table 6.1: Summarised results for different approaches of initialisation

		moving average					simple average	EKF
		0.5s	**1s**	**5s**	**10s**	**20s**		
accel. bias (m/s^2)	***x***	0.000	0.000	0.000	0.000	0.000	0.000	0.026
	y	0.000	0.000	0.000	0.000	0.000	0.000	-0.018
	z	0.000	0.000	0.000	0.000	0.000	0.000	0.000
gyro. bias $(°/s)$	***r***	0.146	0.141	0.146	0.146	0.144	0.139	0.143
	p	-0.028	-0.030	-0.028	-0.029	-0.029	-0.030	-0.037
	h	-0.057	-0.059	-0.059	-0.060	-0.059	-0.060	-0.058
initial att. (°)	***r***	1.302	1.289	1.301	1.301	1.300	1.290	1.121
	p	-0.097	-0.095	-0.087	-0.088	-0.084	-0.265	-0.169
	h	324.980	324.980	324.980	324.980	324.980	324.980	324.954

The initialisation results of moving average at the intervals of $5s$, $10s$ and $20s$ are relatively consistent. In contrast, the initial attitudes, especially the pitch angles, resulted from the moving average at the intervals of $0.5s$ and $1s$ are slightly different from the majority. For the simple average, all the measurements are averaged with equal weight. The initial roll and pitch angles are noticeably different from the majority, while the estimated gyroscope bias in *r*-axis is slightly smaller.

Through the averaging method, more precise accelerometer outputs are provided for direct attitude estimation. According to eqn. A1.11, the accelerometer biases can only be determined from the differences between the norm of accelerometer outputs and the reference gravity acceleration. In this thesis, the accelerometer outputs are

assumed accurate such that the difference is resolved into the estimation of gravity anomaly. The accelerometer biases therefore cannot be determined, which are theoretically undetermined and should be all zeros. However, the EKF results do not agree with the assumption. On the contrary, the estimated magnitudes of accelerometer biases are considerably large.

In practice, the measurement error model has introduced an additional correlation with the attitudes such that the attitude errors are resolved into the accelerometer biases. In addition, the initial attitudes are optimised from the previous measurements, while the additional inertial measurements are redundant. The measurement errors and noises are therefore contributed to the estimation of accelerometer biases. Since the random noises are accumulated in the accelerometer biases in different axes, the compensated measurements are no longer consistent with the actual attitudes, especially for low-cost inertial sensors. Consequently, the excessive attitude errors, as well as the accelerometer biases, are progressively accumulated.

To conclude, the moving average at around $5s$ to $10s$ interval can sufficiently improve the precision of inertial measurements and provide reliable initialisation results. Since the measurement error models are established from the mathematical models for initialisation, the initial covariance of navigation system can be propagated and updated by the EKF to establish the correlation between the system states.

6.1.2. Sensor Bias Recalibration

The estimation of sensor bias is one of the major factors for the performance of a navigation system. After the system initialisation, the sensor turn-on biases are estimated and compensated. For low-cost sensors, the growth of sensor uncertainties

and the bias drifts are relatively larger, which would introduce additional variability for the implementation.

For a typical INS/GNSS solution, the GNSS measurement noises are generally random and large, which would not cause significant impact to the sensor recalibration. In contrast, the reference trajectory is estimated by the TAP solution that any track defect may cause bias to the nominal trajectory. In addition, the train oscillations would further contribute to the discrepancies between INS and TAP navigation results.

In general, the measurements are considered zero-mean and randomly distributed. Any systematic discrepancy between the measurements and the predicted navigation results indicates the system navigation biases which are caused by the inertial sensors. The systematic discrepancies for RBN solution, however, are also impacted by the train oscillations.

To examine the actual impacts, the profiles of accelerometer and gyroscope biases are estimated and shown in Figure 6.1 and Figure 6.2 respectively. The original sensor biases are coloured in red, while the revised results are coloured in green.

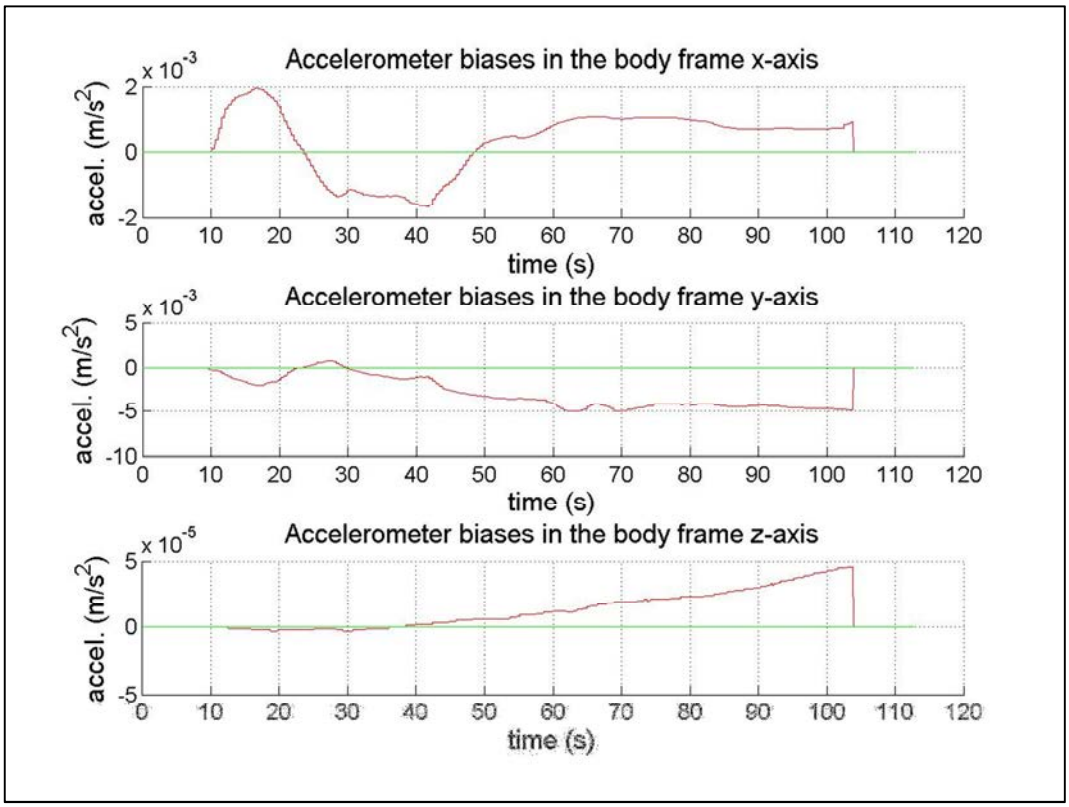

Figure 6.1: RBN derived accelerometer biases

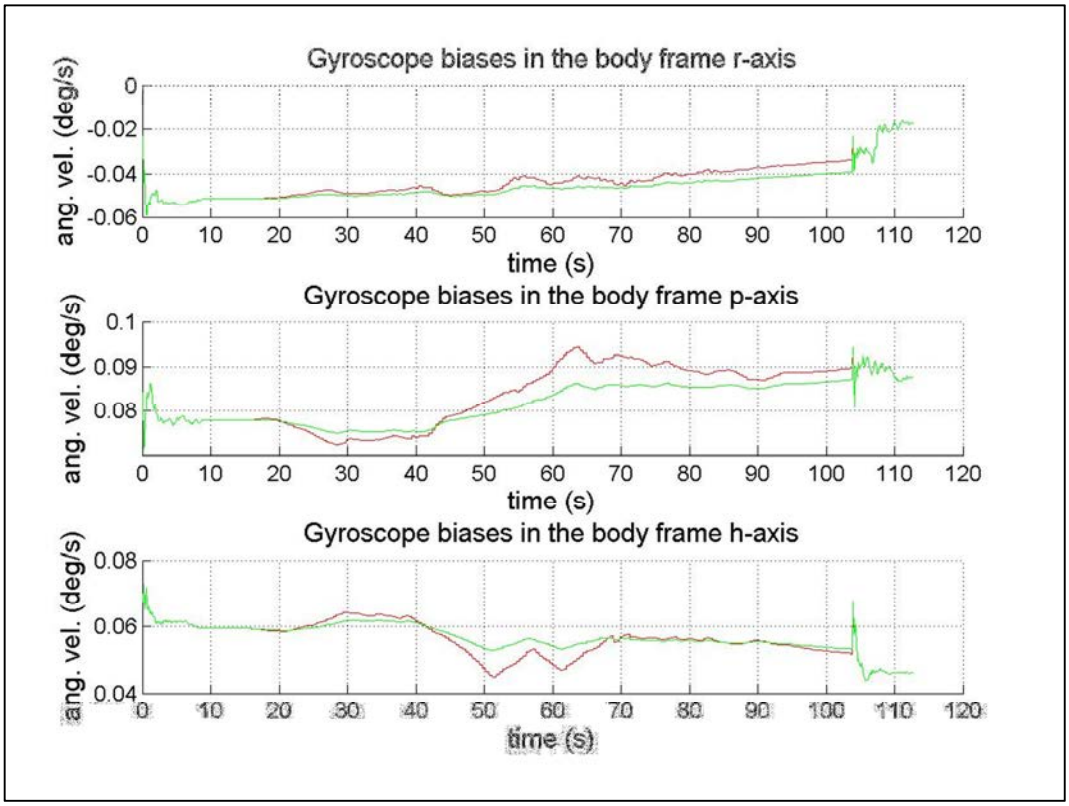

Figure 6.2: RBN derived gyroscope biases

The sensor biases have generally drifted at the rate specified by the manufacturer. According to the results, the changes of sensor biases are relatively rapid and abnormal through the recalibration with the constrained train motion. Although the navigation solution is continuously constrained, the incorrect sensor biases would introduce excessive navigation errors. Consequently, the adaptive measurement covariance would be increased, while the TAP constraint would be loosened.

From the estimation results, the sensor biases at the initialisation and finalisation phases are coherent, such that the drifts of sensor biases are small. To minimise the impacts of incorrect sensor biases, the dynamic displacement and misalignment terms can be added to the navigation system error state and propagated with the filtering process, such that the systematic errors can be alternatively resolved into the corresponding terms. However, the navigation system remains unchanged in this thesis to maintain the simplicity and independence of the components. Alternatively, an individual complementary filter could be applied to remove the short-term impacts and excessive errors from the sensor biases.

For the accelerometer, the measurements in y and z axes are constrained by the track, while the measurement in x axis contributes to train motion and is not controlled. The accelerometer bias in x axis is therefore nearly unobservable. Although the track constraints provide redundancies to calibrate the accelerometer biases in y and z axes, the bias are greatly correlated to the attitude errors which are biased by the train oscillations. As a result, accelerometer biases are neglected unless the dynamic train motion is precisely modelled and compensated.

6.1.3. Additional Track Uncertainties

From the navigation results, the angular discrepancy in the *p* axis indicated that a track defect may exist in the experimental section such that the pitch errors are over-constrained by the inaccurate TAP solution. To retain the physical motion, additional track uncertainties regarding the position and attitude are introduced to the measurement error models. The recomputed velocity and attitude profiles are illustrated in Figure 6.3 and Figure 6.4 respectively The previous results are coloured in red and the recomputed results with additional track uncertainties are coloured in green.

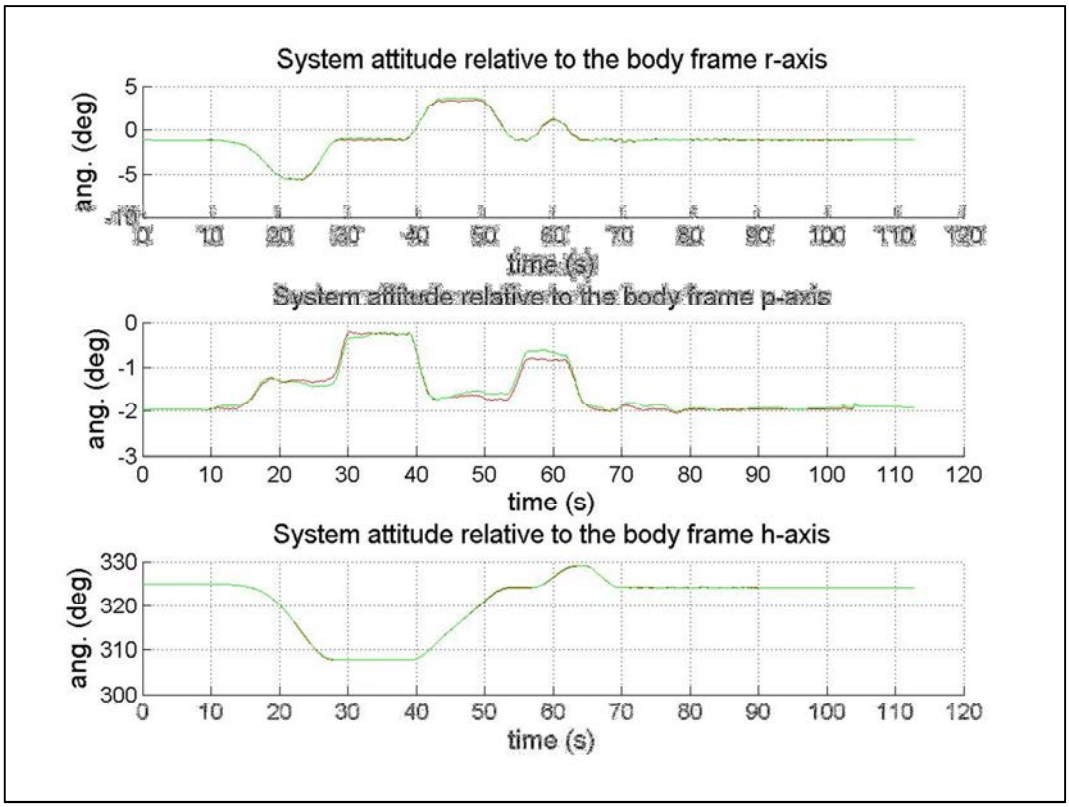

Figure 6.3: RBN derived attitudes with additional track uncertainties

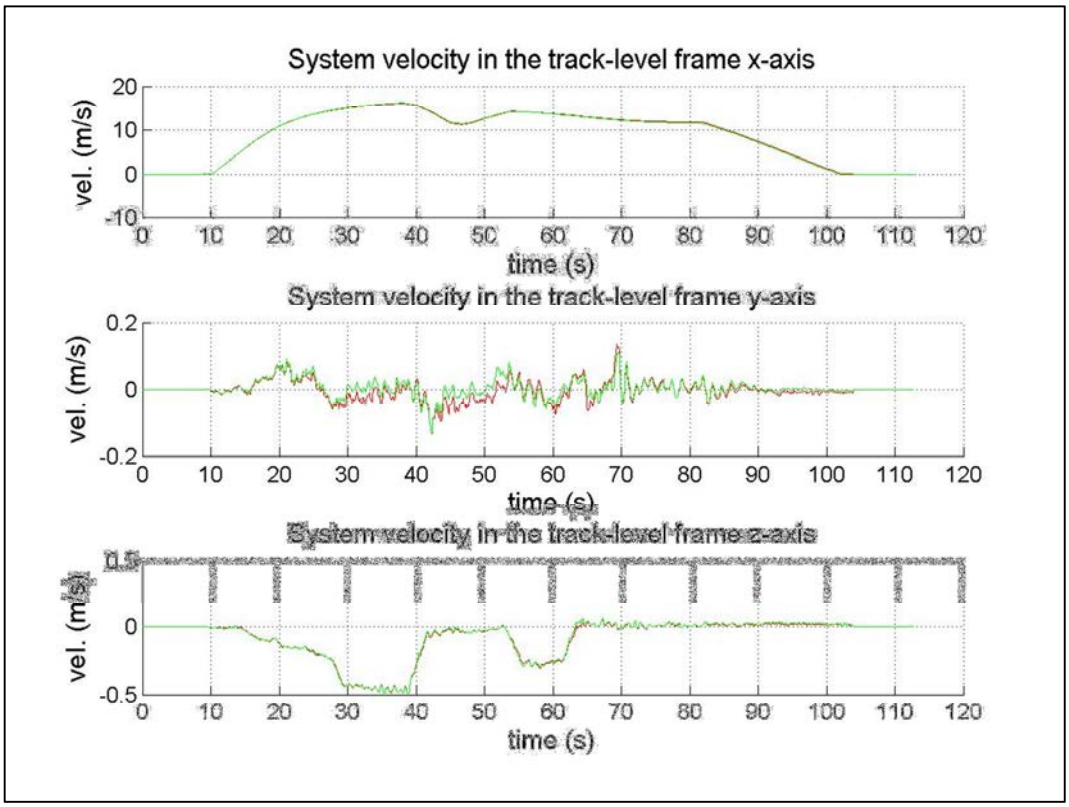

Figure 6.4: RBN derived velocities with additional track uncertainties

From Figure 6.3, the estimated attitudes, especially the pitch, are less constrained, such that the recovery of actual track geometry is more accurate. According to Figure 6.4, the velocity profiles in the *t*-frame *y* and *z* axes are slightly smoothened, which are considered closer to the actual motion because of the loosened constraints. The resultant chainage, however, has changed from $1088.2m$ to $1083.4m$ so the longitudinal position error is slightly larger. A possible reason to this outcome is that the track uncertainties are not correctly optimised. To validate the performance of RBN solution, further investigation and analysis will be conducted in later sections.

6.1.4. Dynamic Motion for Train Oscillation

Although the RBN solution employs TAP results for error control, the train oscillations would introduce biases to the error control process. The dynamic misalignment and displacement are estimated from the discrepancies between TAP and navigation results as shown in Figure 6.5 and Figure 6.6 respectively.

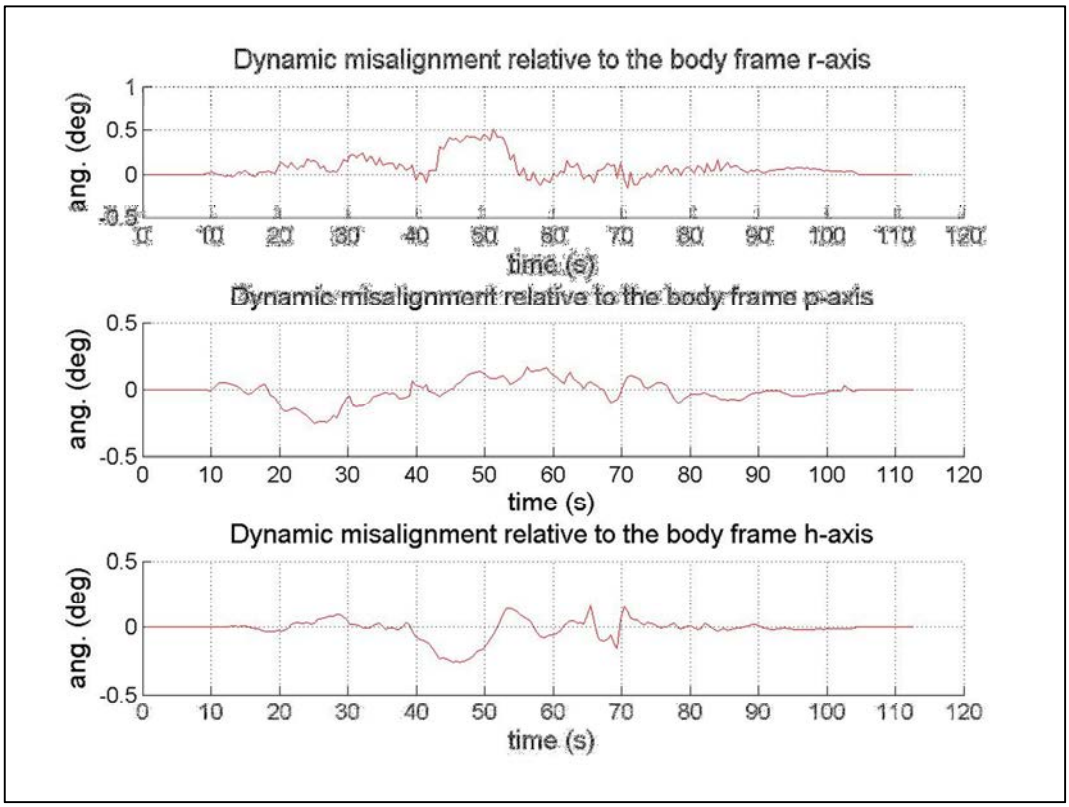

Figure 6.5: Dynamic misalignment of *a*-frame relative to the b-frame

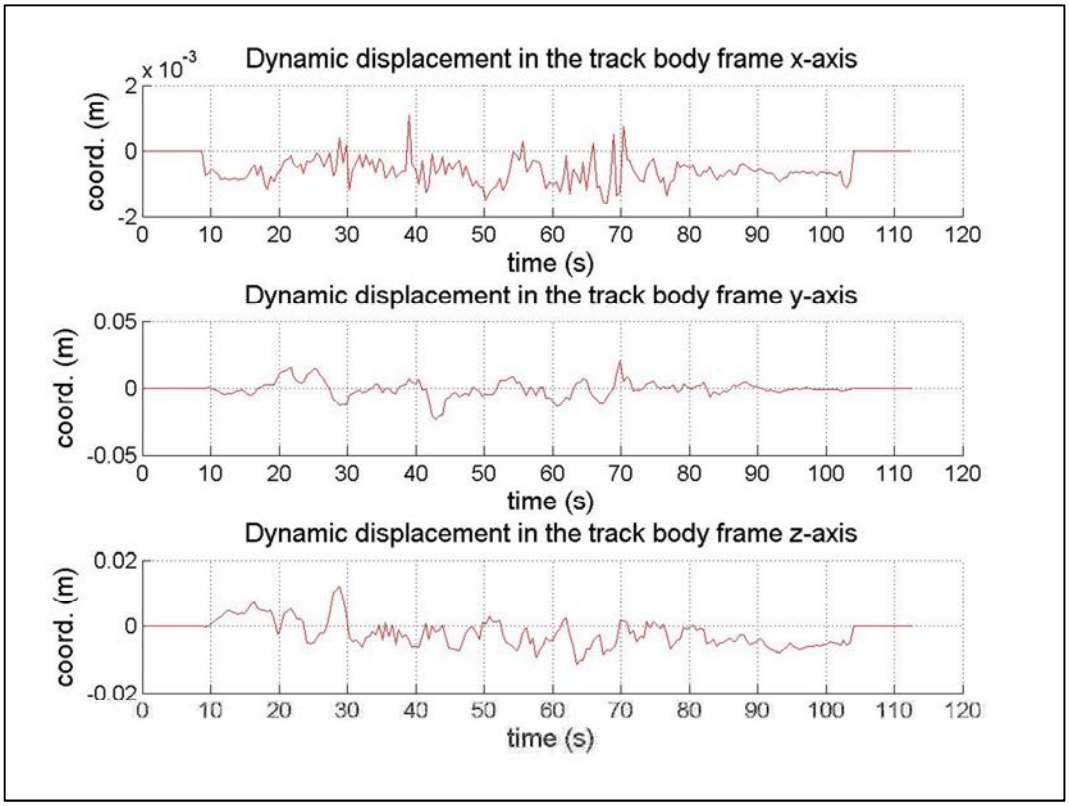

Figure 6.6: Dynamic displacement resolved into the *a*-frame

According to Figure 6.5, the frequency and magnitude of train oscillations in the roll axis are relatively higher than that in other axes, which conforms with previous predictions. Although the non-zero values may indicate the attitude errors or inaccurate constant misalignment, the biased misalignment may be caused by uncompensated physical track defects.

During the period from around $40s$ to $70s$, a noticeable heading misalignment can be found at curved sections with a magnitude near $\pm 0.2°$. The heading misalignment is possibly caused by the inaccuracy of track-to-train transition correction or chainage-originated TAP attitude errors.

A low-rate oscillation can be observed from the dynamic misalignment in the *p* axis. The rate of pitch misalignment changes with time, which does not correspond to the characteristics of high-frequency train oscillation or long-term sensor bias drift. As a result, the dynamic misalignment indicates the existence of track defect.

In Figure 6.6, the longitudinal dynamic displacement should be theoretically zero. The non-zero errors are mainly caused by transformation errors, such that the non-zero offsets are resolved into the *x* axis of the *a*-frame. In contrast, the lateral dynamic displacement is relatively large (generally bounded by $0.02m$), which is possibly caused by uncompensated track-to-train transition errors, transformation of offsets or uncompensated train vibrations.

The high-frequency train oscillations are fundamentally compensated through the estimated dynamic misalignment. From the profile of vertical dynamic displacement, a constant rate of drift is discovered, which may indicate the existence of uncompensated sensor biases or physical track defects.

6.2. Multi-IMU Navigation Results

In section 6.1, abnormal patterns have been identified from the navigation results, which may be caused by sensor errors or physical train motion. To clarify the source of errors, the navigation results are recomputed by employing both the primary and secondary sensors in this section. Through the comparison of individual navigation results, the discrepancies are independent of train motion and track defects, which are primarily caused by sensor errors.

The primary and secondary IMUs are separately processed by individual processing units, which are time tagged with internal sensor clock and are not synchronised. As a result, a constant time difference can be found between the two sets of measurement data. To facilitate the analysis, the results are stored and shown with respect to chainage.

6.2.1. Discrepancies between Navigation Results

After the initial study of navigation results, the overall accuracy is yet to be maximised. For further investigation, the navigation results are individually estimated from the primary and secondary solutions, which are coloured in red and green respectively. The attitude profiles and discrepancies (primary – secondary) are summarised in Figure 6.7 and Figure 6.8 respectively.

The attitude, velocity and position errors of both sets of navigation results are tabulated in Table 6.2.

Table 6.2: The attitude, velocity and position errors from the two sensors

IMU	Attitude Error (°)			Velocity Error (*m/s*)			Position Error (*m*)		
	r	***p***	***h***	***x***	***y***	***z***	***x***	***y***	***z***
1	0.023	-0.012	0.023	-0.012	0.023	-0.012	-9.444	-0.001	-0.005
2	0.030	-0.011	0.030	-0.011	0.030	-0.011	8.934	-0.003	-0.004

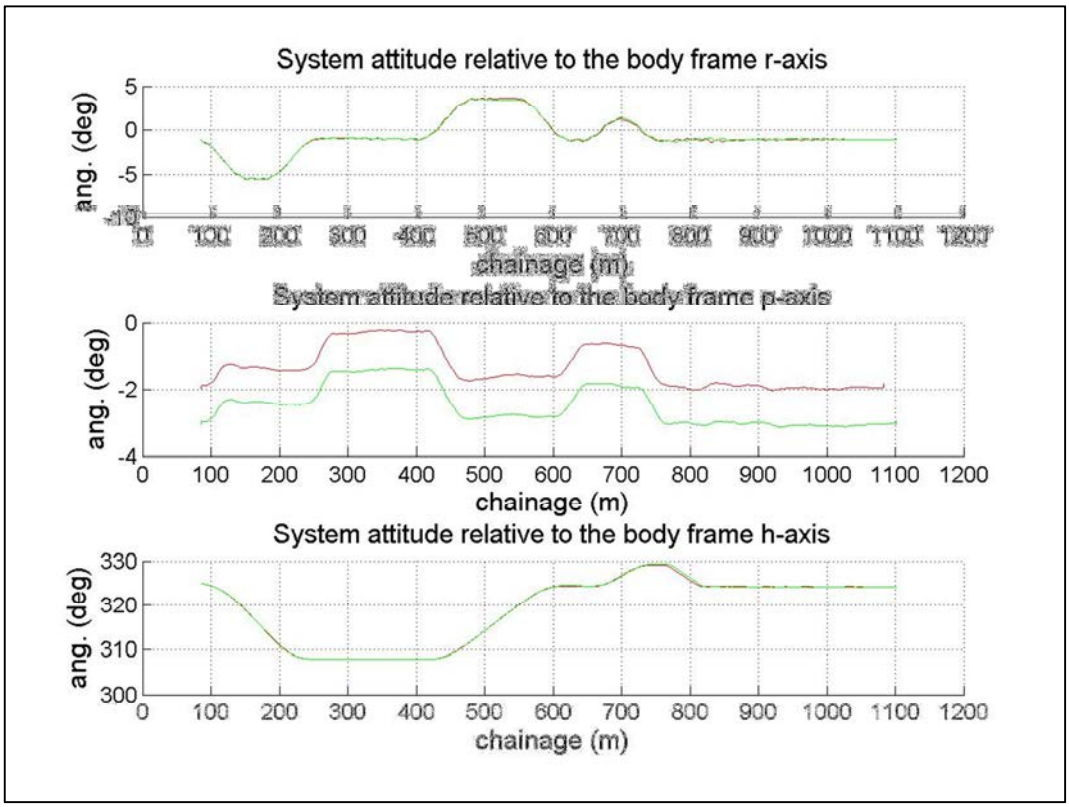

Figure 6.7: System attitudes estimated from the two sensors

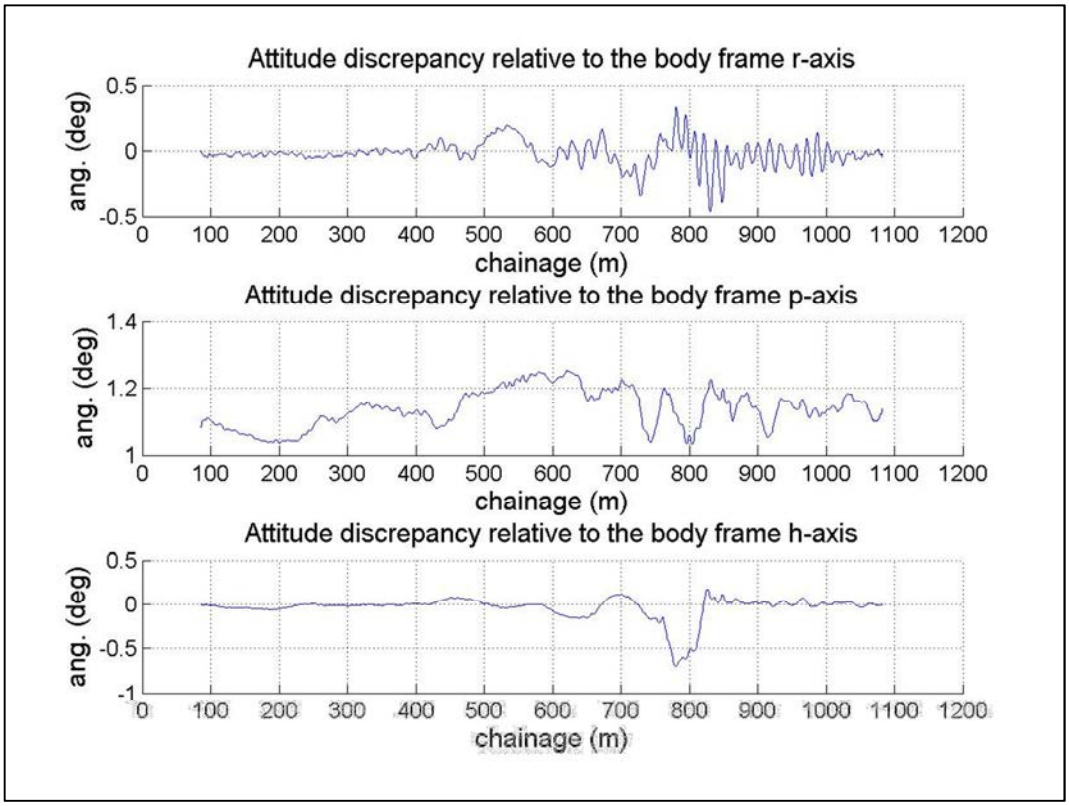

Figure 6.8: Attitude discrepancies between the two sensors

According to Figure 6.7, the attitude patterns are consistent with each other in all axes. The angular discrepancies are estimated by subtracting the secondary results from the primary results as shown in Figure 6.8, while a constant angular offset of around 1.1° is found in the p axis. The small angular discrepancies indicate the consistence of the results, which are progressively increased after chainage $450m$. The standard deviations of angular discrepancies in the roll, pitch and heading axes are 0.09°, 0.06° and 0.13° respectively, which represent the angular uncertainties caused by sensor and chainage errors. Although the sensors are well aligned in roll and heading axes, abnormal patterns can be identified after chainage $450m$. To investigate the causes of discrepancies, the velocity profiles and discrepancies are summarised in Figure 6.9 and Figure 6.10 respectively.

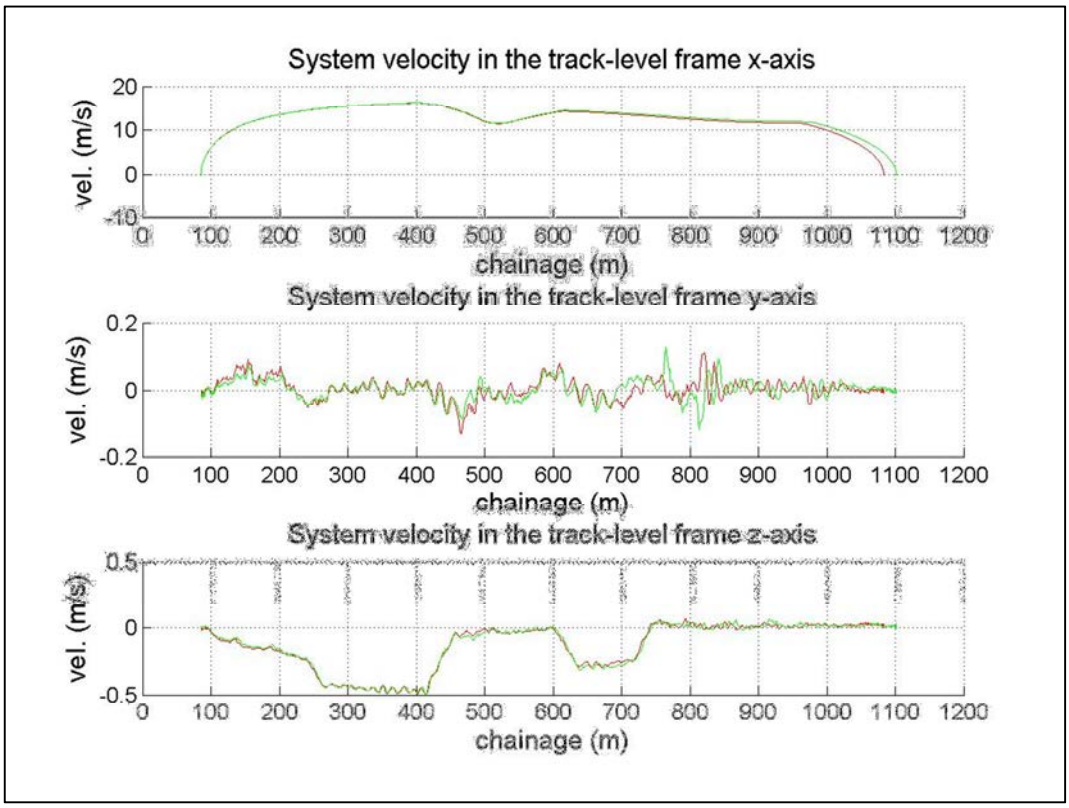

Figure 6.9: System velocities estimated from the two sensors

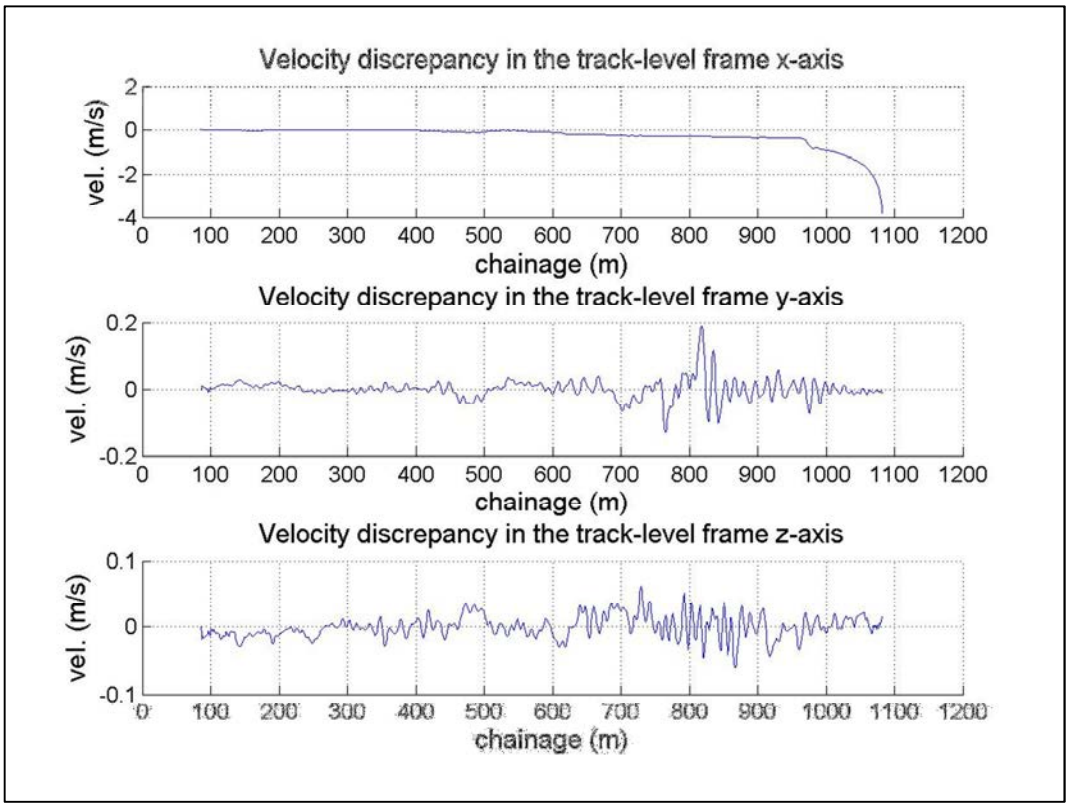

Figure 6.10: Velocity discrepancies between the two sensors

According to Figure 6.9, both sets of the results are generally consistent in the first half of the motion, which denote that the train motion has been correctly captured and represented. However, the velocity profiles of the secondary solution have shifted away from that of the primary solution at about $18.4m$ at the end of train motion (shown in Table 6.2). In Figure 6.10, the velocity discrepancies in the *y* and *z* axes oscillate at around zero and are bounded by $0.2\,m/s$ and $0.05\,m/s$ respectively, while discrepancies in all axes have been progressively accumulated after chainage $450m$.

From the results, a noticeable heading error can be seen at around chainage $450m$, such that the velocity is incorrectly resolved into the lateral direction. Consequently, the velocity error in the longitudinal track direction are gradually integrated into chainage error. In the meanwhile, the roll errors are caused by the chainage error as

shown in the Figure 5.12, which are accumulated at a rate and rebounded at around $550m$ where the train has entered into curve section with opposite radius.

Since both of the navigation solutions are theoretically identical under the same train motion and track conditions, the discrepancies of navigation results are primarily resulted from the sensor measurement errors.

6.2.2. Uncompensated Dynamic Motion

Since the RBN solution is implemented with several assumptions for train dynamics, the actual motion such as track-to-train transition, train vibration nature, or relative motion between train car and bogies may not be accurately compensated. The differences between partially compensated motion (from TAP) and estimated motion (from navigation solution) are represented by the dynamic misalignment and displacement as illustrated in Figure 6.11 and Figure 6.12 respectively.

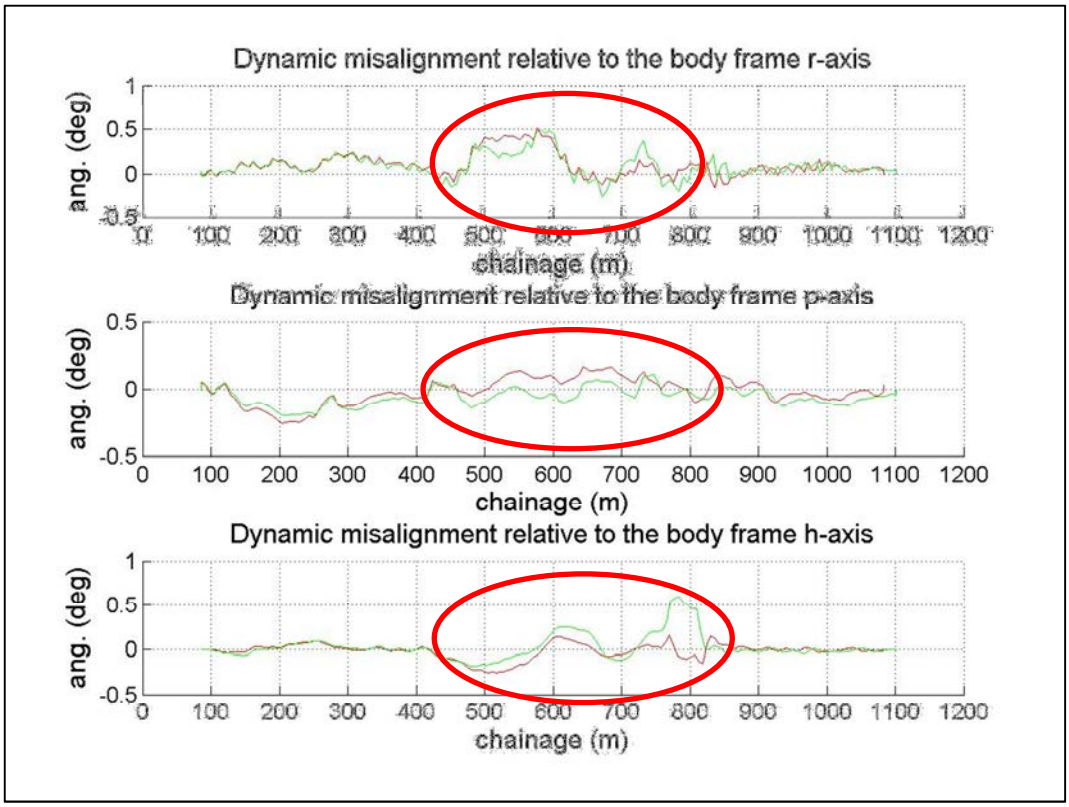

Figure 6.11: Dynamic misalignment estimated from the two sensors

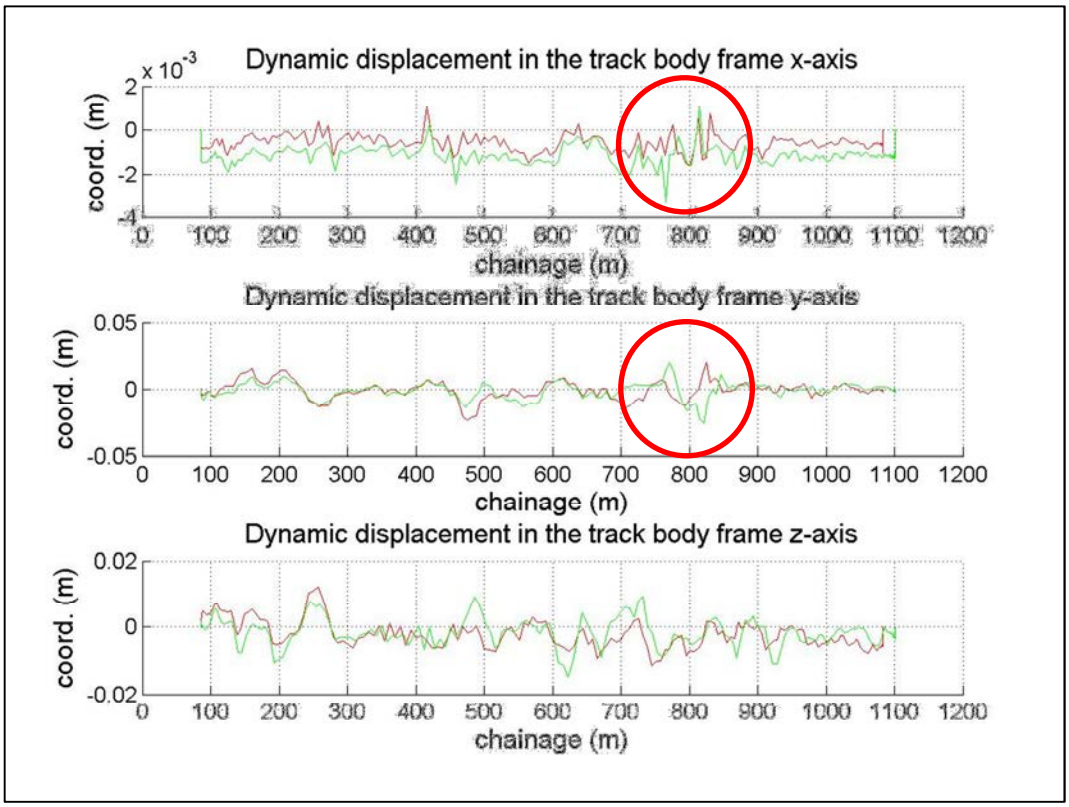

Figure 6.12: Dynamic displacement estimated from the two sensors

The dynamic misalignment and displacement between both solutions are generally coherent but slightly different at around $500m$ to $800m$, especially the roll and heading. Since the discrepancies are probably caused by the uncompensated misalignment errors, an empirically determined correction profile can be estimated to minimise the error of reference track results by removing high rate vibrations.

It is noted that the dynamic displacement is more localised when compared to the misalignment. This is resulted from an additional attitude compensation for CUPT that the part of the train motion has been removed from the dynamic displacement. In contrast, the dynamic misalignment is estimated without additional corrections with respect to the train motion.

According to the measurement error models, the covariance matrices regarding the dynamic motion are determined by the adaptive method. The attitude differences between the TAP solution and the navigation results, as well as the relevant

covariance, would be reduced. However, the attitude correction profile retrieved from the navigation results may be biased by uncompensated chainage error and low rate train oscillations, which is not appropriate for direct physical track correction until a more comprehensive solution has been established. In addition, the dynamic misalignment and displacement may be caused by the train motion which may be not be consistent for each run.

6.2.3. Combine Navigation Solution

As illustrated in these results, the sensor errors have introduced noticeable discrepancies into the navigation results. To minimise the impacts of sensor errors, both the primary and secondary measurement data are applied to a combined navigation solution.

It is noted that the angular misalignment between the primary and secondary sensors are relatively stable as both are attached at a rigid platform. The discrepancies between two sets of accelerometer measurement data are therefore approximately constant. To simplify the implementation, the primary navigation system is retained, while the secondary sensor measurement data are only applied for smoothing the primary inertial measurements by a complementary filter.

After implementing the combined navigation solution, the system attitudes, velocities, dynamic misalignment and displacement are closely aligned with previous results, but the chainage error has been reduced from $-9.4m$ to $-5.2m$ by the same set of system parameters.

6.3. Repeated Navigation Results

To examine the performance and repeatability of the RBN solution, three sets of experimental data (including the previous set of data) were individually collected

along the same section of track. The corresponding information including the date, time and period of motion, are summarised in Table 6.3.

Table 6.3: Summary of data collection

Set	Date of collection	Time	Period of time (second)			Track section	
			Initial	Motion	Final	From	To
A	13/08/2015	18:06	8.5	95.0	8.5	HAH	POL
B	13/10/2015	21:24	18.1	90.0	18.1	HAH	POL
C	30/10/2015	20:27	29.4	88.0	26.7	HAH	POL

6.3.1. Physical Track Conditions

The accuracy of track reference, especially the attitudes, is a primary concern for the performance of RBN solution. To investigate the physical track conditions, the navigation solutions are optimised such that the chainage errors are bounded within sub-metre-level, which can be implemented by slightly adjusting the uncertainties of track reference attitude regarding the physical track conditions. Figure 6.13 shows the attitude profiles of solution A, B and C which are coloured in red, green and blue respectively.

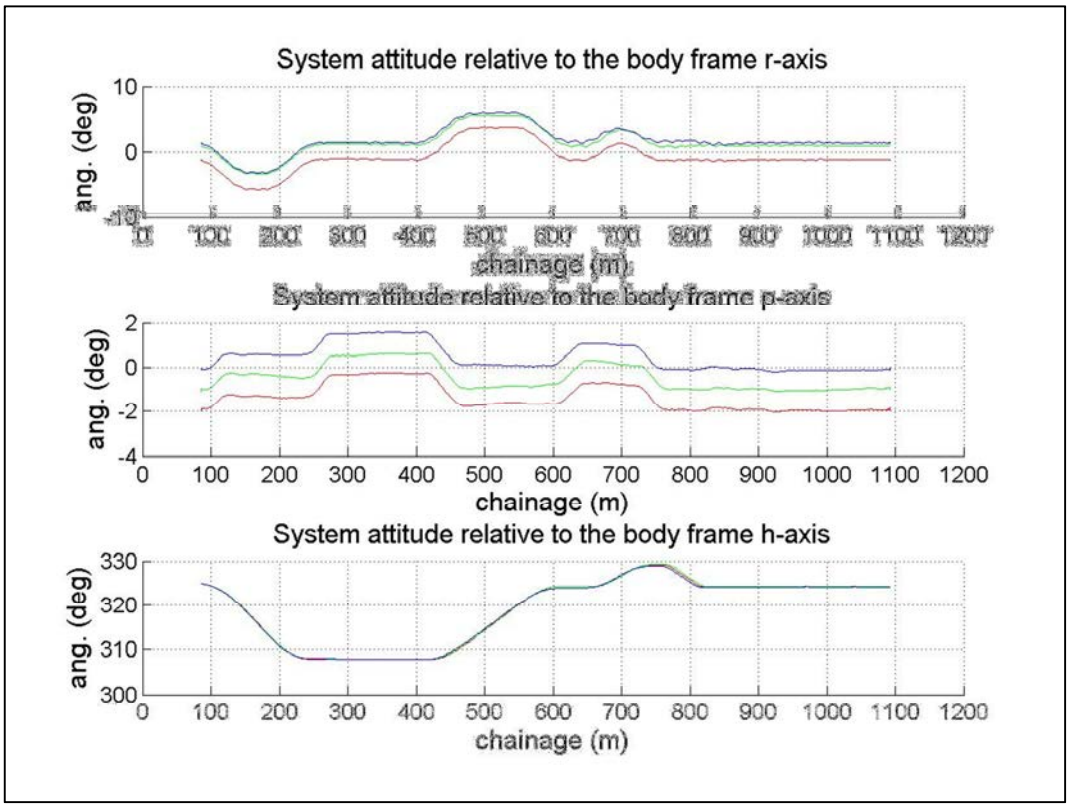

Figure 6.13: System attitudes estimated from the three sets of data

As shown in Figure 6.13, the curves of three solutions are rather consistent. The constant angular offsets are caused by the constant misalignment of the system as it was placed on the floor of the carriage relative to the track reference. Since the chainage errors are not compensated, the curve patterns are slightly offset along the chainage axis. The results show that the major train oscillations in the *r* and *p* axes are rather coherent. The relative distortions between the curves are most likely caused by the over-constraint problems mentioned previously. The physical train attitudes are retrieved by subtracting the TAP attitudes from the system attitudes, which are expressed in form of dynamic misalignment as shown in Figure 6.14.

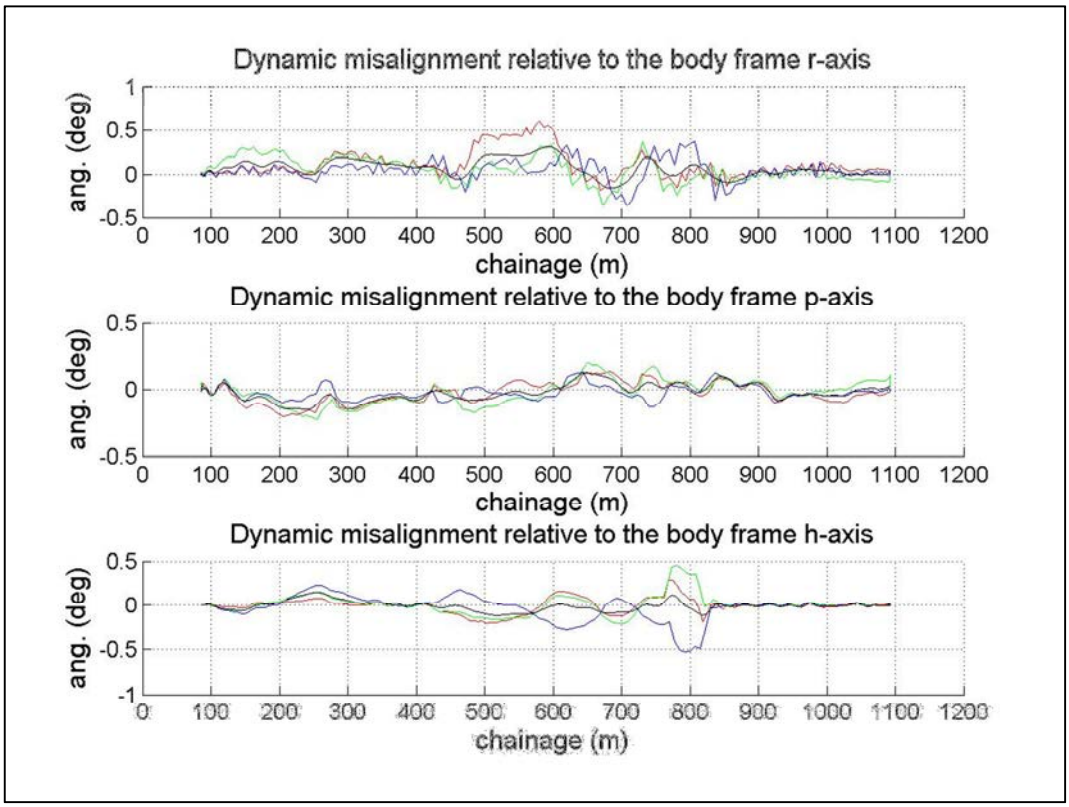

Figure 6.14: Dynamic misalignment estimated from the three sets of data

The relative discrepancies may be caused by the chainage-originated track errors, independent train motion or inappropriate weights for navigation error control. To remove the high-rate train oscillations and the discrepancies of train motion, the results are smoothened and averaged. As illustrated in Figure 6.14, the curves which are coloured in black represent the general dynamic misalignment within the experimental section after compensating the run-to-run variations. The low-rate train motion and track attitude errors are remained in the resultant misalignment.

6.3.2. Train Motion and Velocity

In addition to the track conditions, the train velocities have been resolved into the *t*-frame and represented in Figure 6.15 for further investigation.

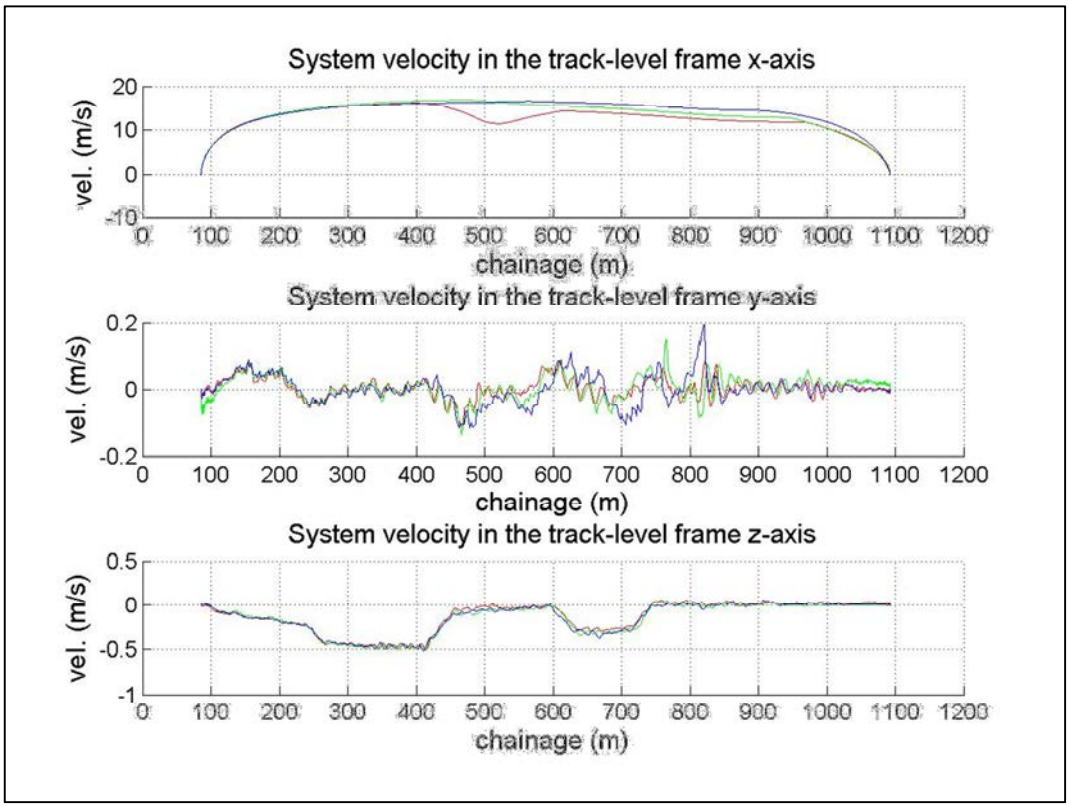

Figure 6.15: System velocities estimated from the three sets of data

Since the train acceleration and braking are computer controlled with feedback of velocity data, the run-to-run velocity profiles should be slightly different with varying operational conditions. The run-to-run variations for the velocity in the *x* axis are rather small during the train accelerating phase, while the braking curves are similar at a train speed under $5\,m/s$.

The velocity profiles in *y* and *z* axes are closely aligned. The discrepancies in *y* axis can be found at around $450m$ to $800m$, which are probably resolved from the run-to-run variations of train velocity. It is noted that the high-rate velocity oscillations in the *y* axis are sometimes consistent, which conform to the findings in attitude results. The position differences between the TAP estimates and the navigation results are represented by the dynamic displacement as illustrated in Figure 6.16.

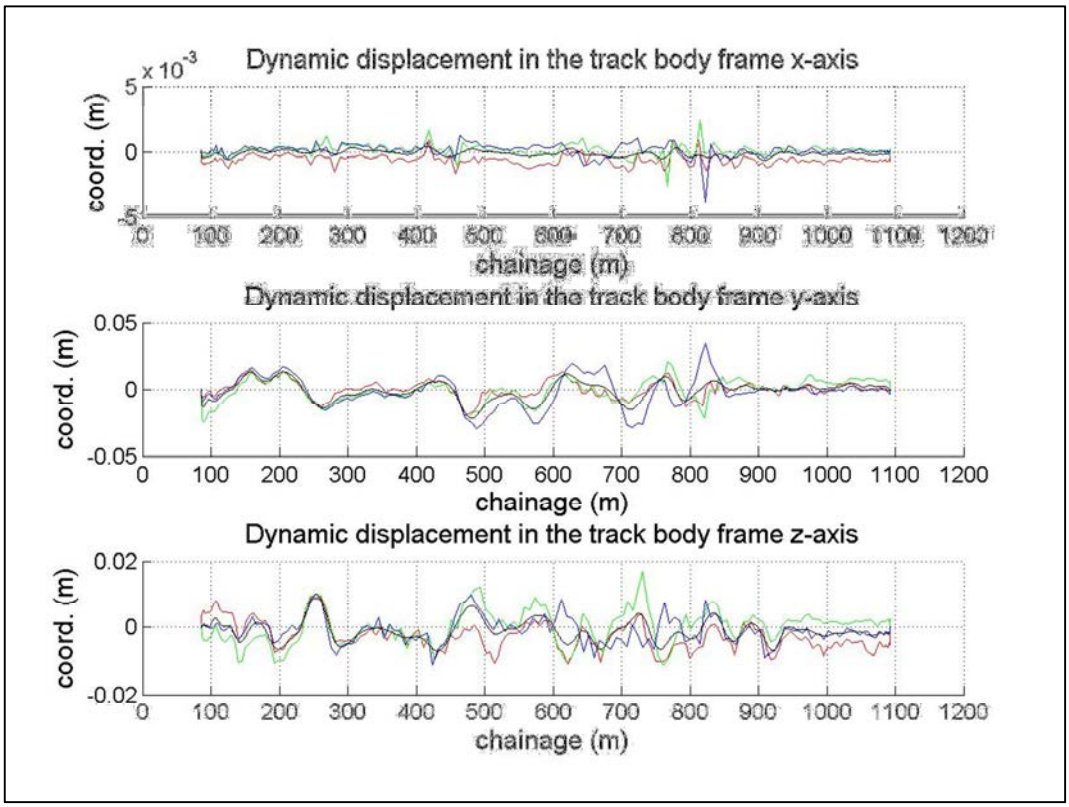

Figure 6.16: Dynamic displacement estimated from the three sets of data

Similar patterns can be found in the dynamic displacement profiles, while the run-to-run variations are directly proportional to estimated velocities in the corresponding axes. However, it is found that the dynamic displacement and velocity, as well as the dynamic misalignment, for solution C are slightly different from the averaged results, which may be caused by inappropriate weight control.

In summary, the train motion is generally consistent within the same track section even travelling at different train speeds.

6.3.3. Repeatability of Navigation Results

In this section, the navigation results are computed from the three independent sets of experimental data such that the run-to-run sensor errors and train motion are independent. In general, the resultant dynamic misalignment and displacement are zero-mean, which indicate the correctness of additional compensation to the TAP

estimates. The RMS of smoothened dynamic misalignment and displacement (high rate train motion removed) are computed from the averaged results, which are shown in Table 6.4.

Table 6.4: RMS of dynamic misalignment and displacement from averages

Solution	RMS of misalignment (°)			RMS of displacement (m)		
	r	*p*	*h*	*x*	*y*	*z*
A	0.097	0.035	0.062	0.001	0.004	0.003
B	0.087	0.041	0.091	0.000	0.005	0.003
C	0.108	0.049	0.141	0.000	0.007	0.003

Although the run-to-run variations are expected, similarity can be found from the profiles of navigation results. Table 6.4 shows that the RMS of dynamic misalignment for solution C is slightly larger than others, while the RMS of dynamic displacement for all the three solutions are small (millimetre-level).

The long-term variations from zero-mean are primarily caused by the track defects. In contrast, the low-rate variations (period of 100-metre-level) are mainly caused by any systematic nature of train motion or uncompensated errors from the TAP estimates, while the high-rate variations (period of 10-metre-level) indicate the resultant train motion compensated by the bogies.

According to the optimised results, the high rate train motions can be measured by and recovered from the RBN solution. In addition, the long-term variations and low rate temporary variations can be retrieved from the three sets of navigation results, which are rather consistent over repeated runs as shown in Table 6.4. Apart from the accuracy, the RBN solution can be an alternative method to continuously monitor the train motion, while the variations of entire track geometry can be repeatedly measured.

6.4. Validation with Alternative Track Section

To confirm the RBN solution a set of data was collected on 13/10/2015 for another section of track. The section is the eastbound track connected from TKO station to HAH station. The navigation results illustrated in this section were computed based on the knowledge gained from the initial study, while several system parameters were empirically reweighed.

6.4.1. General Navigation Results

The profiles of attitude are shown in Figure 6.17. The estimated velocities are resolved in the *t*-frame and shown in Figure 6.18. The results of the standalone INS and the RBN solution are plotted in the figures relative to time, which are coloured in red and green respectively.

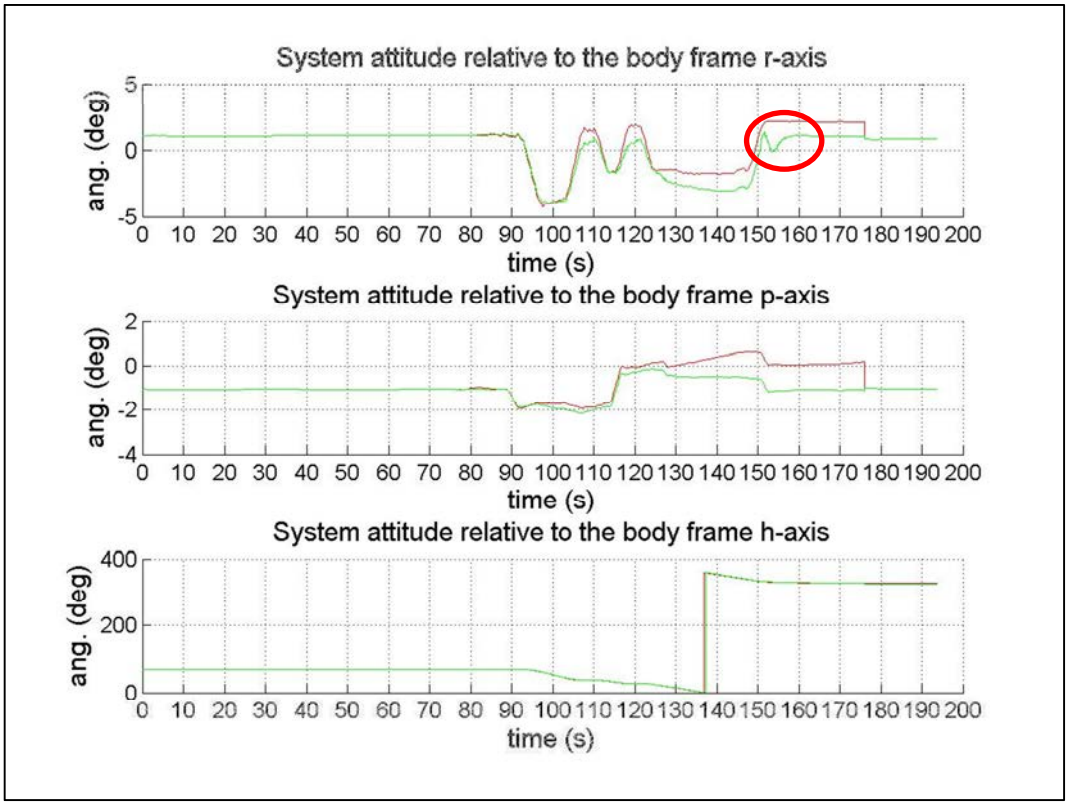

Figure 6.17: INS and RBN derived system attitudes

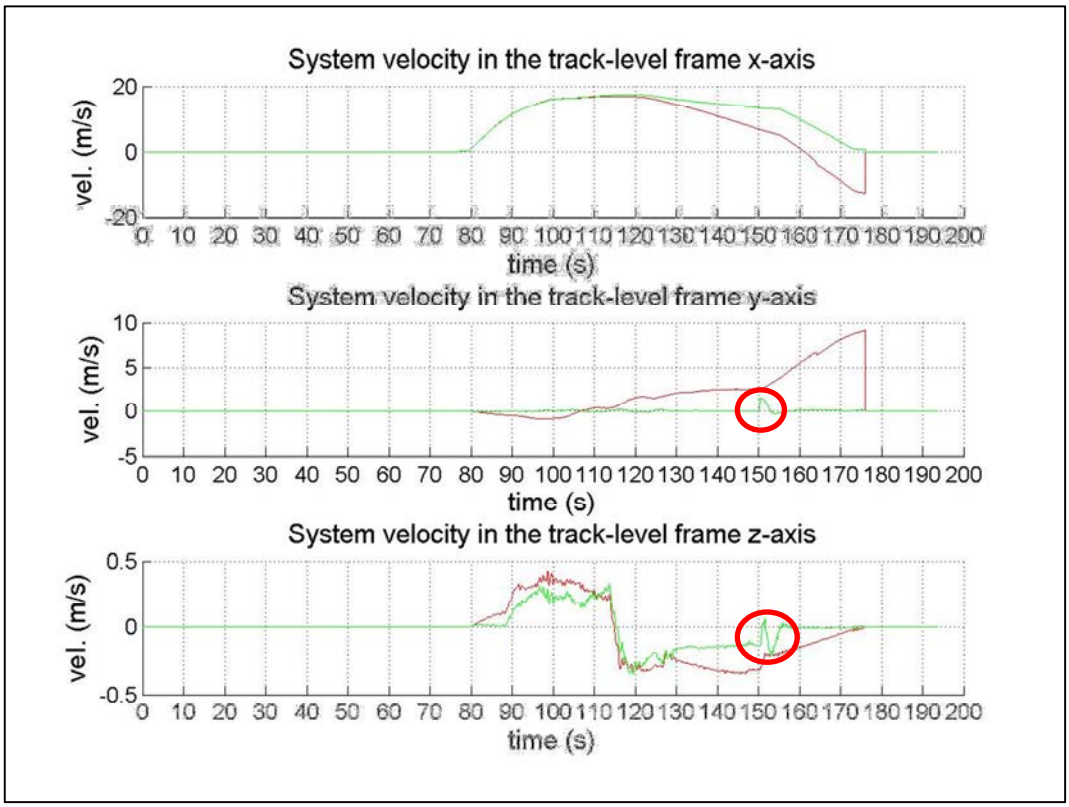

Figure 6.18: INS and RBN derived system velocities

According to the navigation results, the drifts in attitude and velocity errors are greatly controlled by the RBN solution. However, an abnormal roll error can be detected at around $155s$, which lead to an additional velocity error in both the y and z axes. The abnormal error is mainly caused by chainage-originated track attitude errors. However, the navigation results are optimised such that the chainage error should be insignificant to that magnitude of attitude error.

6.4.2. Incorrectness of Track Data

To verify the source of error, the navigation results are compared with the TAP estimated system attitudes. Figure 6.19 shows the system attitudes which are derived from the TAP solution and the standalone INS.

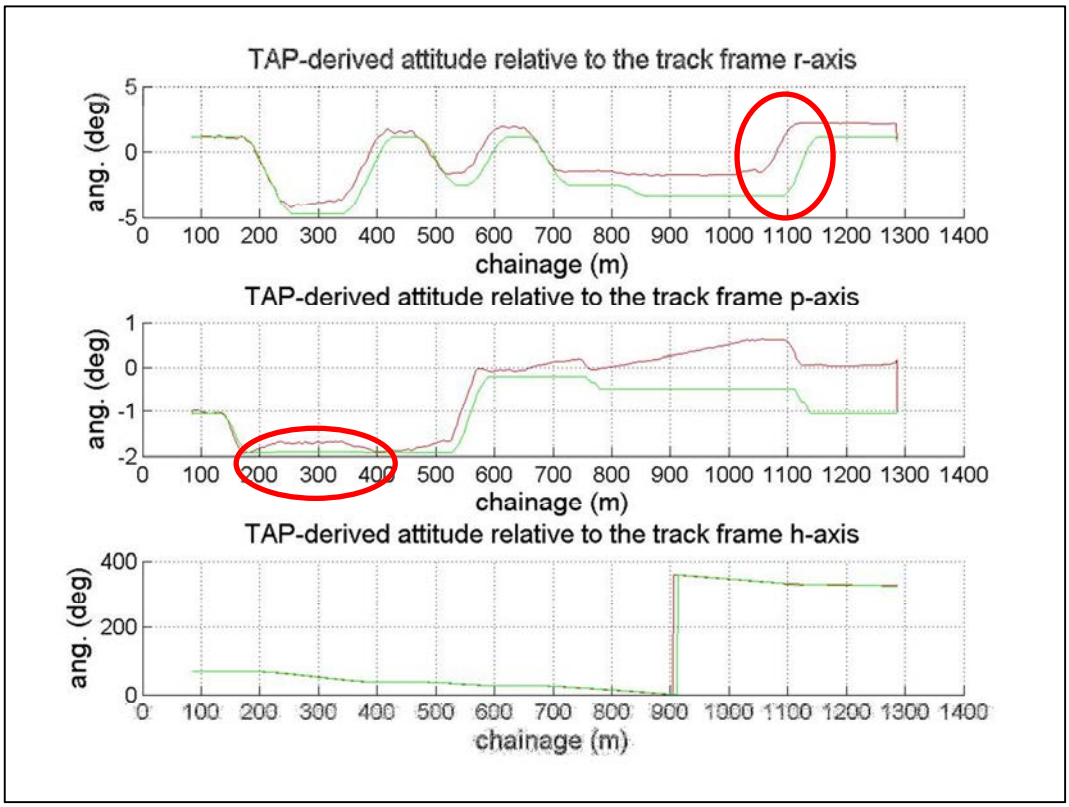

Figure 6.19: INS and TAP derived system attitudes

It is found that the pitch and heading profiles are generally coherent by ignoring the drifts of attitude caused by uncompensated sensor biases. In contrast, the roll profiles are shifted in the chainage direction by few metres.

In addition, abnormal patterns can be identified from the INS derived pitch angles from around $200m$ to $400m$, and from around $1050m$ to $1150m$, which indicate that the track alignment data is not absolutely consistent with the physical track.

Investigation revealed that the track alignment data for the TKO to HAH section is the design data and not compiled from as-built survey records. The actual track alignment is probably modified from the original track alignment design. As a result, the discrepancies between the incorrectly defined track data and the physical track geometry are estimated by the RBN solution and are illustrated in Figure 6.20.

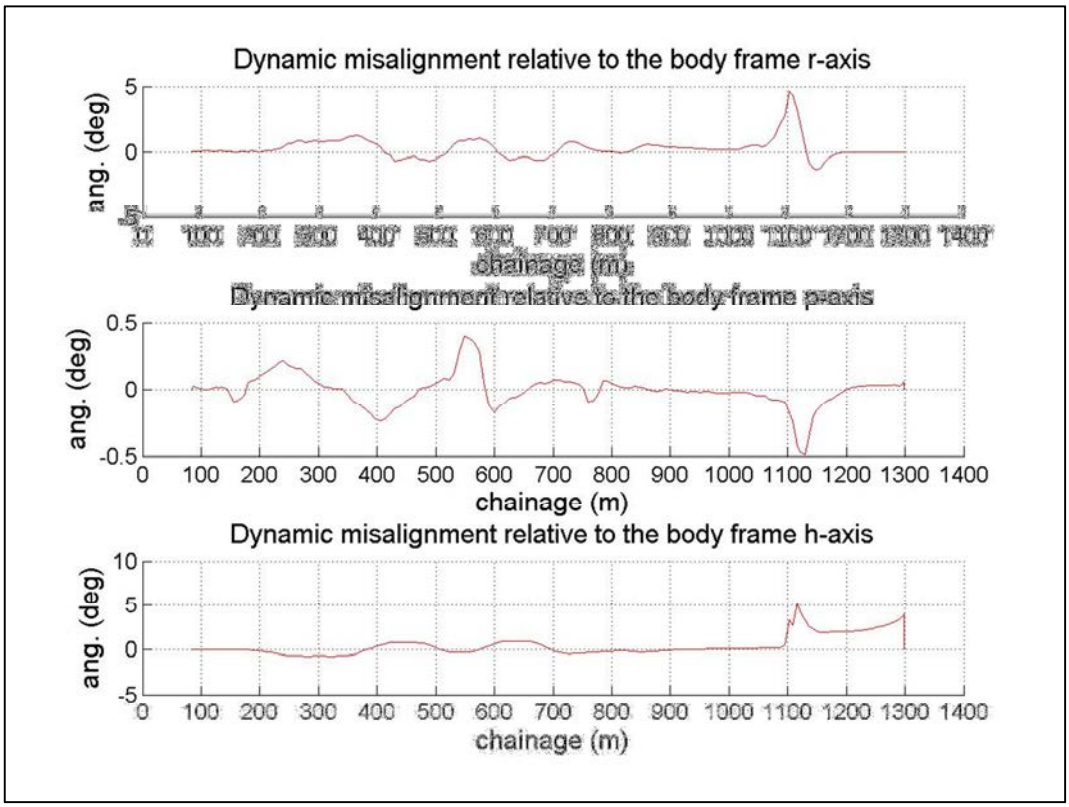

Figure 6.20: Dynamic misalignment estimated from RBN

6.5. Performance and Deficiencies of RBN

Through the system implementation, different sets of navigation results are represented and analysed in previous sections, while the impacts of sensor errors, train motion and track data correctness have been illustrated and discussed. In this section, the results are summarised for the performance and deficiencies of RBN.

6.5.1. Practical Accuracy of RBN

In the rail-bound environment, the chainage is a primary factor for train localisation, which is a one-dimensional horizontal distance defined with the track alignment. For RBN solution, the chainage error is a primary indicator for the accuracy of navigation results, while the lateral and vertical position are constrained by the physical track through the TAP estimates. In general, results illustrated that the longitudinal position accuracy varies from few decimetres to over ten metres, which

slightly depends on the weighting of track uncertainties. The redundant navigation results explicitly indicated a 10-metre discrepancy under the identical track conditions and train motion. It implies that the excessive position errors are potentially resulted from the impacts of sensor errors.

6.5.2. Correctness of Attitude and Velocity

Apart from the absolute position errors, the system attitude and velocity profiles are represented and analysed. The RBN results demonstrated a great improvement for the accumulation of attitude errors, while the physical train motion, as well as track defects, can be accurately retrieved.

It is noted that the VUPT is suggested but not applied in this thesis. The attitude error control has provided an alternative measure to diminish the growth of velocity errors. Although the navigation results are not examined with external control data, the velocity accuracy can be validated by the misclosures at the end of train motion.

In addition, the repeatability of solution has been illustrated by three independent sets of navigation results. The nominal discrepancies between the TAP results and the RBN results can be determined from the navigation records, which are represented in dynamic misalignment and displacement. After the removal of high rate oscillations, the additional train motion and track defects are generalised in form of dynamic misalignment and displacement record.

6.5.3. Dynamic Weight Control

Although the train motion and track defects can be generalised into a record of dynamic misalignment and displacement, the direct error compensation was not applied in this thesis. It is mentioned that the adaptive method is employed to estimate the uncertainties of train motion, which is a dynamic weight control process.

After the error compensation, the discrepancies between TAP estimates and system results, as well as the resultant adaptive noises, would be notably reduced, such that the relative weight for navigation error control would increase. As a result, the error compensation would be counteracted by the increased weight and is not beneficial to the error control process.

The error compensation has been reserved as a potential measure for accuracy improvement. An alternative weight control and optimisation method is required to tackle the encountered problem, which is a research direction beyond this thesis.

6.5.4. Track Alignment Errors

The performance of RBN solution is verified and examined on the basis of correct track alignment data. In section 6.4, the impacts of incorrect track alignment data have been illustrated. Although an accurate navigation solution cannot be achieved, the attitude and velocity errors can be identified from the results through appropriate weight control. The resultant misalignment and displacement represented part of the track alignment errors, which require further study to recover the actual differences between the track data and physical geometry.

Chapter 7: Conclusion and Recommendations

Problems related to GNSS outages, which are currently unsolved for general inertial navigation applications, have greatly hampered the potential development of mobile mapping into other fields. In railway environments, mobile mapping technology is usually employed for engineering applications, such as track survey, tunnel mapping and clearance measurement, while its potential application in other areas such as real-time train control and infrastructure monitoring (particularly in tunnels) are yet to be exploited.

To enhance the potential of MMS in underground railway systems, a GNSS-free solution for train navigation and georeferencing has been developed. This thesis presents and validates the concept of the Rail-bound Navigation (RBN) solution by replacing the GNSS component of a POS with track constraints. The result is georeferencing technique that can be applied in all railway systems and in underground railways in particular. RBN forms the basis of a wide range of applications such as Underground Railway Laser Scanning (URLS), real time train control, and full time infrastructure monitoring.

7.1. Summary for Rail-bound Navigation

In a railway environment, the train motion is fundamentally bounded by the rail track meaning that the track alignment data can be utilised to constrain the train motion sensed by an INS. In general, the navigation system is aligned with the nominal track alignment at constant angular and linear differences, while the dynamic train motion introduces additional uncertainties to the discrepancies between the track alignment data and the navigation results. Both of these aspects have been considered and incorporated into the formation and validation of the RBN solution.

7.1.1. Formulation of RBN Structure

The RBN solution is primarily maintained by inertial navigation results, which provides alternative error control regarding typical INS/GNSS configuration. The fundamentals of INS, such as the inertial sensor errors, INS mechanisation, system initialisation and relevant error models, are summarised in Appendix 1.

To quantify the track constraints, a TAP solution is established to retrieve the track position and attitude from alignment parameters for the error control process. In Chapter 3, the generalised functional models, error models and essential considerations have been presented for the development of a TAP solution. Through the appropriate chainage updating methods, the TAP can provide an alternative navigation reference with three-dimensional position and attitude.

Regarding the train dynamics, the fusion of INS and TAP is more complicated than a typical INS/GNSS integration. In Chapter 4, the structure of the RBN solution has been introduced and discussed in detail. The INS/TAP integration is implemented through an EKF process and the measurement error models are developed to estimate the navigation errors and their uncertainties. In addition, several assumptions were made for the train motion behaviour such that the track-to-train transition and train-to-body misalignment are introduced to compensate for the systematic discrepancies between the actual train motion and the TAP estimates. As a result, a valid relationship between the inertial navigation and the track constraints has been established.

7.1.2. Validation of RBN Performance

Following the formulation of the RBN solution, a prototype navigation system was designed and implemented in Chapter 5 for the validation of the hypotheses. A preliminary experiment was carried out with a simulated rail-bound motion to obtain initial knowledge for the potentials and deficiencies of the RBN solution. To verify the theoretical accuracy of TAP estimation, a set of track alignment sample data from Hong Kong's MTRC was used. The chainage errors were simulated to estimate the impacts to TAP navigation errors, which are consistent with the propagated uncertainties.

Through the implementation of the RBN, the coherent attitude patterns between TAP estimates and INS results have illustrated the correctness of the TAP solution. Although the longitudinal position error is not minimised, a significant improvement in attitude and velocity was produced by the RBN solution.

In Chapter 6, the performance of RBN solution is further optimised and analysed through redundant measurements and independent experiments. Through analysis of the data, it is seen that the general accuracy of the RBN solution mainly depends on the sensor quality and the weight for error control. By comparing the navigation results from redundant sensor measurements, the impacts of sensor errors were clearly identified as they were found to cause 10-metre level position discrepancies. The impacts of sensor errors can be diminished by data smoothing and increasing the weight of TAP estimates, especially for the pitch angle.

In addition, three independent sets of experimental data were collected for the same section of track. The dynamic misalignment and displacement are generally coherent, while the run-to-run variations are mainly caused by the uncompensated train motion.

After filtering the high rate oscillations, the averaged misalignment and displacement indicated the physical track defects and the uncompensated low rate train motion, which can be further employed to monitor the track geometry. Through the analysis of the RBN results, the incorrectness of track data can be indicated from any abnormal dynamic misalignment.

7.2. Significance and Implications of the RBN Solution

Through the formulation and validation of the RBN solution, the research objectives have been accomplished with satisfactory results. Despite the poor inertial sensor quality, the accuracy of attitude and velocity can be vastly improved with RBN in a GNSS-free environment without additional control data and post-processing. The significance and potential of the RBN solution is illustrated.

7.2.1. Originality of RBN Concept

The formulation of the RBN concept originated from the demands of railway systems. In highly urbanised cities, underground rapid transit is generally the backbone of public transformation, which requires highly automated train control, accurate train localisation and safety enforcement. Mobile mapping technology, which can provide individual navigation results and spatial measurements, is particularly valuable for multi-purposes applications, such as alternative train localisation, precise speed monitoring, continuous track deformation monitoring, tunnel condition monitoring and train detection. In general, typical MMS are designed for above-ground applications, which are usually built with high performance sensors to minimise the impacts of GNSS outages. As a result, the system cost and the necessity of post-process have hampered the feasibility of continuous railway applications.

In principle, the train motion is fundamentally bounded by the physical track and is predefined by the track alignment, indicating that the GNSS component can be alternatively replaced by the track constraints. The sensor requirements, as well as the necessity of post-process, are therefore reduced on account of the continuous error control process.

Despite the potential benefits, the integration of mobile mapping technology and railway systems has received little attention. A GNSS-free train navigation solution, RBN, was thus formulated to establish a basis and research direction for the integration of mobile mapping technology and railway systems.

7.2.2. Realisation of Track Constraints

Through the formulation of the RBN concept, a comprehensive method is required to realise the track constraints. Consequently, the concept of TAP solution was developed from the typical curve approximations from engineering surveying, which has been generalised into a series of functional models and the georeferencing of track geometry. The three-dimensional position, as well as the track attitudes, can be determined to utilise the track alignment data and completely realise the track constraints.

The TAP solution forms the backbone of the RBN solution. It provides a way to realise a GNSS-free inertial navigation solution with loosened requirements of post-process, external control data and measurements, which facilitates the development of mobile mapping technology towards real-time applications.

7.2.3. Notable Performance

Following the realisation of track constraints, the INS/TAP integration was implemented on the basis of further optimisation, including chainage updates, track-

to-train transition, train-to-body constant and dynamic misalignment, and the transition of fine alignment process, which aims at modelling and compensating for the discrepancies between the nominal track constraints and the actual train motion.

The experimental results have illustrated a great improvement by using a prototype system with consumer grade MEMS IMUs. Despite the longitudinal position errors caused by sensor quality, the attitude and velocity profiles have demonstrated that the train motion can be precisely retained by the RBN solution, while the accumulation of navigation errors has been greatly constrained without external data and measurements.

Furthermore, the results of repeated experiments have indicated the potential of track monitoring and track error compensation, while the nature of train vibrations and motion, or track defects can be examined from the navigation results.

7.3. Summary of RBN Errors

In this thesis, a series of error control processes were involved in addition to the fundamental INS/TAP integration, which formulated the backbone of the RBN solution. The navigation performance, however, is constrained by the relevant error sources with different impacts. Through the discussion and analysis, major error sources and their correlations are identified, classified and summarised in this section.

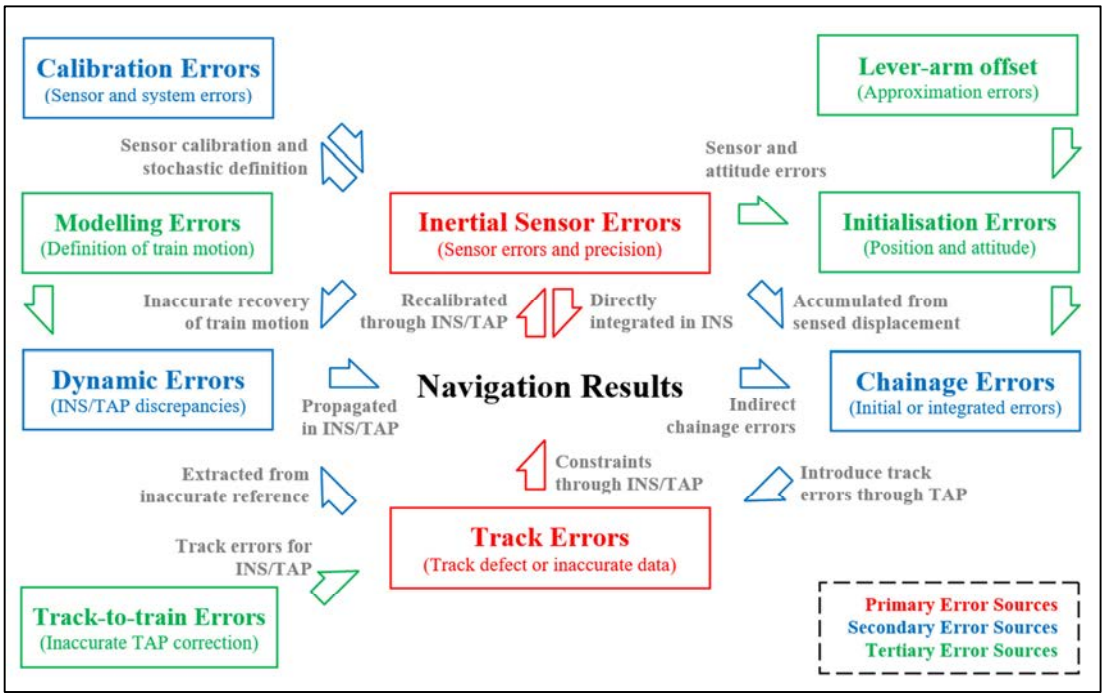

Figure 7.1: RBN error sources and their correlations

The error sources for RBN solution can be defined and classified into primary, secondary and tertiary levels regarding their impacts and characteristics. The major errors identified in this thesis are represented in Figure 7.1 with corresponding colours and descriptions, which are concisely summarised in sections 7.3.1, 7.3.2 and 0.

7.3.1. Primary RBN Errors

The primary error sources for RBN solution are the inertial sensor errors and track errors. They are the major constraints which directly restrict the navigation performance. In addition, the growth of these errors would constitute alternative sources of error such that their impacts would be further enlarged.

The inertial sensor errors (or quality) are the primary factors to indicate the accuracy and precision of an INS. For less precise inertial sensors such as consumer-grade sensors, the stochastic relationships for INS/TAP may not be valid under the rapid

growth of navigation uncertainties. The navigation system would be over-constrained by the track and introduces biases by propagating to the recalibrated sensor errors.

At the meanwhile, the track errors resulted from track defects, inaccurate or incorrect track data, would have great impact to the navigation results and diverge the solution.

7.3.2. Secondary RBN Errors

Through the RBN structure, secondary error sources, such as calibration errors, chainage errors, and dynamic errors, are resulted from the growth of primary error sources, which are directly or indirectly correlated to the navigation results.

The calibration approach for sensors is mainly constrained by the quality of sensors, such as physical and stochastic characteristics, which would introduce different levels of calibration errors (or remaining errors after calibration). These errors would propagate and be integrated to the navigation results through the INS mechanisation. In addition, it may diverge the solution by inappropriate stochastic definition.

In this thesis, the chainage is maintained by an INS and indirectly constrained by RBN solution such as the attitude error control. The magnitude of chainage error is therefore proportional to the growth of inertial sensor errors and introduce track errors by inaccurate chainage.

The train motion, which is defined as the discrepancies between INS and TAP estimates, has to be extracted and modelled in term of dynamic errors. The dynamic errors are directly affected by the INS estimates and the track errors, which constitute the relationships between the track reference and the moving train. The growth of primary errors may lead to invalid RBN conditions and loss of train motion.

7.3.3. Tertiary RBN Errors

In the development of RBN solution, several error sources, such as the lever-arm offset, initialisation errors, train motion modelling errors and train-to-train errors, are directly correlated to several errors sources and less significant to the navigation solution. They are classified into tertiary level of errors and are controlled under assumptions in this thesis.

7.4. Research Restrictions and Limitations

Throughout the study, the research direction and content were repeatedly modified regarding the changes of project conditions. The actual performance of the RBN solution cannot be demonstrated in absolute terms, while a comprehensive analysis of accuracy is not available. Furthermore, several assumptions have been made to facilitate the formulation of solution, which have also limited the research scope.

7.4.1. Absence of High-grade Inertial Sensor

Since a survey-grade MMS or INS was not available, a prototype system was built with consumer grade MEMS IMUs. A large proportion of time was spent on the preparation of hardware, and establishing data processing methods and sensor characteristics. Through the implementation, results indicated that the sensor errors have caused a significant impact to the absolute position accuracy. Thus, the present study has only explored the relative performance of attitude and velocity. In addition, the practical performance of the RBN solution would be significantly enhanced by employing higher grade sensors, such as industrial-grade IMUs, but the potential improvement is currently unknown.

7.4.2. Lack of Access to Railway and Train Control Data

The research access to the MTR facilities has been withdrawn because of a change of staff. Therefore, the experiments were merely performed with minimum installation by carrying the devices as luggage. The inertial measurements are the only available data for the implementation of the RBN solution, while the train control data is not accessible for further optimisation. Consequently, the potential improvement by integrating the RBN with train control data remains uncertain.

Although the track alignment design data was provided from the MTRC for research purposes, the HAH to POL section is the only available track alignment data for implementing the RBN solution. The access to as-built survey record is denied regarding the change of personnel, while the track alignment has been modified from the design data. As a result, only a single set of track alignment data is available to examine the general performance that restrict the generalisation of the RBN results.

7.4.3. Simplifications Resulted from Assumptions

A fundamental assumption has been made for the interaction between the train body and the bogies that a bogie is rotatable and constantly fixed with the train at a point. In practice, the bogie has a much more complicated structure for compensating the train motion, while the behaviours for various types of bogie are very different. This simplification may introduce excessive position and attitude errors to the system.

Although the sensor biases and scale errors were calibrated, an accurate gravity acceleration is not employed throughout the calibration. This may lead to a scale error and propagated into absolute velocity and position errors. In addition, the stochastic model for the propagation of sensor error uncertainties has been

established with manufacturer's specification which may not be accurate or may cause uncertainties to the practical accuracy.

In this thesis, a typical INS system model has been employed and maintained for future optimisation, while the TAP position and attitude are independently estimated. The estimated navigation errors are assumed as zero-mean and characterised by the innovation covariance. However, the uncompensated train motion has biased the solution, which has been incorrectly resolved into the drifts of sensor biases. Although the impacts were reduced by a complementary filter, a more rigorous method is necessary.

7.5. Recommendations and Future Improvements

Despite the encountered restrictions and limitations, the concept of the RBN solution has been realised and validated through the experiments. This study has illustrated the potential performance of RBN solution rather than its actual performance. Consequently, a number of possible improvements are recommended for future research.

7.5.1. A Comprehensive Performance Analysis

Since the prototype navigation system cannot provide satisfactory measurement accuracy, a comprehensive performance analysis is not applied to the RBN solution. Regarding the improvement demonstrated in this study, the actual performance of RBN solution should be remarkable if a higher grade INS was applied. It is recommended to implement the RBN solution to a more advanced INS for further investigation, such that a comprehensive performance analysis would be meaningful to indicate the absolute improvement by comparing the RBN solution to alternative error control methods.

7.5.2. Train Control Data Fusion

In this study, the navigation results are exclusively constrained by the TAP estimates, which have already illustrated a significant improvement in attitude and velocity. To maximise the long-term position accuracy, train control data fusion, such as train speed and position, is strongly recommended, such that the characteristics of train control and railway systems can be utilised. In the meanwhile, the RBN solution may provide precise information for train motion by interacted with train control system.

7.5.3. Error Modelling for Train Motion

Since a number of assumptions have been made to simplify the compensation of train motion, the navigation results are slightly biased by the compensation errors. To achieve a more rigorous solution, the track-to-train transition, the nature of bogie compensation and the lateral overturning effects are some of the recommended research directions to establish the error models for train motion dynamics and replace the adaptive measurement noise method.

7.5.4. Track Deformation Record

The physical track defects, which have been identified from the navigation results, are retrieved as dynamic misalignment and displacement. This study demonstrates the feasibility of continuous track monitoring through a misalignment record relative to the alignment chainage. Through the use of more advanced sensors and rigorous train motion dynamics, possible track deformation can be indicated by compared to the up-to-date record, which facilitate the track maintenance. In the meanwhile, the track error compensation can be applied to improve the RBN error control with advanced error models for train dynamics. A more thoughtful study is recommended to handle the spatial errors and the detection of track defects.

7.5.5. Rail-bound Mobile Mapping

Since the primary originality of the RBN solution is to facilitate the integration of mobile mapping technology and railway systems, it is highly recommended to investigate the performance of the RBN solution through the acquisition mobile mapping data. Thus, the feasibility of tunnel condition and structural monitoring can be examined through the analysis of mapping data accuracy. Additionally, the potential of intermittent chainage correction through the identified landmarks provides another potential research direction.

7.5.6. Further Integration with Railway System

In general, this study presents a potential train navigation and georeferencing solution for railway systems and demonstrates the implications of improvement by employing the RBN solution. In addition, RBN may provide several potential development directions for the integration of mobile mapping technology and railway and train control systems as shown in Figure 7.2, including the URLS, train signalling and timetable management, railway system maintenance and Automatic Train Operation (ATO).

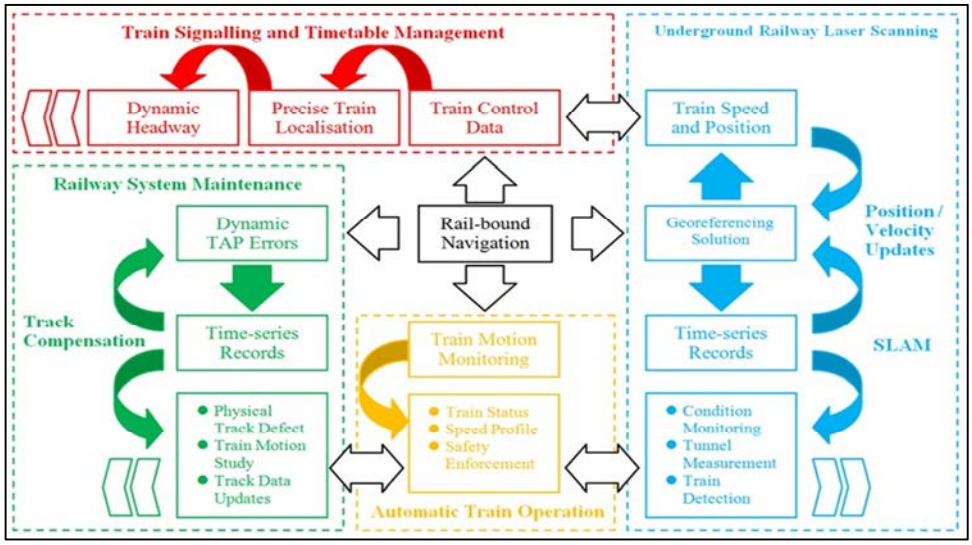

Figure 7.2: Potential development aspects for comprehensive integration

Through the interaction with train control data, a more precise train localisation can be determined from RBN, which provides an alternative solution for dynamic headway calculation and updates. The train separation can be potentially reduced for maximising the route capacity while the train safety is maintained by URLS. Additionally, the RBN solution provides a full time measurement such that a track deformation record can be established for facilitating the track maintenance, while the track record can be applied to improve the RBN accuracy.

By compensating for the track defects, the train motion can be retrieved from the navigation results from the RBN solution, which establish an indicator to the train health status (e.g. train vibrations). In addition, the RBN and URLS provide alternative sources of train-borne measurements (e.g. precise train speed and localisation, acceleration and braking measurement, train and obstacle detection) supporting the ATO.

In conclusion, RBN deserves further studies to discover its potential, which can facilitate the development in both the mobile mapping and railway system.

Appendix 1 - Inertial Navigation Basis

To facilitate the development of RBN solution, the fundamentals of inertial navigation are reviewed for navigation system design and implementation. An overview of inertial sensors and relevant models, including the essential navigation equations for system mechanisation and initialisation, are summarised prior to the design of an INS.

A1.1. Overview of Inertial Sensors

For the minimal necessary configuration, an INS maintains the navigation solution from inertial measurements which are collected by inertial sensors such as accelerometers and gyroscopes. Therefore, the quality of the inertial sensors or the IMU has a considerable contribution to the overall navigation performance that the sensor errors should be properly handled prior to the implementation of a navigation system.

In general, sensor errors comprise systematic errors and zero-mean random errors. The systematic errors are usually deterministic, which can be compensated through appropriate calibration. The random errors are considered to be non-deterministic and cannot be compensated. However, they are usually handled by a stochastic model for capturing the statistical properties after accounting for systematic errors.

A1.1.1. Systematic Errors

The characteristics of systematic errors of accelerometers and gyroscopes can be indicated by the effects of differences between signal input and output, which have been discussed by Titterton and Weston (2004); Grewal et al. (2007); Farrell (2008);

Groves (2008). The error characteristics are generally classified by the patterns regarding the physical features as shown in Figure A1.1.

With respect to performance requirements, physical and mathematical models have been developed to compensate for the fixed errors through a calibration process. The physical models are derived with respect to the principles of physics for the correction of recognisable errors such as zero-constant and scale error. In addition, mathematical models are empirically defined to remove systematic errors with specific patterns.

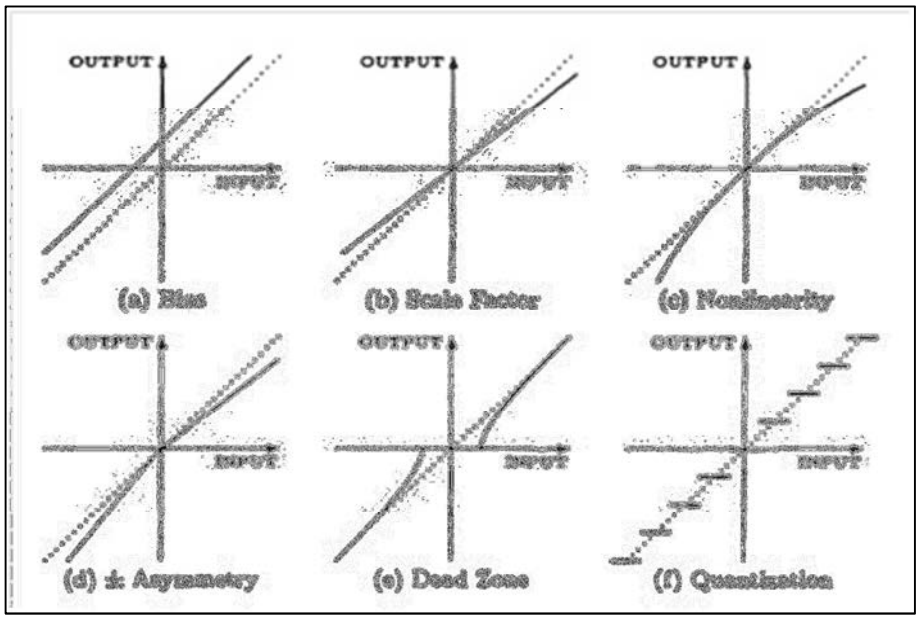

Figure A1.1: Typical sensor error characteristics (Grewal et al., 2007)

By considering the general error sources, the physical error models for accelerometer and gyroscope can be described by eqn. 3.11 and eqn. 3.12 respectively, which are summarised from Farrell (2008).

$$\mathbf{f}_{ib}^{b} = (\mathbf{I} - \delta\mathbf{S}_a)\left(\tilde{\mathbf{f}}_{ib}^{b} - \delta\mathbf{b}_a - \delta\mathbf{n}_a - \boldsymbol{\nu}_a\right) \tag{A1.1}$$

where $\mathbf{f}_{ib}^{b}$ and $\tilde{\mathbf{f}}_{ib}^{b}$ are the actual and raw accelerometer measurements respectively; $\delta\mathbf{S}_a$ is a diagonal matrix of accelerometer scale factor error; $\delta\mathbf{b}_a$ is the accelerometer

bias; $\delta\mathbf{n}_a$ is the accelerometer non-linear scale factor; and $\boldsymbol{v}_a$ is the accelerometer random noise.

$$\boldsymbol{\omega}_{ib}^{b} = \left(\mathbf{I} - \delta\mathbf{S}_g\right)\left(\tilde{\boldsymbol{\omega}}_{ib}^{b} - \delta\mathbf{b}_g - \delta\mathbf{k}_g - \boldsymbol{v}_g\right) \tag{A1.2}$$

where $\boldsymbol{\omega}_{ib}^{b}$ and $\tilde{\boldsymbol{\omega}}_{ib}^{b}$ are the actual and raw gyroscope measurements respectively; $\delta\mathbf{S}_g$ is a diagonal matrix of gyroscope scale factor error; $\delta\mathbf{b}_g$ is the gyroscope bias; $\delta\mathbf{k}_g$ is the gyroscope g-sensitivity; and $\boldsymbol{v}_g$ is the gyroscope random noise.

It is noted that the choice of error terms depends on the sensor characteristics and the performance requirements. For low cost sensors such as consumer grade IMUs, the sensor noises (v_a and v_g) may be too large that the systematic errors are not observable.

A1.1.2. Random Errors

Through the compensation of systematic errors, a variety of random errors are resulted from uncontrollable conditions such as temperature, pressure and electronic noise. The random errors are considered to be zero-mean, which are usually described as a lump-sum of uncompensated error sources such as white noise, exponentially correlated noise, random-walk errors, harmonic noise and "$1/f$" noise (Grewal et al., 2007).

Appropriate stochastic models are usually applied to define the random processes and capture the sensor noise characteristics. For a typical aided INS solution, a stochastic model is required to characterise the time-correlated measurement errors and determine the optimal weighting for integrating the INS and aiding data sources through a Kalman filter.

Prior to the implementation of navigation system, the stochastic model parameters can be estimated through methods such as auto-correlation function, power spectral density and auto-regressive moving average through laboratory calibration. Regarding the research objectives, the stochastic modelling and sensor calibration process are not further explained.

A1.2. Mechanisation of Inertial Navigation Systems

Since the experiments conducted in this research are located in a low-latitude region (Hong Kong, 22.4°N), the INS is mechanised in the *n*-frame without the singularity problem that occurs in polar regions. In this section, the elemental INS mechanisation equations are summarised for a *n-e-d* implementation, which are defined for an EKF implementation. The mechanisation equations basically follow the convention of Farrell (2008) and Groves (2008) with minimal modifications, which are elaborated in Appendix 2.

A1.2.1. Inertial Navigation Equations

An INS maintains its navigation solution by the changes of position, velocity and attitude relative to a coordinate frame, which involves the computation with a series of transformation, integration and compensation of inertial motion. The navigation equations for the rates of position, velocity and attitude are mechanised in the *n*-frame, which are summarised in eqn. A1.3, eqn. A1.4 and eqn. A1. 5 respectively.

$$\dot{\mathbf{r}}^n = \begin{bmatrix} \frac{1}{R_M + h} & 0 & 0 \\ 0 & \frac{1}{(R_N + h)\cos\varphi} & 0 \\ 0 & 0 & -1 \end{bmatrix} \mathbf{v}_{eb}^n \tag{A1.3}$$

where $\dot{\mathbf{r}}^n$ is the rate of changes in curvilinear coordinates; $\mathbf{v}_{eb}^n = [v_N \quad v_E \quad v_D]^T$ are the Earth-relative velocities expressed in the *n*-frame.

$$\dot{\mathbf{v}}_{eb}^n = -(\boldsymbol{\Omega}_{en}^n + 2\boldsymbol{\Omega}_{ie}^n)\mathbf{v}_{eb}^n + \mathbf{f}_{ib}^n + \mathbf{g}^n \tag{A1.4}$$

where $\mathbf{f}_{ib}^n = \mathbf{C}_b^n \mathbf{f}_{ib}^b$ is the acceleration sensed in the *b*-frame and transformed into the*n*-frame; $\mathbf{g}^n = [0 \quad 0 \quad g]^T$ is the normal gravity acceleration represented in the *n*-frame; $\boldsymbol{\Omega}_{en}^n$ is the skew matrix of the turn rate of the*n*-frame relative to the *e*-frame; $\boldsymbol{\Omega}_{ie}^n$ is the skew matrix of the rotation rate of the*e*-frame relative to the *i*-frame.

$$\dot{\mathbf{C}}_b^n = \mathbf{C}_b^n \boldsymbol{\Omega}_{ib}^b - (\boldsymbol{\Omega}_{ie}^n + \boldsymbol{\Omega}_{en}^n)\mathbf{C}_b^n \tag{A1.5}$$

where $\boldsymbol{\Omega}_{ib}^b$ is the skew matrix of angular velocity ($\boldsymbol{\omega}_{ib}^b$) sensed in the *b*-frame relative to the *i*-frame.

A1.2.2. Inertial Navigation Updates

The rates of changes in position, velocity and attitude are described by the continuous-time navigation equations. To implement an INS, a discrete time solution is required regarding the discrete-time measurement samples, while the integration and compensation of inertial measurements are performed in sequence.

The attitude is usually updated prior to velocity and position, which can be integrated through several methods, including DCM, quaternion, rotation vector and Euler angles. An approximation of direct attitude updates is shown in eqn. A1.6 in the form of DCM.

$$\mathbf{C}_b^n(t_1) \approx \mathbf{C}_b^n(t_0)\left(\mathbf{I} + \boldsymbol{\Omega}_{ib}^b \Delta t\right) - (\boldsymbol{\Omega}_{ie}^n + \boldsymbol{\Omega}_{en}^n)\mathbf{C}_b^n(t_0)\Delta t \tag{A1.6}$$

where $\mathbf{C}_b^n(t_1)$ and $\mathbf{C}_b^n(t_0)$ are the current and previous transformation matrices; t_1 and t_0 are the time epochs where $t_1 > t_0$; $\Delta t = t_1 - t_0$ is the sampling time interval. Following the attitude integration, the velocity and position integration are relatively straight forward, which are shown in eqn. A1.7 and eqn. A1.8 respectively.

$$\mathbf{v}_{eb}^n(t_1) = \mathbf{v}_{eb}^n(t_0) + \Delta t\left[\frac{1}{2}\left(\mathbf{C}_b^n(t_1) + \mathbf{C}_b^n(t_0)\right)\mathbf{f}_{ib}^n - (\boldsymbol{\Omega}_{en}^n + 2\boldsymbol{\Omega}_{ie}^n)\mathbf{v}_{eb}^n(t_0) + \mathbf{g}^n\right] \quad \text{(A1.7)}$$

where $\mathbf{v}_{eb}^n(t_1)$ and $\mathbf{v}_{eb}^n(t_0)$ are the current and previous Earth-relative velocities.

$$\mathbf{r}^n(t_1) = \mathbf{r}^n(t_0) + \frac{\Delta t}{2}\mathbf{D}[\mathbf{v}_{eb}^n(t_1) + \mathbf{v}_{eb}^n(t_0)] \quad \text{(A1.8)}$$

where $\mathbf{r}^n(t_1)$and $\mathbf{r}^n(t_0)$ are the current and previous position in the *n*-frame.

The computation flow of inertial navigation updates is simplified and illustrated in Figure A1.2. The inertial measurements are transformed into the *n*-frame, which are integrated and compensated for navigation updates from initial position, velocity and attitude without external sources of information.

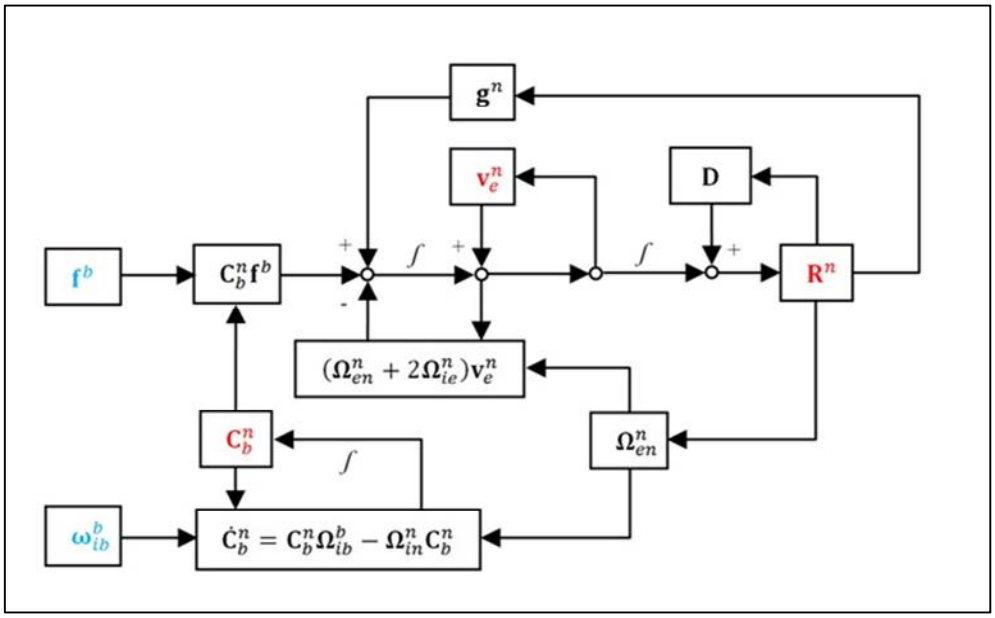

Figure A1.2: Computation flow diagram for an INS

A1.3. System Initialisation and Alignment

Since an INS is a dead reckoning solution by maintaining the position and attitude changes through the sensed motion and rotation, the initial position, velocity and attitude are required to solve the ambiguity problems of system.

A1.3.1. Position and Velocity Initialisation

In general, an INS requires external sources for initialising position, such as GNSS position or manual input, while the earth-relative velocity can be initialised by zero-input through stationary initialisation or by external velocity reference. Some systems may employ low-grade IMUs and are mechanised in a localised reference frame for small-area navigation or indoor positioning, which require only the arbitrary position by disregarding the global effects, such as Earth's rotation and the rotation of the *n*-frame relative to the *e*-frame.

For railway environments, the navigation area is sufficiently large (over kilometres) that the global positional changes would introduce significant impacts to the navigation solution. The INS is therefore implemented in the *n*-frame and requires georeferenced position. Through the TAP, the chainage of reference is required to determine the reference position and support the position initialisation. The stationary initialisation can be merely implemented when the train temporarily stops at a station. Providing position and speed data through the train control system, dynamic initialisation is achievable for more flexible operation.

A1.3.2. Initial Sensor Alignment

For a strap-down INS, the sensor alignment is performed to determine the initial values of transformation between the *b*-frame and the reference frame, which is conventionally achieved through one of four methods (Grewal et al., 2007):

- **Optical alignment:** it can be performed by optical line-of-sight measurements to ground-based directions for near-Earth applications, or by star tracking in space or near-space.
- **Gyrocompass alignment:** it employs the sensed acceleration to determine the local vertical and the sensed Earth rotation to determine the direction of north. In addition, latitude can be determined from the angle between the Earth rotation vector and the horizontal. This method requires stationary initialisation and is time-consuming, which is only applicable to land-based vehicles.
- **Transferred alignment:** it can be done in a moving host vehicle by velocity matching with another aligned INS.
- **GNSS-aided alignment:** the alignment variables are estimated by position matching with GNSS through the integrated INS/GNSS implementation. This does not require stationary vehicle during alignment process, which needs a period of time to settle the navigation errors to acceptable levels.

The proposed RBN solution is capable of direct GNSS replacement with TAP for position matching for dynamic initialisation process. However, it depends on the availability and accuracy of the reference chainage. Dynamic TAP-aided alignment is recommended only if an alternative train localisation method is applicable.

Alternatively, gyrocompass alignment is preliminarily considered to be more suitable in railway systems as the host train would repeatedly stop at station platforms with pre-defined chainage. The relevant gyrocompass alignment equations for the formation of rotation matrix have been derived and broadly reviewed by Titterton and Weston (2004), Bekir (2007) and Grewal et al. (2007), and utilises the measurements of accelerometers and gyroscopes. The gyrocompass alignment, however, requires highly accurate and precise sensors and a certain period of time,

which introduces additional restrictions to system implementation. For low cost MEMS IMUs, the sensor biases and measurement noises are considerably large that which are be suitable for conventional navigation and gyrocompass alignment.

The self-alignment process can be generalised and decomposed into sensor levelling and heading processes. The sensor *b*-frame is firstly levelled by matching the sensed acceleration with the local vertical to determine the roll and pitch angles, then followed by a heading process. The accelerometer levelling is described by eqn. 3.19, which is summarised from Bekir (2007) and Groves (2008).

$$\begin{bmatrix} \hat{\phi} \\ \hat{\theta} \end{bmatrix} = \begin{bmatrix} \tan^{-1}\left(-f_y/-f_z\right) \\ \tan^{-1}\left(f_x/\sqrt{f_y^2+f_z^2}\right) \end{bmatrix} \tag{A1.9}$$

where $\hat{\phi}$ and $\hat{\theta}$ are the estimated roll and pitch angles respectively; f_x, f_y and f_z are the accelerometer outputs in *x*, *y* and *z* axes respectively.

The roll and pitch estimation shown in eqn. A1.9 merely utilises the accelerometer outputs. The error equations of roll and pitch are linearised and shown in eqn. A1.10. While the errors are propagated from the accelerometer outputs, the errors of accelerometer outputs are considered to be independent.

$$\begin{bmatrix} \delta\hat{\phi} \\ \delta\hat{\theta} \end{bmatrix} = \begin{bmatrix} 0 & \dfrac{f_z}{f_z^2+f_y^2} & -\dfrac{f_y}{f_z^2+f_y^2} \\ -\dfrac{\sqrt{f_y^2+f_z^2}}{\|f\|^2} & \dfrac{f_x f_y}{\|f\|^2\sqrt{f_y^2+f_z^2}} & \dfrac{f_x f_z}{\|f\|^2\sqrt{f_y^2+f_z^2}} \end{bmatrix} \begin{bmatrix} \delta f_x \\ \delta f_y \\ \delta f_z \end{bmatrix} \tag{A1.10}$$

where $\|f\| = \sqrt{f_x^2+f_y^2+f_z^2}$ is the magnitude of accelerometer outputs.

Regarding the error equation shown in eqn. A1.10, the angular errors are inversely proportional to the magnitude of accelerometer outputs. For land-based applications,

the ratio of gravity acceleration (about $1g$) and accelerometer noise (about $0.1mg$ to $10mg$) is considerably large, which is applicable to a wide range of sensors. For low cost IMUs, the angular precision can be improved by averaging the accelerometer outputs over time when the host train is stationary.

A1.3.3. Sensor Error Compensation

In addition to the calibrated and compensated errors, the sensor instability, such as turn-on biases and time-correlated biases, should also be handled through the INS implementation. During the system initialisation and alignment processes, the uncompensated gyroscope and accelerometer biases can be estimated as shown in eqn. A1.11 which is summarised from Bekir (2007).

$$\begin{bmatrix} \delta\hat{\boldsymbol{\omega}}_{ib}^{b} \\ \delta\hat{\mathbf{f}}_{ib}^{b} \end{bmatrix} = \begin{bmatrix} \tilde{\boldsymbol{\omega}}_{ib}^{b} - \omega_{ie}\hat{\mathbf{C}}_{n}^{b}\begin{bmatrix} \cos\hat{\varphi} \\ 0 \\ -\sin\hat{\varphi} \end{bmatrix} \\ \tilde{\mathbf{f}}_{ib}^{b} - \hat{\mathbf{C}}_{n}^{b}\begin{bmatrix} 0 \\ 0 \\ g \end{bmatrix} \end{bmatrix} \tag{A1.11}$$

When stationary, the gyroscope and accelerometer outputs are assumed to be zero values after the compensation of Earth's rotation rate and gravity acceleration respectively. The sensor biases are therefore estimated from the sensor outputs, which are maintained and continuously calibrated through a Kalman filter process.

A1.4. System Error Control

Since an INS is updated with relative measurements, navigation and sensor errors are propagated with time that the long-term accuracy of standalone navigation solution depends greatly on the IMU quality, the system initialisation accuracy, and the nature of motion. In accordance with such deficiency, the aided inertial navigation solution is usually implemented through a filtering process such as a Kalman filter,

complementary filter, and particle filter. The filtering process aims to model and propagate the system state and noises, which regulates the error control process through external measurement updates.

A1.4.1. Navigation Error Models

Since the EKF operates with a linearised dynamics model, the navigation equations of the rate of position (eqn. A1.3), velocity (eqn. A1.4) and attitude (eqn. A1.5) are linearised with respect to the system error state. The continuous-time dynamics model is summarised and presented in eqn. A1.12 with the derivatives elaborated in Appendix 2.

$$\begin{bmatrix} \delta\dot{\mathbf{r}} \\ \delta\dot{\mathbf{v}} \\ \dot{\boldsymbol{\rho}} \end{bmatrix} = \begin{bmatrix} \mathbf{F}_{rr} & \mathbf{F}_{rv} & \mathbf{F}_{r\rho} \\ \mathbf{F}_{vr} & \mathbf{F}_{vv} & \mathbf{F}_{v\rho} \\ \mathbf{F}_{\rho r} & \mathbf{F}_{\rho v} & \mathbf{F}_{\rho\rho} \end{bmatrix} \begin{bmatrix} \delta\mathbf{r} \\ \delta\mathbf{v} \\ \boldsymbol{\rho} \end{bmatrix} + \begin{bmatrix} \mathbf{0} & \mathbf{0} \\ \hat{\mathbf{C}}_b^n & \mathbf{0} \\ \mathbf{0} & -\hat{\mathbf{C}}_b^n \end{bmatrix} \begin{bmatrix} \delta\mathbf{f}_{ib}^b \\ \delta\boldsymbol{\omega}_{ib}^b \end{bmatrix} \tag{A1.12}$$

where $\delta\mathbf{r}$ are the position errors; $\delta\mathbf{v}$ are the velocity errors; $\boldsymbol{\rho} = [\epsilon_n \quad \epsilon_e \quad \epsilon_d]^T$ are the attitude errors; $\mathbf{0}$ is a 3×3 zero matrix; the subcomponents of $\mathbf{F}$ matrix are the corresponding derivatives.

The sensor errors are involved in the propagation of navigation errors, which are time correlated and change slowly with time. The sensor errors are therefore integrated with the system error state and controlled through an appropriate stochastic model.

A1.4.2. Sensor Error Models

The deterministic errors of accelerometers and gyroscopes, such as biases, scale factors, and orthogonality misalignments, are generally modelled and compensated through pre-calibration, while the time correlated sensor noises are handled by

stochastic models and characterised by random processes, such as random walk, Gauss-Markov and Auto-Regressive (AR) processes (Noureldin et al., 2013).

For an aided INS process, the inertial sensor bias drifts are primarily modelled with a Kalman filtering process, while the additional errors terms are introduced for further performance requirements. The error models, however, are also considered on account of sensor quality, numerical stability and observability.

To implement the prototype system, a first order Gauss-Markov process is employed to model the random noises associating with the accelerometer and gyroscope biases (Noureldin et al., 2013). Accordingly, a general system model for an INS is summarised in eqn. A1.13, while only the drifts of sensor bias are involved in the system.

$$\begin{bmatrix} \delta\dot{\mathbf{r}} \\ \delta\dot{\mathbf{v}} \\ \dot{\boldsymbol{\rho}} \\ \delta\dot{\mathbf{f}}_{ib}^{b} \\ \delta\dot{\boldsymbol{\omega}}_{ib}^{b} \end{bmatrix} = \begin{bmatrix} \mathbf{F}_{rr} & \mathbf{F}_{rv} & \mathbf{F}_{r\rho} & \mathbf{0} & \mathbf{0} \\ \mathbf{F}_{vr} & \mathbf{F}_{vv} & \mathbf{F}_{v\rho} & -\hat{\mathbf{C}}_{b}^{n} & \mathbf{0} \\ \mathbf{F}_{\rho r} & \mathbf{F}_{\rho v} & \mathbf{F}_{\rho\rho} & \mathbf{0} & \hat{\mathbf{C}}_{b}^{n} \\ \mathbf{0} & \mathbf{0} & \mathbf{0} & -\mathbf{T}_{f}^{-1} & \mathbf{0} \\ \mathbf{0} & \mathbf{0} & \mathbf{0} & \mathbf{0} & -\mathbf{T}_{\omega}^{-1} \end{bmatrix} \begin{bmatrix} \delta\mathbf{r} \\ \delta\mathbf{v} \\ \boldsymbol{\rho} \\ \delta\mathbf{f}_{ib}^{b} \\ \delta\boldsymbol{\omega}_{ib}^{b} \end{bmatrix} + \begin{bmatrix} \mathbf{0} & \mathbf{0} & \mathbf{0} & \mathbf{0} \\ -\hat{\mathbf{C}}_{b}^{n} & \mathbf{0} & \mathbf{0} & \mathbf{0} \\ \mathbf{0} & \hat{\mathbf{C}}_{b}^{n} & \mathbf{0} & \mathbf{0} \\ \mathbf{0} & \mathbf{0} & \mathbf{I} & \mathbf{0} \\ \mathbf{0} & \mathbf{0} & \mathbf{0} & \mathbf{I} \end{bmatrix} \begin{bmatrix} \mathbf{v}_{f} \\ \mathbf{v}_{\omega} \\ \mathbf{w}_{f} \\ \mathbf{w}_{\omega} \end{bmatrix} \qquad \text{(A1.13)}$$

where $\mathbf{T}_{f}^{-1}$ and $\mathbf{T}_{\omega}^{-1}$ are the diagonal matrices of reciprocals of the correlation time associated with accelerometer biases and gyroscope biases respectively; $\mathbf{v}_{f}$ and $\mathbf{v}_{\omega}$ are the measurement noises of accelerometers and gyroscopes; $\mathbf{w}_{f}$ and $\mathbf{w}_{\omega}$ are the spectral densities of accelerometers and gyroscopes specified by the manufacturer.

The sensor error models are applied for sensor noise propagation, which regulate the growth of navigation noises. Through an EKF process, the stochastic modelling is important for optimal weight estimation of measurement updates and continuous calibration of sensor biases. The general Kalman filtering process can be found in Appendix 3.

Appendix 2 - INS Error Models

In Appendix 1, the INS mechanisation equations and error models are summarised for the establishment of the navigation system, which are further elaborated in the following sections. The mechanisation equations and error models are derived on the basis of Farrell (2008) and Groves (2008) with minimal modifications.

A2.1. Kinematic Equations for Position

For the implementation in the *n*-frame, the geodetic position is represented by $\mathbf{r}^n = [\varphi \quad \lambda \quad h]^T$. The derivatives of geodetic position can be determined from the Earth-relative velocity $\mathbf{v}_e^n = [v_n \quad v_e \quad v_d]^T$ through a curvilinear transformation as shown in eqn. A2.1.

$$\begin{aligned} \dot{\mathbf{r}}^n &= \mathbf{D}\mathbf{v}_e^n \\ \begin{bmatrix} \dot{\varphi} \\ \dot{\lambda} \\ \dot{h} \end{bmatrix} &= \begin{bmatrix} \frac{1}{R_M + h} & 0 & 0 \\ 0 & \frac{1}{(R_N + h)\cos\varphi} & 0 \\ 0 & 0 & -1 \end{bmatrix} \begin{bmatrix} v_n \\ v_e \\ v_d \end{bmatrix} \end{aligned} \tag{A2.1}$$

where **D** is the transformation of the linear magnitude from *n-e-d* resolving axes to the curvilinear magnitude; R_M and R_N are the radii of curvature in the meridian and prime vertical.

A2.2. Kinematic Equations for Velocity

For a strapdown inertial navigation, the time rate of change of velocity is derived from the accelerometer measurements sensed in the *b*-frame relative to the *i*-frame, which is progressively transformed to the *n*-frame with the compensation of frame rotations as elaborated in the following section.

A2.2.1. Inertial Position and Earth-relative Velocity

The position vector of a point relative to centre of the Earth can be transformed from *i*-frame to the *e*-frame through $\mathbf{C}_i^e$. The rate of change for position measured in the *e*-frame, the earth-relative velocity, can be expressed in eqn. A2.2.

$$\mathbf{v}_e = \dot{\mathbf{r}}^e \tag{A2.14}$$

where $\mathbf{v}_e$ is the Earth-relative velocity vector; $\dot{\mathbf{r}}^e = \mathbf{C}_i^e \dot{\mathbf{r}}^i$ is the first differential of position vector in the *e*-frame. By representing the velocity vector in the *i*-frame, the rotation of the *e*-frame with respect to the *i*-frame can be derived with the derivative of position through the theorem of Coriolis:

$$\begin{aligned} \mathbf{v}_e^i + \boldsymbol{\Omega}_{ie}^i \mathbf{r}^i &= \frac{d}{dt}\mathbf{r}^i \\ \frac{d^2}{dt^2}\mathbf{r}^i &= \frac{d}{dt}\mathbf{v}_e^i + \frac{d}{dt}\left(\boldsymbol{\Omega}_{ie}^i \mathbf{r}^i\right) \\ &= \frac{d}{dt}\mathbf{v}_e^i + \boldsymbol{\Omega}_{ie}^i\left(\mathbf{v}_e^i + \boldsymbol{\Omega}_{ie}^i \mathbf{r}^i\right) \end{aligned} \tag{A2.15}$$

where $\mathbf{v}_e^i$ is the Earth-relative velocity vector in the *i*-frame; $\mathbf{r}^i$ is the position vector in the *i*-frame; $\boldsymbol{\Omega}_{ie}^i$ is the skew-symmetric matrix of Earth rotation rate in the *i*-frame. By rearranging the terms in eqn. A2.3, the Earth-relative acceleration in the *i*-frame can be described as eqn. A2.4.

$$\begin{aligned} \frac{d}{dt}\mathbf{v}_e^i &= \frac{d^2}{dt^2}\mathbf{r}^i - \boldsymbol{\Omega}_{ie}^i\left(\mathbf{v}_e^i + \boldsymbol{\Omega}_{ie}^i \mathbf{r}^i\right) \\ &= \frac{d^2}{dt^2}\mathbf{r}^i - \boldsymbol{\Omega}_{ie}^i \boldsymbol{\Omega}_{ie}^i \mathbf{r}^i - \boldsymbol{\Omega}_{ie}^i \mathbf{v}_e^i \end{aligned} \tag{A2.16}$$

where $\frac{d}{dt}\mathbf{v}_e^i$ is the acceleration relative to the Earth in the *i*-frame; $\frac{d^2}{dt^2}\mathbf{R}^i$ is the inertial acceleration; $\boldsymbol{\Omega}_{ie}^i \boldsymbol{\Omega}_{ie}^i \mathbf{R}^i$ is the term of local centripetal acceleration; $\boldsymbol{\Omega}_{ie}^i \mathbf{v}_e^i$ is the term of Coriolis acceleration. With the substitution of specific force and local

gravity acceleration, the equation can be finalised for the time derivative of earth's relative velocity in the *i*-frame as shown in eqn. A2.5.

$$\frac{d}{dt}\mathbf{v}_e^i = \mathbf{f}^i + \mathbf{g}^i - \mathbf{\Omega}_{ie}^i \mathbf{v}_e^i \tag{A2.17}$$

where $\mathbf{f}^i$ is the specific force in the *i*-frame; $\mathbf{g}^i$ is the local gravity vector in the *i*-frame.

A2.2.2. Velocity Derivative in the Earth Frame

After deriving the basis of the dynamic equations and related terms in the *i*-frame, the Earth-relative velocity vector ($\mathbf{v}_e^i$) in the *i*-frame can be transformed into the *e*-frame with the consideration of the Earth's rotation rate. The time rate of change of Earth-relative velocity in the *e*-frame is defined with the rotation of the *e*-frame relative to the *i*-frame as shown in eqn. A2.6.

$$\begin{aligned} \mathbf{v}_e^e &= \mathbf{C}_i^e \mathbf{v}_e^i \\ \dot{\mathbf{v}}_e^e &= \mathbf{C}_i^e \left(\dot{\mathbf{v}}_e^i - \mathbf{\Omega}_{ie}^i \mathbf{v}_e^i \right) \\ &= \mathbf{C}_i^e \left(\mathbf{f}^i + \mathbf{g}^i - \mathbf{\Omega}_{ie}^i \mathbf{v}_e^i - \mathbf{\Omega}_{ie}^i \mathbf{v}_e^i \right) \\ &= \mathbf{f}^e + \mathbf{g}^e - 2\mathbf{\Omega}_{ie}^e \mathbf{v}_e^e \end{aligned} \tag{A2.18}$$

where $\mathbf{C}_i^e$ is the rotation matrix for the transformation from the *i*-frame to the *e*-frame; $\mathbf{v}_e^e$ is the Earth-relative velocity vector in the *e*-frame; $\mathbf{f}^e = \mathbf{C}_b^e \mathbf{f}^b$ is the specific force in the *e*-frame, which is transformed from the *b*-frame; $\mathbf{g}^e$ is the local gravity acceleration vector in the *e*-frame.

A2.2.3. Velocity Derivative in the Navigation Frame

The Earth-relative velocity vector ($\mathbf{v}_e^i$) in the *i*-frame can be transformed to the navigation frame with the consideration of the Earth's rotation rate and the transport

rate. The time rate of change of earth-relative velocity in the *n*-frame is elaborated in eqn. A2.7.

$$\begin{aligned}\mathbf{v}_e^n &= \mathbf{C}_i^n \mathbf{v}_e^i \\ \dot{\mathbf{v}}_e^n &= \mathbf{C}_i^n\left(\dot{\mathbf{v}}_e^i - \boldsymbol{\Omega}_{in}^i \mathbf{v}_e^i\right) \\ &= \mathbf{C}_i^n\left(\mathbf{f}^i + \mathbf{g}^i - \boldsymbol{\Omega}_{ie}^i \mathbf{v}_e^i - \boldsymbol{\Omega}_{ie}^i \mathbf{v}_e^i\right) \\ &= \mathbf{f}^n + \mathbf{g}^n - (\boldsymbol{\Omega}_{en}^n + 2\boldsymbol{\Omega}_{ie}^n)\mathbf{v}_e^n \end{aligned} \quad \text{(A2.19)}$$

where $\boldsymbol{\Omega}_{in}^n = \boldsymbol{\Omega}_{en}^n + \boldsymbol{\Omega}_{ie}^n$ is the sum of transport rate and the Earth's rotation rate; $\boldsymbol{\Omega}_{en}^n$ is the transport rate for the *n*-frame relative to the *e*-frame; $\boldsymbol{\Omega}_{ie}^n$ is the Earth's rotation rate in the *n*-frame; $\mathbf{f}^n = \mathbf{C}_b^n \mathbf{f}^b$ is the specific force in the *n*-frame, which can be transformed from the *b*-frame; $\mathbf{g}^n = [\zeta_g \quad -\eta_g \quad g]^T$ is the local gravity vector in the *n*-frame. The term $(\boldsymbol{\Omega}_{en}^n + 2\boldsymbol{\Omega}_{ie}^n)$ can be expressed into eqn. A2.8.

$$\begin{aligned}\boldsymbol{\Omega}_{en}^n + 2\boldsymbol{\Omega}_{ie}^n &= \begin{bmatrix} 0 & \dot{\lambda}\sin\varphi & -\dot{\varphi} \\ -\dot{\lambda}\sin\varphi & 0 & -\dot{\lambda}\cos\varphi \\ \dot{\varphi} & \dot{\lambda}\cos\varphi & 0 \end{bmatrix} + 2\omega_{ie}\begin{bmatrix} 0 & \sin\varphi & 0 \\ -\sin\varphi & 0 & -\cos\varphi \\ \dot{0} & \cos\varphi & 0 \end{bmatrix} \\ &= \begin{bmatrix} 0 & (\dot{\lambda}+2\omega_{ie})\sin\varphi & -\dot{\varphi} \\ -(\dot{\lambda}+2\omega_{ie})\sin\varphi & 0 & -(\dot{\lambda}+2\omega_{ie})\cos\varphi \\ \dot{\varphi} & (\dot{\lambda}+2\omega_{ie})\cos\varphi & 0 \end{bmatrix} \end{aligned} \quad \text{(A2.20)}$$

where $\boldsymbol{\omega}_{en}^n = [\dot{\lambda}\cos\varphi \quad -\dot{\varphi} \quad -\dot{\lambda}\sin\varphi]^T$ is the transport rate vector due to position change; $\boldsymbol{\omega}_{ie}^n = \omega_{ie}[\cos\varphi \quad 0 \quad -\sin\varphi]^T$ is the Earth's rotation rate vector.

A2.3. Kinematic Equations for Attitude

Since the angular velocities are sensed by the gyroscope in the *b*-frame relative to the *i*-frame, the time rate of change of the direction cosine matrix in the *n*-frame can be determined through transformation and compensation of angular velocity between the frames as shown in eqn. A2.9.

$$\begin{aligned}\dot{\mathbf{C}}_b^n &= \mathbf{C}_b^n \boldsymbol{\Omega}_{nb}^b \\ &= \mathbf{C}_b^n\left(\boldsymbol{\Omega}_{ib}^b - \boldsymbol{\Omega}_{in}^b\right)\end{aligned}$$

$$= \mathbf{C}_b^n \boldsymbol{\Omega}_{ib}^b - \mathbf{C}_b^n \mathbf{C}_n^b (\boldsymbol{\Omega}_{ie}^n + \boldsymbol{\Omega}_{en}^n) \mathbf{C}_b^n$$
$$= \mathbf{C}_b^n \boldsymbol{\Omega}_{ib}^b - (\boldsymbol{\Omega}_{ie}^n + \boldsymbol{\Omega}_{en}^n) \mathbf{C}_b^n \quad \text{(A2.21)}$$

where $\boldsymbol{\Omega}_{ib}^b$ is the skew matrix of angular velocity ($\boldsymbol{\omega}_{ib}^b$) sensed in the *b*-frame relative to the *i*-frame.

A2.4. Error State Dynamic Model

Through the linearization of kinematic navigation equations, the dynamic model can be derived with respect to the error state, which is employed for the extended Kalman filtering process. The navigation errors and sensor bias errors for a basic INS can be defined with an error state model as illustrated in eqn. A2.10.

$$\begin{aligned} \delta \mathbf{x}_n &= [\delta\varphi \quad \delta\lambda \quad \delta h \quad \delta v_n \quad \delta v_e \quad \delta v_d \quad \epsilon_n \quad \epsilon_e \quad \epsilon_d]^T \\ \delta \mathbf{x}_s &= [\delta f_x \quad \delta f_y \quad \delta f_z \quad \delta\omega_x \quad \delta\omega_y \quad \delta\omega_z]^T \end{aligned} \quad \text{(A2.22)}$$

where $\mathbf{x}_n$ and $\mathbf{x}_n$ are the navigation error state vector and the sensor error state vector respectively; $\delta\mathbf{r} = [\delta\varphi \quad \delta\lambda \quad \delta h]^T$ are the position errors; $\delta\mathbf{v} = [\delta v_n \quad \delta v_e \quad \delta v_d]^T$ are the Earth-relative velocity errors; $\boldsymbol{\rho} = [\epsilon_n \quad \epsilon_e \quad \epsilon_d]^T$ are the attitude errors; $\delta\mathbf{f}^b = [\delta f_x \quad \delta f_y \quad \delta f_z]^T$ are the accelerometer errors; $\delta\boldsymbol{\omega}_{ib}^b = [\delta\omega_x \quad \delta\omega_y \quad \delta\omega_z]^T$ are the gyroscope errors.

A2.4.1. Linearised Position Error Equation

The kinematic equation for position as illustrated in eqn. B.1 can be linearised in the form of eqn. A2.11, while $\mathbf{F}_{rr}$, $\mathbf{F}_{rv}$ and $\mathbf{F}_{r\rho}$ are the derivatives with respect to the error states.

$$\begin{aligned} \dot{\mathbf{r}} &= \mathbf{f}_r(\hat{\mathbf{r}}, \hat{\mathbf{v}}) + \mathbf{F}_{rr}\delta\mathbf{r} + \mathbf{F}_{rv}\delta\mathbf{v} + \mathbf{F}_{r\rho}\,\boldsymbol{\rho} \\ \delta\dot{\mathbf{r}} &= \mathbf{F}_{rr}\delta\mathbf{r} + \mathbf{F}_{rv}\delta\mathbf{v} + \mathbf{F}_{r\rho}\,\boldsymbol{\rho} \end{aligned} \quad \text{(A2.23)}$$

$$\mathbf{F}_{rr} = \begin{bmatrix} 0 & 0 & \dfrac{-\hat{v}_n}{\left(R_M + \hat{h}\right)^2} \\ \dfrac{\hat{v}_e \sin\hat{\varphi}}{\cos^2\hat{\varphi}\left(R_N + \hat{h}\right)} & 0 & \dfrac{-\hat{v}_e}{\cos\hat{\varphi}\left(R_N + \hat{h}\right)^2} \\ 0 & 0 & 0 \end{bmatrix} \tag{A2.24}$$

$$\mathbf{F}_{rv} = \begin{bmatrix} \dfrac{1}{R_M + \hat{h}} & 0 & 0 \\ 0 & \dfrac{1}{\cos\varphi\left(R_N + \hat{h}\right)} & 0 \\ 0 & 0 & -1 \end{bmatrix} \tag{A2.25}$$

$$\mathbf{F}_{r\rho} = \begin{bmatrix} 0 & 0 & 0 \\ 0 & 0 & 0 \\ 0 & 0 & 0 \end{bmatrix} \tag{A2.26}$$

A2.4.2. Linearised Velocity Error Equation

The kinematic equation for velocity as illustrated in eqn. B.7 can be rearranged and linearised in the form of eqn. B.15, while $\mathbf{F}_{vr}$, $\mathbf{F}_{vv}$ and $\mathbf{F}_{v\rho}$ are the derivatives with respect to the error states.

$$\begin{aligned} \dot{\hat{\mathbf{v}}} &= \hat{\mathbf{f}}^n + \hat{\mathbf{g}}^n - \left(\widehat{\boldsymbol{\Omega}}_{en}^n + 2\widehat{\boldsymbol{\Omega}}_{ie}^n\right)\hat{\mathbf{v}}^n \\ &= \hat{\mathbf{C}}_b^n\left(\tilde{\mathbf{f}}^b - \Delta\hat{\mathbf{f}}^b\right) + \hat{\mathbf{g}}^n - \left(\widehat{\boldsymbol{\Omega}}_{en}^n + 2\widehat{\boldsymbol{\Omega}}_{ie}^n\right)\hat{\mathbf{v}}^n \\ &= \left(\mathbf{I} - \boldsymbol{\Omega}_\rho\right)\mathbf{C}_b^n\mathbf{f}^b + \hat{\mathbf{C}}_b^n\left(\Delta\mathbf{f}^b - \Delta\hat{\mathbf{f}}^b\right) + \hat{\mathbf{g}}^n - \left(\widehat{\boldsymbol{\Omega}}_{en}^n + 2\widehat{\boldsymbol{\Omega}}_{ie}^n\right)\hat{\mathbf{v}}^n \\ \dot{\mathbf{v}} &= \mathbf{f}^n + \mathbf{g}^n - \left(\widehat{\boldsymbol{\Omega}}_{en}^n + 2\widehat{\boldsymbol{\Omega}}_{ie}^n\right)\hat{\mathbf{v}}^n - \boldsymbol{\Omega}_\rho\mathbf{f}^n + \hat{\mathbf{C}}_b^n\delta\mathbf{f}^b - \delta\mathbf{g}^n \\ \delta\dot{\mathbf{v}} &= -\left(\widehat{\boldsymbol{\Omega}}_{en}^n + 2\widehat{\boldsymbol{\Omega}}_{ie}^n\right)\delta\mathbf{v} - \left(\delta\widehat{\boldsymbol{\Omega}}_{en}^n + 2\delta\widehat{\boldsymbol{\Omega}}_{ie}^n\right)\hat{\mathbf{v}}^n + \boldsymbol{\Omega}_\rho\mathbf{f}^n - \hat{\mathbf{C}}_b^n\delta\mathbf{f}^b + \delta\mathbf{g}^n \\ &= \mathbf{F}_{vp}\delta\mathbf{r} + \mathbf{F}_{vv}\delta\mathbf{v} + \mathbf{F}_{v\rho}\,\boldsymbol{\rho} - \mathbf{C}_b^n\delta\mathbf{f}^b \end{aligned} \tag{A2.27}$$

where $\boldsymbol{\Omega}_\rho$ is the skew symmetric matrix of attitude errors.

$$\mathbf{F}_{vr} = \begin{bmatrix} -2\omega_{ie}\hat{v}_e - \dfrac{\hat{v}_e^2}{\cos\hat{\varphi}\,(R_N+\hat{h})} & 0 & \dfrac{-\hat{v}_n\hat{v}_d}{(R_M+\hat{h})^2} + \dfrac{\hat{v}_e^2\tan\hat{\varphi}}{(R_N+\hat{h})^2} \\ 2\omega_{ie}(\cos\hat{\varphi}\,\hat{v}_n - \sin\hat{\varphi}\,\hat{v}_d) + \dfrac{\hat{v}_e\hat{v}_n}{\cos^2\hat{\phi}\,(R_N+\hat{h})} & 0 & -\dfrac{\hat{v}_n\hat{v}_e\tan\hat{\varphi} + \hat{v}_d\hat{v}_e}{(R_N+\hat{h})^2} \\ 2\omega_{ie}\sin\hat{\varphi}\,\hat{v}_e & 0 & \dfrac{\hat{v}_n^2}{(R_M+\hat{h})^2} + \dfrac{\hat{v}_e^2}{(R_N+\hat{h})^2} \end{bmatrix} \quad \text{(A2.28)}$$

$$\mathbf{F}_{vv} = \begin{bmatrix} \dfrac{\hat{v}_d}{R_M+\hat{h}} & -2\left(\omega_{ie}\sin\hat{\varphi} + \dfrac{\hat{v}_e\tan\hat{\varphi}}{R_N+\hat{h}}\right) & \dfrac{\hat{v}_n}{R_N+\hat{h}} \\ 2\omega_{ie}\sin\hat{\varphi} + \dfrac{\hat{v}_e\tan\hat{\varphi}}{R_N+\hat{h}} & \dfrac{\hat{v}_d + \hat{v}_n\tan\hat{\phi}}{R_M+\hat{h}} & 2\omega_{ie}\cos\hat{\varphi} + \dfrac{\hat{v}_e}{R_N+\hat{h}} \\ -\dfrac{2\hat{v}_n}{R_M+\hat{h}} & -2\left(\omega_{ie}\cos\hat{\varphi} + \dfrac{\hat{v}_e}{R_N+\hat{h}}\right) & 0 \end{bmatrix} \quad \text{(A2.29)}$$

$$\mathbf{F}_{v\rho} = \begin{bmatrix} 0 & f_d & -f_e \\ -f_d & 0 & f_n \\ f_e & -f_n & 0 \end{bmatrix} \quad \text{(A2.30)}$$

A2.4.3. Linearised Attitude Error Equation

The kinematic equation for attitude as illustrated in eqn. A2.9 can be written in the form of vector as shown in eqn. A2.19, while the term $\delta\boldsymbol{\omega}_{in}^{b}$ can be determined by eqn. A2.20.

$$\dot{\boldsymbol{\rho}} = \hat{\mathbf{C}}_b^n\left(\delta\boldsymbol{\omega}_{ib}^b - \delta\boldsymbol{\omega}_{in}^b\right) \quad \text{(A2.31)}$$

$$\begin{aligned} \boldsymbol{\omega}_{in}^b &= \mathbf{C}_n^b\boldsymbol{\omega}_{in}^n \\ \hat{\boldsymbol{\omega}}_{in}^b + \delta\boldsymbol{\omega}_{in}^b &= \hat{\mathbf{C}}_n^b(\mathbf{I} - \boldsymbol{\Omega}_\rho)(\hat{\boldsymbol{\omega}}_{in}^n + \delta\boldsymbol{\omega}_{in}^n) \\ \delta\boldsymbol{\omega}_{in}^b &= \hat{\mathbf{C}}_n^b\left(\delta\boldsymbol{\omega}_{in}^n - \boldsymbol{\Omega}_\rho\hat{\boldsymbol{\omega}}_{in}^n\right) \end{aligned} \quad \text{(A2.32)}$$

By substituting eqn. A2.20 into eqn. A2.19, the attitude equation can be linearised into eqn. A2.21, while $\mathbf{F}_{\rho r}$, $\mathbf{F}_{\rho v}$ and $\mathbf{F}_{\rho\rho}$ are the derivatives with respect to the error states.

$$\dot{\boldsymbol{\rho}} = \hat{\mathbf{C}}_b^n\delta\boldsymbol{\omega}_{ib}^b - \hat{\mathbf{C}}_b^n\hat{\mathbf{C}}_n^b\left(\delta\boldsymbol{\omega}_{in}^n - \boldsymbol{\Omega}_\rho\hat{\boldsymbol{\omega}}_{in}^n\right)$$

$$= \hat{\mathbf{C}}_b^n \delta\boldsymbol{\omega}_{ib}^b - \delta\boldsymbol{\omega}_{in}^n - \boldsymbol{\Omega}_{in}^n \boldsymbol{\rho}$$
$$= \mathbf{F}_{\rho r}\delta\mathbf{r} + \mathbf{F}_{\rho v}\delta\mathbf{v} + \mathbf{F}_{\rho\rho}\,\boldsymbol{\rho} + \hat{\mathbf{C}}_b^n \delta\boldsymbol{\omega}_{ib}^b \tag{A2.33}$$

$$\mathbf{F}_{\rho r} = -\frac{\delta\boldsymbol{\omega}_{in}^n}{\delta\hat{\mathbf{r}}}$$
$$= \begin{bmatrix} \omega_{ie}\sin\hat{\varphi} & 0 & \dfrac{\hat{v}_e}{\left(R_N+\hat{h}\right)^2} \\ 0 & 0 & \dfrac{-\hat{v}_n}{\left(R_M+\hat{h}\right)^2} \\ \omega_{ie}\cos\hat{\varphi} + \dfrac{\hat{v}_e}{\left(R_N+\hat{h}\right)\cos^2\hat{\varphi}} & 0 & \dfrac{-\hat{v}_e\tan\hat{\varphi}}{\left(R_N+\hat{h}\right)^2} \end{bmatrix} \tag{A2.34}$$

$$\mathbf{F}_{\rho v} = -\frac{\delta\boldsymbol{\omega}_{in}^n}{\delta\hat{\mathbf{v}}}$$
$$= \begin{bmatrix} 0 & \dfrac{-1}{R_N+\hat{h}} & 0 \\ \dfrac{1}{R_M+\hat{h}} & 0 & 0 \\ 0 & \dfrac{\tan\hat{\varphi}}{R_N+\hat{h}} & 0 \end{bmatrix} \tag{A2.35}$$

$$\mathbf{F}_{\rho\rho} = -\boldsymbol{\Omega}_{in}^n$$
$$= \begin{bmatrix} 0 & -\dfrac{\hat{v}_e\tan\hat{\varphi}}{R_N+\hat{h}} - \omega_{ie}\sin\hat{\varphi} & \dfrac{\hat{v}_n}{R_M+\hat{h}} \\ \dfrac{\hat{v}_e\tan\hat{\varphi}}{R_N+\hat{h}} + \omega_{ie}\sin\hat{\varphi} & 0 & \dfrac{\hat{v}_e}{R_N+\hat{h}} + \omega_{ie}\cos\hat{\varphi} \\ -\dfrac{\hat{v}_n}{R_M+\hat{h}} & -\dfrac{\hat{v}_e}{R_N+\hat{h}} - \omega_{ie}\cos\hat{\varphi} & 0 \end{bmatrix} \tag{A2.36}$$

Appendix 3 - Kalman Filter Basis

For typical inertial navigation solution, the Kalman filter is usually employed to integrate the navigation results with other sensors and data. To facilitate the development, the RBN solution is established on the basis of the typical INS mechanisation and Kalman filtering solution, while the fundamentals of Kalman filter are reviewed and summarised here.

A3.1. Fundamental Principles of Kalman Filter

The Kalman filter is an algorithm which utilise a bundle of measurements with respect to time for estimating unknown variables by compensating measurement errors and processing errors. It is an estimator for the state of a linear dynamic system perturbed by the Gaussian white noise, while the measurements are used and processed with linear functions of system state with additive Gaussian white noise (Grewal and Andrews, 2008). In general, the Kalman filter has the following properties (Farrell, 2008):

- The estimate is unbiased;
- The estimate is minimum mean-squared error estimate with Gaussian distribution;
- The estimate is the minimum of positive definite quadratic cost function and non-decreasing function of estimation error;
- The Kalman filter is an optimal state estimation algorithm for linear system;
- The residual state error is orthogonal to all previous measurements;
- The measurement residual is white;
- The effects of initial conditions decay with time.

A3.2. Models for Kalman Filter

The Kalman filter algorithm generally involves a two-step process: the prediction updates and measurement updates, while the process model and measurement model are formulated in a linear form. For the state transition, the process model is formulated as a dynamic model with physical properties, which is employed for prediction updates from previous state as shown in eqn. A3.1.

$$\mathbf{x}_t = \mathbf{F}_t\mathbf{x}_{t-1} + \mathbf{B}_t\mathbf{u}_{t-1} + \mathbf{w}_t \quad \text{(A3.1)}$$

where $\mathbf{x}$ is the system state vector; $\mathbf{u}$ is the control vector; $\mathbf{F}_t$ is the state transition model; $\mathbf{B}_t$ is the control-input model; and $\mathbf{w}_t$ is the process noise assumed to be zero-mean multivariate normal distribution with covariance $\mathbf{Q}_t$. The system state is defined for variables of interest while the dynamic model is derived for prediction updates. The relationship between the physical measurements and the variables is defined by a measurement model.

$$\mathbf{z}_t = \mathbf{H}_t\mathbf{x}_t + \mathbf{v}_t \quad \text{(A3.2)}$$

where $\mathbf{z}_t$ is the measurements; $\mathbf{H}_t$ is the measurement model relating the state and measurements; $\mathbf{v}_t$ is the measurement noise assumed to be zero-mean multivariate normal distribution with covariance $\mathbf{R}_t$.

A3.3. Kalman Filter Processes

Following the established process model, the prediction of state estimate can be performed by the dynamic model as shown in eqn. A3.3, while the covariance of state estimate is propagated through eqn. A3.4.

$$\hat{\mathbf{x}}_{t|t-1} = \mathbf{F}_t\hat{\mathbf{x}}_{t-1|t-1} + \mathbf{B}_t\mathbf{u}_{t-1} \quad \text{(A3.3)}$$

$$\mathbf{P}_{t|t-1} = \mathbf{F}_t \mathbf{P}_{t-1|t-1} \mathbf{F}_t^T + \mathbf{Q}_t \quad \text{(A3.4)}$$

Since the dynamic model involves processing noise, the state estimate requires further adjustment by external measurements to constrain the growth of process uncertainties. For measurement updates, the difference between measurements and estimated measurements from the state estimate is defined as the measurement residual or innovation (eqn. A3.5), while the corresponding covariance is propagated through eqn. A3.6.

$$\tilde{\mathbf{y}}_t = \tilde{\mathbf{z}}_t - \mathbf{H}_t \hat{\mathbf{x}}_{t|t-1} \quad \text{(A3.5)}$$

$$\mathbf{S}_t = \mathbf{H}_t \mathbf{P}_{t|t-1} \mathbf{H}_t^T + \mathbf{R}_t \quad \text{(A3.6)}$$

The Kalman gain is a weighing factor determined by the covariance of state estimate and the covariance of innovation, which is summarised in eqn. A3.7. Consequently, the Kalman gain is employed to weigh the state correction (eqn. A3.8) and update the state covariance (eqn. A3.9).

$$\mathbf{K}_t = \mathbf{P}_{t|t-1} \mathbf{H}_t^t \mathbf{S}_t^{-1} \quad \text{(A3.7)}$$

$$\hat{\mathbf{x}}_{t|t} = \hat{\mathbf{x}}_{t|t-1} + \mathbf{K}_t \tilde{\mathbf{y}}_t \quad \text{(A3.8)}$$

$$\mathbf{P}_{t|t} = (\mathbf{I} - \mathbf{K}_t \mathbf{H}_t) \mathbf{P}_{t|t-1} \quad \text{(A3.9)}$$

Since the prediction updates and measurement updates are individually performed, they can be processed at different rates. For an aided navigation system, the prediction process is operated to provide navigation results and uncertainties at a given rate. The measurement updating process is then performed at the sample rate of measurements for error control.

A3.4. Kalman Filter for Non-linear System

For navigation applications such as inertial navigation, the system dynamic equations and the measurement equations are non-linearly defined. Since the Kalman filter algorithm is a linear quadratic estimation, it cannot be directly applied to a non-linear system. The general approaches for non-linear filtering are linearised Kalman filter and extended Kalman filter. For a non-linear system, the dynamic model and the measurement model can be derived by eqn. A3.10 and eqn. A3.11 respectively.

$$\begin{aligned}
\dot{\mathbf{x}}(t) &= \dot{\bar{\mathbf{x}}}(t) + \delta\dot{\mathbf{x}}(t) \\
&= \mathbf{f}(\mathbf{x}(t), \mathbf{u}(t), t) + \mathbf{w}(t) \\
&= \mathbf{f}(\bar{\mathbf{x}}(t) + \delta\mathbf{x}(t), \mathbf{u}(t), t) + \mathbf{w}(t) \\
&= \mathbf{f}(\bar{\mathbf{x}}(t), \mathbf{u}(t), t) + \left.\frac{\partial \mathbf{f}}{\partial \mathbf{x}(t)}\right|_{\mathbf{x}=\bar{\mathbf{x}}} \delta\mathbf{x}(t) + \mathbf{w}(t) \\
\delta\dot{\mathbf{x}}(t) &= \mathbf{F}(\bar{\mathbf{x}}, \mathbf{u}, t)\delta\mathbf{x}(t) + \mathbf{w}(t)
\end{aligned} \tag{A3.10}$$

where $\mathbf{x}(t) = \bar{\mathbf{x}}(t) + \delta\mathbf{x}(t)$ is linearized by approximation with error state; $\mathbf{F}(\bar{\mathbf{x}}(t), \mathbf{u}(t), t) = \left.\frac{\partial \mathbf{f}}{\partial \mathbf{x}(t)}\right|_{\mathbf{x}=\bar{\mathbf{x}}}$ is the derivative of dynamic model relative to error state.

$$\begin{aligned}
\mathbf{y}(t) &= \mathbf{h}(\mathbf{x}(t), t) + \mathbf{v}(t) \\
&= \mathbf{h}(\bar{\mathbf{x}}(t) + \delta\mathbf{x}(t), t) + \mathbf{v}(t) \\
&= \mathbf{h}(\bar{\mathbf{x}}(t), t) + \left.\frac{\partial \mathbf{h}}{\partial \mathbf{x}(t)}\right|_{\mathbf{x}=\bar{\mathbf{x}}} \delta\mathbf{x}(t) + \mathbf{v}(t) \\
\boldsymbol{z}(t) &= \mathbf{y}(t) - \bar{\mathbf{y}}(t) \\
&= \mathbf{H}(\bar{\mathbf{x}}(t), t)\, \delta\mathbf{x}(t) + \mathbf{v}(t)
\end{aligned} \tag{A3.11}$$

where $\mathbf{H}(\bar{\mathbf{x}}(t), t) = \left.\frac{\partial \mathbf{h}}{\partial \mathbf{x}(t)}\right|_{\mathbf{x}=\bar{\mathbf{x}}}$ is the derivative of measurement model relative to error state.

The linearised error dynamics is defined for using the linear Kalman filter to estimate the approximation of a non-linear system through the first-order linearisation. The error state is estimated from the Kalman filter process, while the state estimate can be

obtained by correction to state with the estimated error state. The implementation of non-linear filtering can be performed by linearised Kalman filter or extended Kalman filter.

A3.4.1. Linearised Kalman filter

The linearised Kalman filter is employed in some applications with predetermined trajectory, such as orbiting satellites (Farrell, 2008). In case that the nominal trajectory is available, parts of the calculation can be done off-line as the measurements do not affect the calculation of system parameters, such as state transition model, measurement model, the weight matrices, or Kalman gain. The remaining measurement updates are left for on-line computation.

Through the linearised Kalman filter, real-time operation is more feasible since the data processing can be simplified. The computation is similar to the fundamental approach with the error state definition and its linearised measurement model.

A3.4.2. Extended Kalman Filter

For general applications, the navigation trajectory cannot be accurately pre-determined with the design of navigation system. Extended Kalman Filter (EKF) can be used to serve for non-linear filtering in INS process, the nominal trajectory is defined to be equal to the estimated trajectory with inertial sensor measurements, such that the state estimation computation is dependent on measurements. If the state is observable from the measurements and the measurements are accurate enough (Farrell, 2008):

- The state estimate should be near to the actual state;
- The linearisation should be accurate; and
- The performance should be sufficiently good.

However, it is possible that the linearisation would be inaccurate and the estimate may rapidly diverge if the initial estimate is of poor accuracy or the process is incorrectly modelled. Regarding the first-order EKF, more terms can be retained for higher-order linearisation, which reduce the errors in choosing the first order Taylor series approximation as a linearising process (Al-Shabi, 2011). The use of higher order terms of Taylor series approximation can reduce the truncation error due to the neglected terms, especially for highly non-linear systems. The implementation of higher-order system model, however, may not be feasible for fast computation due to increased system non-linearity.

Since the EKF works on first-order approximation, iteration can be performed to improve the accuracy. The iterative EKF repeats the computation at current time step by refining the nominal state estimate and re-linearising the measurement equations. The iterative solution can provide better performance than basic EKF, especially for high system non-linearity (Wan and Merwe, 2001). Through iterations, the computation load would be much higher and more processing time is required.

A3.4.3. Unscented Kalman Filter

The Unscented Kalman Filter (UKF) is considered a sigma-point Kalman filter, which is a derivative-free alternative to EKF and provides superior performance at an equivalent computational complexity (Wan and Merwe, 2001).

For typical EKF, the state distribution is propagated through the first-order linearisation of non-linear system, while the posterior mean and covariance could be corrupted (Terejanu, 2009). The use of UKF overcomes the problem by using a deterministic sampling approach known as unscented transform (UT) to select a minimal set of sample point called sigma points for propagating mean and

covariance estimates through non-linear transformations, which avoids linearization by taking explicit derivatives as in general EKF.

Each sigma point is propagated through the non-linearity yielding in the end a cloud of transformed points, while the newly estimated mean and covariance are then computed based on the statistics (Terejanu, 2009). UKF can be implemented by different available methods of unscented transform, such as general UKF, simplex UKF, or spherical UKF (Al-Shabi, 2011).

A3.4.4. Particle Filter

The Particle Filter (PF) is a Sequential Importance Sampling (SIS) algorithm relies on handling the multi-dimensional integrals numerically, which is an alternative method for non-linear processing avoiding the linearization of the models. It is a sequential Monte Carlo method based on particle representations of probability densities, which can be applied to any state-space model and generalize the traditional Kalman filtering methods (Arulampalam et al., 2002).

Similar to UKF, the particle filter uses dynamic simulation of sample points as entrained "particles" carried forward in time through non-linear dynamics, then reconstruct the propagated mean and covariance matrix from the propagated samples (Grewal and Andrews, 2008). The sampling statistics are used for implementing the Kalman measurement update. Particle filter can be more accurate than UKF with enough particles (Grewal and Andrews, 2008).

The particle filters are also being used or enhanced for implementing aided inertial navigation for sensor integration (Gustafsson et al., 2002; Georgy et al., 2011), which can accommodate for arbitrary inertial sensor characteristics and motion dynamics.

REFERENCES

Al-Shabi, M. A. (2011). The General Toeplitz/Observability Smooth Variable Structure Filter. Ph. D. Thesis. McMaster University.

Aggarwal, P., Syed, Z., Noureldin, A. & El-Sheimy, N. (2010). MEMS-based Integrated Navigation. London: Artech House.

Almagbile, A., Wang, J. & Ding, W. (2010). Evaluating the Performance of Adaptive Kalman Filter Methods in GPS/INS Integration. Journal of Global Positioning Systems, 9(1), 33-40. http://dx.doi.org/10.5081/jgps.9.1.33

Arduino. (2016). In Arduino. Retrieved from https://www.arduino.cc/

Arulampalam, M. S., Maskell, S., Gordon, N. and Clapp, T. (2002). A Tutorial on Particle Filters for Online Nonlinear/Non-Gaussian Bayesian Tracking. IEEE Transactions on Signal Processing. Vol.50 (2).

Bailey, T. & Durrant-Whyte, H. (2006). Simultaneous Localization and Mapping (SLAM): Part II State of the Art. IEEE Robot. & Autom. Mag., 13(3), 108-117. http://dx.doi.org/10.1109/MRA.2006.1678144

Baltsavias, E. P. (1999a). A Comparison between Photogrammetry and Laser Scanning. ISPRS Journal of Photogramm. and Remote Sens., 54(2-3), 83-94. http://dx.doi.org/10.1016/S0924-2716(99)00014-3

Baltsavias, E. P. (1999b). Airborne Laser Scanning: Basic Relations and Formulas. ISPRS Journal of Photogramm. and Remote Sens., 54(2-3), 199-214. http://dx.doi.org/10.1016/S0924-2716(99)00015-5

Baltsavias, E. P. (1999c). Airborne Laser Scanning: Existing Systems and Firms and Other Resources. ISPRS Journal of Photogramm. and Remote Sens., 54(2-3), 164-198. http://dx.doi.org/10.1016/S0924-2716(99)00016-7

Barber, D., Mills, J. & Smith-Voysey, S. (2008). Geometric Validation of a Ground-based Mobile Laser Scanning System. ISPRS Journal of Photogramm. and Remote Sens., 63(1), 128-141. http://dx.doi.org/10.1016/j.isprsjprs.2007.07.005

Bayoud, F. A., Skaloud, J. & Merminod, B. (2004). Photogrammetry-derived Navigation Parameters for INS Kalman Filter Updates. Proc.of the 20th ISPRS Congress, 35(B5), 252-257. Istanbul, Turkey, 12-23 July 2004. Retrieved from http://www.isprs.org/proceedings/XXXV/congress/comm5/papers/559.pdf

Bekir, E. (2007). Introduction to Modern Navigation Systems. World Scientific.

Boavida, J., Oliveira, A. &Santos, B. (2012). Precise Long Tunnel Survey using the Riegl VMX-250 Mobile Laser Scanning System. In RIEGL Int. Airborne and Mobile User Conf (pp. 1-13). Orlando, FL, USA. 27 February – 01 March 2012. Retrieved from http://www.artescan.net/files/temps/documentos/1334120073_precise_long_tunnel_survey_using_the_riegl_vmx-250_mobile_laser_scanning_system.pdf

Bossler, J. D. & Toth, C. K. (1996). Feature Positioning Accuracy in Mobile Mapping: Results obtained by the GPSVan^{TM}. Int. Arch. of Photogramm. and Remote Sens., ISPRS Comm. IV, 31(B4), 139-142. Retrieved from http://www.isprs.org/proceedings/xxxi/congress/part4/139_XXXI-part4.pdf

Bufton, J. L. (1989). Laser Altimetry Measurements from Aircraft and Spacecraft. Proc. of the IEEE, 77(3), 463-477. http://dx.doi.org/10.1109/5.24131

Cai, G., Chen, B. M. & Lee, T. H. (2011). Unmanned Rotorcraft Systems. Springer. http://dx.doi.org/10.1007/978-0-85729-635-1

Cant deficiency. (n.d.). In Wikipedia, the Free Encyclopedia. Retrieved 26 January 2016, from https://en.wikipedia.org/wiki/Cant_deficiency

Chu, C. & Chiang, K. (2012). The Performance of a Tight INS/GNSS/Photogrammetric Integration Scheme for Land Based MMS Applications in GNSS Denied Environments. Int. Arch. of Photogramm., Remote Sens. and Spatial Inf. Sci., 39(B1), 479-484. Retrieved from http://www.int-arch-photogramm-remote-sens-spatial-inf-sci.net/XXXIX-B1/479/2012/isprsarchives-XXXIX-B1-479-2012.pdf

Durrant-Whyte, H. & Bailey, T. (2006). Simultaneous Localization and Mapping (SLAM): Part I The Essential Algorithms. IEEE Robot. & Autom. Mag., 13(2), 99-110. http://dx.doi.org/10.1109/MRA.2006.1638022

Elberink, S. O. & Khoshelham, K. (2015). Automatic Extraction of Railroad Centerlines from Mobile Laser Scanning Data. Remote Sens., 7(5), 5565−5583.

El-Sheimy, N. (1996). The Development of VISAT - A Mobile Survey System for GIS Applications. Ph.D. Dissertation, Department of Geomatics Engineering, The University of Calgary, Calgary, Alberta, Canada.

El-Sheimy, N. (2005). An Overview of Mobile Mapping Systems. Proc. of the FIG Working Week 2005 (pp. 1-24). Cairo, Egypt, 16-21 April 2005. Retrieved from https://www.fig.net/resources/proceedings/fig_proceedings/cairo/papers/ts_17/ts17_03_elsheimy.pdf

El-Sheimy, N. (2008). Georeferencing Component of LiDAR Systems. In Shan, J. & Toth, C. K. (Eds.), Topographic Laser Ranging and Scanning: Principles and Processing (pp. 195-214). Taylor & Francis Group, LLC.

El-Sheimy, N. & Schwarz, K. P. (1999). Navigating Urban Areas by VISAT - A Mobile Mapping System Integrating GPS/INS/Digital Cameras for GIS Applications. The Journal of Navigation, 45(4), 275-285. http://dx.doi.org/10.1002/j.2161-4296.1998.tb02387.x

El-Sheimy, N., Schwarz, K. P. & Gravel, M. (1995). Mobile 3-D Positioning using GPS/INS/Video Cameras. The Mobile Mapping Symposium (pp. 236-249). Ohio State, USA, 24-26 May 1995.

Ellum, C. & El-Sheimy, N. (2002). Land-based Mobile Mapping Systems. Photogramm. Eng. and Remote Sens., 68(1), 13-17 (and 28). Retrieved from http://www.asprs.org/a/publications/pers/2002journal/january/georef.pdf

Elseberg, J., Borrmann, D. & Nüchter, A. (2012). 6DOF Semi-rigid SLAM for Mobile Scanning. IEEE/RSJ Int. Conf. on IROS (pp. 1865-1870). Vilamoura, Portugal, 7-12 October 2012. http://dx.doi.org/10.1109/IROS.2012.6385509

Elseberg, J., Borrmann, D. & Nüchter, A. (2013). Algorithmic Solutions for Computing Precise Maximum Likelihood 3D Point Clouds from Mobile Laser Scanning Platforms. Remote Sens., 5(11), 5871-5906. http://dx.doi.org/10.3390/rs5115871

Explanatory Notes on Geodetic Datums in Hong Kong. (1995). Retrieved from Hong Kong Special Administrative Region Government, Lands Department: http://www.geodetic.gov.hk/smo/gsi/data/pdf/explanatorynotes.pdf

Farrell, J. A. (2008). Aided Navigation: GPS with High Rate Sensors. McGraw Hill Professional.

Farrell, J. A. & Barth, M. (1999). The Global Positioning System and Inertial Navigation (2nd ed.). McGraw Hill.

FreeIMU Calibration. (2014). In Github. Retrieved from https://github.com/mjs513/FreeIMU-Updates/wiki/04.-FreeIMU-Calibration

FreeIMU-Updates. (2016). In Github. Retrieved from https://github.com/mjs513/FreeIMU-Updates

Friess, P. (2006). Toward a Rigorous Methodology for Airborne Laser Mapping. Proc. of Int. Calibration and Orientation Workshop EuroCOW 2006 (pp. 1-7). Castelldefels, Spain, 25-27 January 2006. Retrieved from http://www.isprs.org/proceedings/2006/euroCOW06/euroCOW06_files/papers/PeterFriessEuroCOW_2006.pdf

Georgy, J., Karamat, T. B., Iqbal, U. and Noureldin, A. (2011). Enhanced MEMS-IMU/Odometer/GPS Integration Using Mixture Particle Filter. GPS Solutions. Vol.15 (3).

Goad, C. (1991). The Ohio State University Mapping System: The Positioning Component. Proc. of the 47th Annual Meeting of the Institute of Navigation (pp. 117-120). Williamsburg, VA, 10-12 June 1991.

Gonçalves, J. A., Mendes, R., Araújo, E., Oliveira, A. & Boavida, J. (2012). Planar Projection of Mobile Laser Scanning Data in Tunnels. Int. Arch. Photogramm. Remote Sens. Spat. Inf. Sci., XXXIX-B3, 109–113.

Grejner-Brzezinska, D. A. (2001). Direct Sensor Orientation in Airborne and Land-based Mapping Applications. Retrieved from https://earthsciences.osu.edu/sites/earthsciences.osu.edu/files/report-461.pdf

Grejner-Brzezinska, D. A., Li, R., Haala, N. & Toth, C. K. (2002). Multi-sensor Systems for Land-based and Airborne Mapping: Technology of the Future?.

ISPRS Commision II, WGII/1. China, 20-23 August 2002. Retrieved from http://www.isprs.org/proceedings/XXXIV/part2/paper/005_127.pdf

Grejner-Brzezinska, D. A., Li, R., Haala, N. & Toth, C. K. (2004). From Mobile Mapping to Telegeoinformatics: Paradigm Shift in Geospatial Data Acquisition, Processing, and Management. Photogramm. Eng. & Remote Sens., 70(2), 197-210. Retrieved from http://asprs.org/a/publications/pers/2004journal/february/2004_feb_197-210.pdf

Grewal, M. S. & Andrews, A. P. (2008). Kalman Filtering: Theory and Practice Using MATLAB. Wiley.

Grewal, M. S., Weill, L. R. & Andrews, A. P. (2007). Global Positioning Systems, Inertial Navigation, and Integration. Wiley. http://dx.doi.org/10.1002/0470099720

Groves, P. D. (2008). Principles of GNSS Inertial and Multisensor Integrated Navigation Systems (1st ed.). Artech House.

Groves, P. D. (2013). Principles of GNSS Inertial and Multisensor Integrated Navigation Systems (2nd ed.). Artech House.

Gustafsson, F., Gunnarsson, F., Bergman, N., Forssell, U., Jansson, J., Karlsson, R. and Nordlund, P.-J. (2002). Particle Filters for Positioning, Navigation and Tracking. IEEE Transactions on Signal Processing.

Haala, N., Peter, M., Kremer, J. & Hunter, G. (2008). Mobile LiDAR Mapping for 3D Point Cloud Collection in Urban Areas - A Performance Test. Int. Arch. Photogramm. Remote Sens. Spatial Inf. Sci., 37, 1119-1127.

Hassan, T., Ellum, C. & El-Sheimy, N. (2006a). Bridging Land-based Mobile Mapping using Photogrammetric Adjustments. Proc. of the 2006 ISPRS Commission I Symposium, from Sensors to Imagery (pp. 128-139). Paris, France, 4-6 May 2006. Retrieved from http://www.isprs.org/proceedings/XXXVI/part1/Papers/T10-44.pdf

Hassan, T., Ellum, C., Nassar, S. & El-Sheimy, N. (2006b). Photogrammetric Bridging of GPS/INS in Urban Centers for Mobile Mapping Applications. Proc.

of the ION GNSS 2006 (pp. 604-610). Fort Worth, Texas, USA. Retrieved from https://www.researchgate.net/publication/281638490_Photogrammetric_Bridging_of_GPSINS_in_Urban_Centers_for_Mobile_Mapping_Applications

He, G. & Novak, K. (1992). Automatic Analysis of Highway Features from Digital Stereo-images. Int. Arch. of Photogramm. and Remote Sens., 29(B3), 119-124. Retrieved from http://www.isprs.org/proceedings/XXIX/congress/part3/119_XXIX-part3.pdf

He, G., Novak, K. & Tang, W. (1994). The Accuracy of Features Positioned with the GPSVan. ISPRS Commission II Symposium, 30(2), 480-486.

Hong Kong: The Facts. (2015). Retrieved 20 February 2016 from Hong Kong Special Administrative Region Government, Transport Department: http://www.gov.hk/en/about/abouthk/factsheets/docs/transport.pdf

Hung, R., King, B. & Chen, W. (2015). Conceptual Issues Regarding the Development of Underground Railway Laser Scanning Systems. Int. Journal of Geo-Inf., 4(1), 185-198. http://dx.doi.org/10.3390/ijgi4010185

Hung, R., King, B. & Chen, W. (2016). A Method for the Positioning and Orientation of Rail-bound Vehicles in GNSS-free Environments. ISPRS Annals of the Photogramm. Remote Sens. Spat. Inf. Sci., III-1/W5, 135−142. http://dx.doi.org/10.5194/isprs-annals-III-1-135-2016

Hyyppä, J. (2011). State of the Art in Laser Scanning. In D. Fritsch (Ed.), Photogramm. Week 2011 (pp. 203-216). Retrieved from http://www.ifp.uni-stuttgart.de/publications/phowo11/210Hyyppa.pdf

Hyyppä, J., Wagner, W., Hollaus, M. & Hyyppä, H. (2009). Airborne Laser Scanning. In T. A. Warner, M. D. Nellis & G. M. Foody (Eds.), The SAGE Handbook of Remote Sens. (pp. 199-212). London: SAGE Publications Ltd. http://dx.doi.org/10.4135/9780857021052.n14

Imanishi, A. Tachibana, K. & Tsukahara, K. (2011). The Development of Accuracy Maintenance Method for Mobile Mapping System (MMS) Data at GPS Invisible Area. FIG Working Week 2011 (pp. 1-16). Marrakech, Morocco, 18-

22 May 2011. Retrieved from http://www.fig.net/resources/proceedings/fig_proceedings/fig2011/papers/ts07f/ts07f_imanishi_tachibana_et_al_4982.pdf

Island Line Closed after Metal Debris Hits MTR Train Window. (2012). Retrieved 29 April 2016 from Hong Kong Free Press: http://hongwrong.com/mtr-chaos/

Jwa, Y. & Sonh, G. (2015). Kalman Filter Based Railway Tracking from Mobile LiDAR Data. ISPRS Annals of the Photogramm. Remote Sens. Spat. Inf. Sci., II-3/W5, 159–164.

Kaartinen, H., Kukko, A., Hyyppä, J. & Jaakkola, A. (2012). Benchmarking Mobile Laser Scanning Systems using a Permanent Test Field. Int. Arch. of Photogramm., Remote Sens. and Spatial Inf. Sci., 39(B5), 471-476. Retrieved from http://www.int-arch-photogramm-remote-sens-spatial-inf-sci.net/XXXIX-B5/471/2012/isprsarchives-XXXIX-B5-471-2012.pdf

Kiencke, U. & Nielsen, L. (2000). Automotive Control Systems for Engine, Driveline, and Vehicle. Springer-Verlag,

Klein, I. & Filin, S. (2011). LiDAR and INS Fusion in Periods of GPS Outages for Mobile Laser Scanning Mapping Systems. Int. Arch. of Photogramm., Remote Sens. and Spatial Inf. Sci., 38(5/W12), 231-236. Retrieved from http://www.int-arch-photogramm-remote-sens-spatial-inf-sci.net/XXXVIII-5-W12/231/2011/isprsarchives-XXXVIII-5-W12-231-2011.pdf

Kremer, J. & Grimm, A. (2012). The RailMapper - A Dedicated Mobile LiDAR Mapping System for Railway Networks. Int. Arch. of Photogramm., Remote Sens. and Spatial Inf. Sci., 39(B5), 477-482. Retrieved from http://www.int-arch-photogramm-remote-sens-spatial-inf-sci.net/XXXIX-B5/477/2012/isprsarchives-XXXIX-B5-477-2012.pdf

Kruse, F., Milch, S. & Rohling, H. (2002). Multi Sensor System for Obstacle Detection in Train Applications. GRS 2002. Bonn.

Lau, S. (2014, 10 February). Thousands of passengers delayed after latest MTR breakdown. South China Morning Post. Retrieved April 29, 2016 from:

http://www.scmp.com/news/hong-kong/article/1424673/thousands-passengers-delayed-after-latest-mtr-breakdown

Lawrence, A. (1998). Modern Inertial Technology: Navigation, Guidance, and Control (2nd ed.). New York: Springer.

Leslar, M., Perry, G. & McNease, K. (2012). Using Mobile LiDAR to Survey a Railway Line for Asset Inventory. In ASPRS 2010 Annual Conf., San Diego, California. 26–30 April 2010.

Liu, H., Nassar, S. & El-Sheimy, N. (2010). Two-Filter Smoothing for Accurate INS/GPS Land-Vehicle Navigation in Urban Centers. IEEE Trans. on Veh. Technol., 59(9), 4256-4267. http://dx.doi.org/10.1109/TVT.2010.2070850

Morgan, D. (2009). Using Mobile LiDAR to Survey Railway Infrastructure. Lynx Mobile Mapper. Innovative Technologies for an Efficient Geospatial Management of Earth Resources.

Mostafa, M. & Hutton, J. (2001). Direct Positioning and Orientation Systems: How do they work? What is the Attainable Accuracy?. Proc. of American Society of Photogramm. and Remote Sens. Annual Meeting (pp. 1-11). Retrieved from http://www.applanix.com/media/downloads/articles_papers/POSAV_2001_04_DirectPositioning.pdf

Mostafa, M., Hutton, J. & Reid, B. (2001). GPS/IMU Products - The Applanix Approach. In Fritsch, D. & Spiller, R. (Eds.), Photogramm. Week 2001 (pp. 63-83). Wichmann Verlag, Heidelberg, Germany. Retrieved from http://www.ifp.uni-stuttgart.de/publications/phowo01/Reid.pdf

Nassar, S., Shin, E., Niu, X. & El-Sheimy, N. (2005). Accurate INS/GPS Positioning with Different Inertial Systems Using Various Algorithms for Bridging GPS Outages. Proc. of the ION GNSS 18th Int. Tech. Meeting of the Satellite Division (pp. 1401-1410). CA, USA, 13-16 September 2005. Retrieved from https://www.researchgate.net/publication/281628174_Accurate_INSGPS_Positioning_with_Different_Inertial_Systems_Using_Various_Algorithms_for_Bridging_GPS_Outages

Nassar, S. & Schwarz, K. P. (2002). Bridging DGPS Outages in Kinematic Applications Using a Simple Algorithm for INS Bias Modeling. Proc. of the ION GPS 2002 (pp. 1474-1482). Portland, USA, 24-27 September 2002. Retrieved from http://plan.geomatics.ucalgary.ca/papers/PDF/0703.PDF

Ngo, J. (2013, 18 May). MTR faces HK$15m fine over Yuen Long derailment. South China Morning Post. Retrieved April 29, 2016 from: http://www.scmp.com/news/hong-kong/article/1240668/mtr-corporation-may-face-heavy-fine-train-derailment

Noureldin, A., Karamat, T. B. & Georgy, J. (2013). Fundamentals of Inertial Navigation, Satellite-based Positioning and their Integration. Springer.

Novak, K. (1991). The Ohio State University Mapping System: The Stereo Vision System Component. Proc. of the 47th Annual Meeting of the Institute of Navigation (pp. 121-124). Williamsburg, VA, 10-12 June 1991.

Novak, K. & Bossler, J. D. (1995). Development and Application of the Highway Mapping System of Ohio State University. The Photogramm. Record, 15(85), 123-134. http://dx.doi.org/10.1111/0031-868X.00012

Nüchter, A., Borrmann, D., Koch, P., Kühn, M. & May, S. (2015). A Man-portable, IMU-free Mobile Mapping System. ISPRS Annals of the Photogramm., Remote Sens. and Spatial Inf. Sci., 2(3/W5), 17-23. Retrieved from http://www.isprs-ann-photogramm-remote-sens-spatial-inf-sci.net/II-3-W5/17/2015/isprsannals-II-3-W5-17-2015.pdf

Oh, S.-C., Kim, G.-D., Jeong, W.-T. & Park, Y.-T. (2008). Vision-based Object Detection for Passenger's Safety in Railway Platform. Int. Conf. Control, Autom. Syst. 2008 (pp. 2134–2137). Seoul, Korea.

Passarella, R., Tutuko, B. & Prasetyo, A. P. P. (2011). Design Concept of Train Obstacle Detection System in Indonesia. Int. J. Res. and Rev. in Appl. Sci., 9(3), 453–460.

Petrie, G. (2010). An Introduction to the Technology Mobile Mapping Systems. GEOInformatics (pp. 32-43). Retrieved from

http://www.petriefied.info/Petrie_Mobile_Mapping_Systems_Jan-Feb_2010.pdf

Petrie, G. & Toth, C. K. (2008). Terrestrial Laser Scanners. In Shan, J. & Toth, C. K. (Eds.), Topographic Laser Ranging and Scanning: Principles and Processing (pp. 87-127). Taylor & Francis Group, LLC.

Ponnuswamy, S. (2012). Railway Transportation: Engineering, Operation and Management. Alpha Science.

Press Kit Metro Automation Facts, Figures and Trends - A global bid for automation: UITP Observatory of Automated Metros confirms sustained growth rates for the coming years. (n.d.). Retrieved from International Association of Public Transport: http://www.uitp.org/sites/default/files/Metro%20automation%20-%20facts%20and%20figures.pdf

Processing. (n.d.). In Processing. Retrieved from https://processing.org/

Puente, I., González-Jorge, H., Arias, P. & Armesto, J. (2011). Land-based Mobile Laser Scanning Systems: A Review. ISPRS Workshop, Laser Scanning 2011, 38(5/W12), 163-168. Calgary, Canada, 29-31 August 2011. Retrieved from http://www.int-arch-photogramm-remote-sens-spatial-inf-sci.net/XXXVIII-5-W12/163/2011/isprsarchives-XXXVIII-5-W12-163-2011.pdf

Puente, I., González-Jorge, H., Martínez-Sánchez, J. & Arias, P. (2013). Review of Mobile Mapping and Surveying Technologies. Measurement, 46(7), 2127-2145. http://dx.doi.org/10.1016/j.measurement.2013.03.006

Roncella, R., Remondino, F. & Forlani, G. (2005). Photogrammetric Bridging of GPS Outages in Mobile Mapping. Proc. of Videometrics VIII, SPIE-IS&T Electron. Imaging,5665, 308-319. http://dx.doi.org/10.1117/12.587843

Schwarz, K. P., Chapman, M. A., Cannon, M. W. & Gong, P. (1993). An Integrated INS/GPS Approach to the Georeferencing of Remotely Sensed Data. Photogramm. Eng. & Remote Sens., 59(11), 1667-1674.

Schwarz, K. P. & El-Sheimy, N. (2004). Mobile mapping Systems - State of the Art and Future Trends. Proc. of the 20th Int. ISPRS Congress, 35(B5), 759-768.

Istanbul, Turkey. Retrieved from http://www.isprs.org/proceedings/XXXV/congress/comm5/papers/652.pdf

Soni, A., Robson, S. & Gleeson, B. (2014). Extracting Rail Track Geometry from Static Terrestrial Laser Scans for Monitoring Purposes. Int. Arch. Photogramm. Remote Sens. Spat. Inf. Sci., XL-5, 553–557.

Soni, A. Robson, S. & Gleeson, B. (2015). Optical Non-Contact Railway Track Measurement with Static Terrestrial Laser Scanning to Better than 1.5mm RMS. FIG Working Week 2015. Sofia, Bulgaria.

Suzuki, T., Kitamura, M., Amano, Y. & Hashizume, T. (2010). 6-DOF Localization for a Mobile Robot Using Outdoor 3D Voxel Maps. IEEE/RSJ Int. Conf. on IROS (pp. 5737-5743). http://dx.doi.org/10.1109/IROS.2010.5652983

Tao, C. V. (2000). Mobile Mapping Technology for Road Network Data Acquisition. Journal of Geospatial Eng., 2(2), 1-13. Retrieved from http://www.lsgi.polyu.edu.hk/staff/ZL.Li/vol_2_2/01_tao_c_1.pdf

Terejanu, G. A. (2011). Unscented Kalman Filter Tutorial. University at Buffalo.

Titterton, D. H. & Weston, J. L. (2004). Strapdown Inertial Navigation Technology (2nd ed.). Stevenage: Institution of Electrical Engineers.

The Toolkit. (2013). Retrieved from http://www.instk.org/

Thies, T. (2011). A Vessel-Based Mobile Mapping System - From Sensor Integration to Multipurpose Products. Master's Thesis, HafenCity University, Hamburg, Germany, 28 February 2011. Retrieved from http://www.riegl.com/uploads/tx_pxpriegldownloads/Thies_Thomas__2011_-_A_Vessel-Based_Mobile_Mapping_System__Master_Thesis__HafenCity_University_Hamburg__Germany_part1.pdf

Toschi, I., Rodriguez- Gonzálvez, P., Remondino, F., Minto, S., Orlandini, S. & Fuller, A. (2015). Accuracy Evaluation of a Mobile Mapping System with Advanced Statistical Methods. Int. Arch. of Photogramm., Remote Sens. and Spatial Inf. Sci., XL(5/W4), 245-253. Retrieved from http://www.int-arch-

photogramm-remote-sens-spatial-inf-sci.net/XL-5-W4/245/2015/isprsarchives-XL-5-W4-245-2015.pdf

Toth, C. K. (2009). R&D of Mobile LiDAR Mapping and Future Trends. Proc. of the ASPRS Annual Conf. (pp. 1-7). Baltimore, Maryland. Retrieved from http://www.asprs.org/a/publications/proceedings/baltimore09/0096.pdf

Tsai, G. J., Chiang, K. W., Chu, C. H., Chen, Y. L., El-Sheimy, N. & Habib, A. (2015). The Performance Analysis of an Indoor Mobile Mapping System with RGB-D Sensor. Int. Arch. of Photogramm., Remote Sens. and Spatial Inf. Sci., XL(1/W4), 183-188. Retrieved from http://www.int-arch-photogramm-remote-sens-spatial-inf-sci.net/XL-1-W4/183/2015/isprsarchives-XL-1-W4-183-2015.pdf

Uribe, J. A., Fonseca, L. & Vargas, J. F. (2012). Video Based System for Railroad Collision Warning. 2012 IEEE Int. Carnahan Conf. Secur. Tech., 280–285. Boston.

Ussyshkin, V. (2009). Mobile Laser Scanning Technology for Surveying Application: From Data Collection to End-Products. FIG Working Week 2009 (pp. 1-13). Eilat, Israel, 3-9 May 2009. Retrieved from http://www.fig.net/resources/proceedings/fig_proceedings/fig2009/papers/ts08e/ts08e_ussyshkin_3521.pdf

Ussyshkin, V. & Boba, M. (2008). Performance Characterization of a Mobile LiDAR System: Expected and Unexpected Variables. Proc. of ASPRS Annual Conf. (pp. 1-12). Portland, OR, USA, 28 April - 2 May 2008. Retrieved from http://www.asprs.org/a/publications/proceedings/portland08/0081.pdf

Varesano, F. (2013). FreeIMU: An Open Hardware Framework for Orientation and Motion Sensing.

Wan, E. A. and Merwe, R. V. D. (2001). The Unscented Kalman Filter. Wiley Publishing.

Wehr, A. & Lohr, U. (1999). Airborne Laser Scanning - an Introduction and Overview. ISPRS Journal of Photogramm. and Remote Sens., 54(2-3), 68-82. http://dx.doi.org/10.1016/S0924-2716(99)00011-8

Wever, C. & Lindenberger, J. (1999). Experiences of 10 Years Laser Scanning. In D. Fritsch & R. Spiller (Eds.), Photogramm. Week 1999 (pp. 125-132). Retrieved from http://www.ifp.uni-stuttgart.de/publications/phowo99/wever.pdf

Yang, B. & Fang, L. (2014). Automated Extraction of 3D Railway Tracks from Mobile Laser Scanning Point Clouds. IEEE J. Appl. Earth Obs. Remote Sens., 4750–4761.

Zhao, H., Chiba, M., Shibasaki, R., Shao, X., Cui, J. & Zha, H. (2008). SLAM in a Dynamic Large Outdoor Environment Using a Laser Scanner. IEEE Int. Conf. on Robot. Autom. (pp. 1455-1462). Pasadena, CA, USA, 19-23 May 2008. Retrieved from http://ieeexplore.ieee.org/stamp/stamp.jsp?arnumber=4543407

Zhu, L. & Hyyppä, J. (2014). The Use of Airborne and Mobile Laser Scanning for Modelling Railway Environments in 3D. Remote Sens., 6(4), 3075–3100.

Zlot, R. & Bosse, M. (2014). Efficient Large-Scale 3D Mobile Mapping and Surface Reconstruction of an Underground Mine. In Yoshida, K. & Tadokoro, S. (Eds.), Field and Service Robotics (pp. 479-493). Springer Tracts in Advanced Robotics 92. http://dx.doi.org/10.1007/978-3-642-40686-7_32